

NACA TN 3869

CHAPMAN 1957

# NATIONAL ADVISORY COMMITTEE FOR AERONAUTICS

TECHNICAL NOTE 3869

INVESTIGATION OF SEPARATED FLOWS IN SUPERSONIC  
AND SUBSONIC STREAMS WITH EMPHASIS ON  
THE EFFECT OF TRANSITION

By Dean R. Chapman, Donald M. Kuehn,  
and Howard K. Larson

Ames Aeronautical Laboratory  
Moffett Field, Calif.

Original paper copy from Ken Stetson, retired from AFRL, April 2003. Scanned to PDF at 300 dpi, Prof. S.P. Schneider, Purdue Univ., May 2003. Images scanned in grayscale, appear near quality of original images when viewed on screen at enlarged scale. Posted on public website, since NACA reports are available to public on Langley technical report server (but without grayscale images, so photos are generally unreadable in copies reproduced from microfiche).



Washington

March 1957

## TABLE OF CONTENTS

	<u>Page</u>
SUMMARY . . . . .	1
INTRODUCTION . . . . .	2
NOTATION . . . . .	5
Subscripts . . . . .	6
Superscripts . . . . .	6
APPARATUS AND TEST METHODS . . . . .	7
Wind Tunnel . . . . .	7
Models and Supports . . . . .	7
Test Methods and Techniques . . . . .	8
Variation in Mach number . . . . .	8
Optical techniques . . . . .	9
Transition determination from shadowgraphs . . . . .	9
Boundary-layer trips . . . . .	10
Surface oil-film technique . . . . .	10
RESULTS AND DISCUSSION PERTAINING TO RELATIVE TRANSITION	
LOCATION . . . . .	11
General Survey Illustrating Dominant Importance of	
Relative Transition Location . . . . .	11
Results of initial experiments . . . . .	11
Correlation between transition and occurrence of	
abrupt pressure rise . . . . .	12
Representative pressure distributions for the three	
regimes and results of high-speed motion picture	
studies . . . . .	14
Representative Reynolds number effects for the three	
regimes . . . . .	17
Representative Mach number effects for the three	
regimes . . . . .	18
Significance to wind-tunnel testing . . . . .	19
REYNOLDS NUMBER RANGE FOR PURE LAMINAR SEPARATIONS . . . . .	20
MECHANISM DETERMINING PRESSURE IN SEPARATED REGIONS AND	
THEORETICAL EXPLANATION FOR IMPORTANCE OF TRANSITION	
LOCATION RELATIVE TO REATTACHMENT . . . . .	22
Theoretical Analysis of Leading-Edge Separation . . . . .	23
Experimental Results for Flows With Negligible Boundary-	
Layer Thickness at Separation . . . . .	29
An Explanation of the Importance of Transition Location	
Relative to Reattachment . . . . .	31
CHARACTERISTICS INDEPENDENT OF THE MODE OF INDUCING	
SEPARATION (FREE INTERACTIONS) . . . . .	33
Results for Various Separated Flows . . . . .	34
Difference between subsonic and supersonic	
separations . . . . .	34
Simplified analysis for free-interaction regions . . . . .	35

TABLE OF CONTENTS - Concluded

	<u>Page</u>
Experiments on effects of geometry, Reynolds number, and Mach number for laminar separation . . . . .	38
Experiments on effects of geometry, Reynolds number, and Mach number for turbulent separation . . . . .	40
CONCLUSIONS . . . . .	44
APPENDIX A - ANOMALOUS OIL-FILM OBSERVATIONS . . . . .	46
APPENDIX B - SPECIAL EXPERIMENTS PERTAINING TO THE CROCCO- LEES THEORY . . . . .	48
REFERENCES . . . . .	50
FIGURES . . . . .	55

---

TECHNICAL NOTE 3869

---

INVESTIGATION OF SEPARATED FLOWS IN SUPERSONIC  
AND SUBSONIC STREAMS WITH EMPHASIS ON  
THE EFFECT OF TRANSITION

By Dean R. Chapman, Donald M. Kuehn,  
and Howard K. Larson

SUMMARY

Experimental and theoretical research has been conducted on flow separation associated with steps, bases, compression corners, curved surfaces, shock-wave boundary-layer reflections, and configurations producing leading-edge separation. Results were obtained from pressure-distribution measurements, shadowgraph observations, high-speed motion pictures, and oil-film studies. The maximum scope of measurement encompassed Mach numbers between 0.4 and 3.6, and length Reynolds numbers between 4,000 and 5,000,000.

The principal variable controlling pressure distribution in the separated flows was found to be the location of transition relative to the reattachment and separation positions. Classification is made of each separated flow into one of three regimes: "pure laminar" with transition downstream of reattachment, "transitional" with transition between separation and reattachment, and "turbulent" with transition upstream of separation. By this means of classification it is possible to state rather general results regarding the steadiness of flow and the influence of Reynolds number within each regime.

For certain pure laminar separations a theory for calculating dead-air pressure is advanced which agrees well with subsonic and supersonic experiments. This theory involves no empirical information and provides an explanation of why transition location relative to reattachment is important. A simple analysis of the equations for interaction of boundary-layer and external flow near either laminar or turbulent separation indicates the pressure rise to vary as the square root of the wall shear stress at the beginning of interaction. Various experiments substantiate this variation for most test conditions. An incidental observation is that the stability of a separated laminar mixing layer increases markedly with an increase in Mach number. The possible significance of this observation is discussed.

## INTRODUCTION

Flow separation often is considered as a scourge to many technical devices which depend upon the dynamics of fluids for successful operation, inasmuch as separation often limits the usefulness of these devices. For example, the maximum lift of an airfoil and the maximum compression ratio of a compressor are limited by the occurrence of separation. Separated regions can also occur near a deflected flap, around a spoiler control, in an overexpanded rocket nozzle, behind a blunt base, on the leeward side of an object inclined at large angle of attack, and near the impingement of a shock wave from one body upon the boundary layer of another. Such occurrences make flow separation a very common phenomenon warranting much research effort.

Of the numerous experimental results on separated flows, a few have proved to be applicable throughout the subsonic, transonic, and supersonic speed ranges. The first and most important result involves the phenomenon of boundary-layer transition. In 1914 Prandtl (ref. 1) demonstrated that the pronounced effects of flow separation on the low-speed drag of a bluff body, such as were observed earlier by Eiffel (ref. 2), are determined by the type of boundary-layer flow approaching the separation point; that is, whether it is laminar or turbulent. In the initial post-war years, a number of independent investigations (refs. 3, 4, 5, and 6) were conducted in transonic and supersonic wind tunnels which revealed similar marked effects on compressible flow fields when the boundary layer approaching separation was changed from laminar to turbulent. These experiments leave little doubt that separated flows with transition upstream of separation are fundamentally different from those with transition downstream.

From various experiments on separated flows, a second general result can be detected which may not have been evident at the time the various experiments were conducted, but which is perceptible now through the medium of hindsight coupled with the findings of more recent research. This second result concerns the importance of the location of transition within a separated layer relative to the position of laminar separation. Schiller and Linke (ref. 7) found that even under conditions where the boundary-layer flow remains laminar at separation, the pressure distribution about a circular cylinder depends significantly on how near transition is to the separation position. They observed that an increase in either Reynolds number or turbulence level moved transition upstream in the separated layer to a position closer to separation, and that such movement considerably affected the drag and pressure distribution. Closely related to these findings are some isolated observations that transition location often correlates with an abrupt pressure rise when the separated layer is laminar. This correlation is found within "separation bubbles" on airfoils (ref. 8), and in many other cases, both at low speed and supersonic speed, as is discussed in detail later. Thus with a separated layer remaining laminar, a variation in Reynolds number

changes the location of transition relative to the separation point and this varies the pressure rise associated with transition; the consequence is an effect of Reynolds number on pressure distribution which is especially pronounced in the separated flow behind a base. (See refs. 5 and 6.) An initial approach to the computation of such effects has been made by Crocco and Lees (ref. 9) who consider explicitly the movement of transition along a separated layer. The synoptic result of these various investigations is that the location of transition relative to separation is a variable generally important to separated flows wherein the boundary layer is laminar at separation.

In most previous experiments attention generally has been directed to the type of boundary-layer flow existing at separation and to the relative distance between transition and separation; less attention has been given to the type of boundary-layer flow existing at reattachment and to the relative distance between transition and reattachment. ("Reattachment" is taken herein to mean the localized zone wherein a separated layer either meets a surface or another separated layer.) At sufficiently low Reynolds numbers, a type of separation can exist where transition is downstream of the reattachment zone, or perhaps even nowhere in the flow field. In order to achieve this pure laminar<sup>1</sup> type of separation in a low-speed flow, however, the Reynolds number must be very low (e.g., the order of several thousand for a circular cylinder). In view of the unusually low Reynolds number required, and the fact that the reattachment position is not steady in a subsonic wake, it is understandable that conditions at reattachment previously have received relatively little emphasis in investigations of separated flow. An isolated example of pure laminar separation was observed by Liepmann and Fila (ref. 10) behind a small, half-cylinder, roughness element placed within a subsonic laminar boundary layer.

The present investigation, which is concerned in considerable part with flow conditions near reattachment, was conducted in three phases differing greatly in purpose and scope. Such division was not planned but was dictated by some rather surprising and encouraging results obtained during the initial phase of experimentation, coupled with some major revisions in the wind-tunnel facility made during the interval over which the research was conducted. The initial experiments (conducted in 1953) were concerned with the manner in which Reynolds number variation at supersonic speed affects the separated-flow region upstream of two-dimensional steps of various height. Comparison of the results of the initial experiments with those of other experiments revealed several

---

<sup>1</sup>For reasons explained later, many flows commonly designated as "laminar" separations in previous investigations really are affected significantly by the presence of transition locally in the reattachment zone; such flows are referred to herein as "transitional" separations. Consequently, it is desirable for purposes of emphasis and contradistinction to use an unambiguous terminology, such as "pure laminar," for those flows which truly are unaffected by transition.

---

intriguing similarities among various separated flows on presumably unrelated configurations. These similarities (discussed in detail later) suggested that the location of transition relative to reattachment might be just as fundamental to any separated flow as is the location of transition relative to separation. In order to explore this possibility, a second phase of experiments was conducted with a variety of model shapes rather than just a step. A third phase of experiments was conducted after modifications were made to the wind tunnel which enabled operation over an extended Mach number and Reynolds number range. Inasmuch as an ultimate hope was to improve the understanding of separated flows, it was thought mandatory to include measurements at subsonic as well as supersonic speeds as an integral part of the research. All measurements were made on two-dimensional models.

This report covers three subjects: (1) a general survey of the experimental results grouped according to whether transition is downstream of reattachment, between separation and reattachment, or upstream of separation; (2) a description and experimental test of a theory of the fundamental mechanism near reattachment which governs the dead-air pressure in a separated region (this theory is used to provide an explanation of why transition location relative to reattachment is of importance to separated flows); (3) a simple analysis and pertinent experiments on "free interaction" type flows wherein the boundary layer interacts freely with an external supersonic flow in the manner originally pictured by Oswatitsch and Wieghardt (ref. 11). A preliminary report presenting briefly some of the salient results of this investigation has been published as reference 12.

In the three-year interim over which the present experiments and theoretical research were conducted, various results of other studies appeared which benefited and influenced the course of this research. A thorough investigation of turbulent separation induced by steps and by interaction of oblique shock waves with the turbulent boundary layer on a wind-tunnel wall was published by Bogdonoff (ref. 13) and by Bogdonoff and Kepler (ref. 14). As a result it was deemed unnecessary to investigate turbulent separations for these two cases, except to provide incidental comparisons and checks with their data. Similarly, extensive results of Gadd, Holder, and Regan (ref. 15) became available for the case of shock-wave-induced separation. In these latter experiments, separated flows with transition downstream of reattachment were observed as were fully turbulent flows and flows with transition between separation and reattachment. The importance of transition location relative to reattachment is clearly recognized by Gadd, et al. More recently, the research of Korst, Page, and Childs (ref. 16) became available, in which nearly the same fundamental theoretical mechanism was employed in their calculations of base pressure for thin turbulent boundary layers as that mechanism described and experimentally tested herein for thin laminar boundary layers. Comparison of results from these various recent and independent researches is made later in the report.

## NOTATION

$c_f$	local skin-friction coefficient, $\frac{\tau}{q}$
$\tilde{c}_f$	ratio of $c_{f0}$ at a given $R_{x0}$ to corresponding value at $R_{x0} = 10^6$
$h$	height of step or base
$l_i$	characteristic streamwise length over which interaction takes place
$L$	body length (see fig. 2)
$m$	mass-flow rate per unit span
$M$	Mach number
$p$	pressure
$Pr$	Prandtl number
$q$	dynamic pressure, $\frac{\rho u^2}{2}$
$R$	reattachment point
$R_L, R_{x0}$	Reynolds number, $\frac{u_0 L}{\nu_0}$ and $\frac{u_0 x_0}{\nu_0}$ , respectively
$S$	separation point
$T$	absolute temperature
$u$	velocity
$x$	distance along model measured from leading edge
$\alpha$	angle of attack relative to surface having length $L$
$\gamma$	ratio of specific heats, 1.40 for air
$\delta$	mixing layer or boundary-layer thickness
$\delta^*$	displacement thickness of boundary layer
$\mu$	viscosity coefficient



$\nu$	kinematic viscosity, $\frac{\mu}{\rho}$
$\rho$	density
$\tau$	shear stress

## Subscripts

o	conditions at beginning of interaction in supersonic flow, or at location of minimum pressure in subsonic flow
$\infty$	test-section stream conditions
d	dead air
e	outer edge of mixing layer, or edge of boundary layer
p	plateau conditions (for laminar separation), or peak conditions (for turbulent separation)
r	reattachment point
s	separation point
t	total conditions $\left( \text{e.g., } \frac{T_t}{T} = 1 + \frac{\gamma - 1}{2} M^2 \right)$
*	ratio of quantity to corresponding value at edge of mixing layer $\left( \text{e.g., } T_* \equiv \frac{T}{T_e}, \quad \mu_* \equiv \frac{\mu}{\mu_e}, \text{ etc.} \right)$
w	wall

## Superscripts

'	conditions downstream of reattachment region
-	conditions along dividing streamline of mixing layer

## APPARATUS AND TEST METHODS

## Wind Tunnel

Experiments were conducted in the Ames 1- by 3-foot supersonic wind tunnel No. 1. This tunnel operates continuously with dry air over a range of reservoir pressures. For the initial portion of experiments, the range of tunnel pressures available was limited to between 2.5 and 30 pounds per square inch absolute, and the Mach number was limited to about 2.4. Revisions to the tunnel structure, flexible-plate nozzle, and drive motors were made in 1955 so that subsequent experiments could be made over the range of pressures between about 2 and 60 psia and at Mach numbers up to about 3.6. Subsonic speed control ( $0.4 \leq M_{\infty} \leq 0.8$ ) was obtained by choking the flow downstream of the test section with the flexible, supersonic diffuser.

## Models and Supports

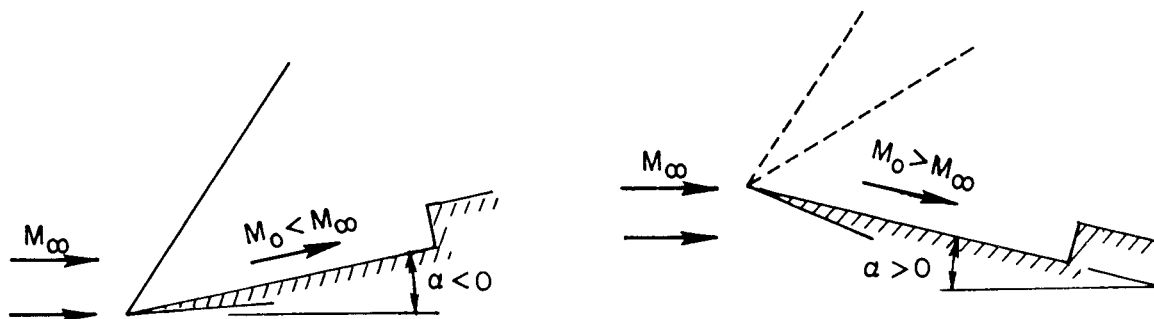
Several types of models with different supports and end plates were employed, each being designed to provide two-dimensional flow conditions. Pressure orifices were located at stations near the center span, and, in most cases, were spaced either 0.05 or 0.10 inch apart. The initial experiments were conducted on step models in an 8-inch-wide two-dimensional channel placed within the 1- by 3-foot test section (see ref. 17 for description of channel). Since use of the channel made model changes and observation rather cumbersome, subsequent experiments were conducted without the channel apparatus by mounting the 8-inch span models on a sting from the rear, and by attaching at both tips relatively small, transparent (lucite), end plates. The photograph in figure 1(a) illustrates the latter method of sting mounting. Since comparison of results obtained with the two methods of mounting showed no significant difference, all subsequent measurements were taken with this latter method of mounting. For those data presented, the flow over the center portion of the model was judged essentially two-dimensional according to three indications: (1) several pressure orifices located spanwise 2 inches off center revealed only small variations of static pressure; (2) the pattern formed by oil film on a model surface (see fig. 1(b)) was normal to the flow direction over a sizable center portion of span; and (3) at all Mach numbers, changing from triangular-shaped to rectangular-shaped end plates had no effect on midspan pressure distribution, and at Mach numbers above about 2.3, even the removal of end plates had no effect. End plates often were not used at the higher Mach numbers, as this enabled better shadowgraphs to be obtained.

Photographs of several models mounted without end plates are presented in figures 1(c), 1(d), and 1(e). The geometry, dimensions, and designations of the various models are given in figure 2. Most

of the models of figure 2 consist of a basic flat plate to which various wedges and steps were fastened to form additional models. This basic flat plate also was used for measurements of boundary-layer-transition Reynolds number to give an indication of wind-tunnel disturbance level. The leading-edge thickness of the flat plate was determined optically to be 0.005 inch. The leading-edge thickness of the other models (for which the surface contour is an integral part of the basic plate) is believed to be approximately the same.

### Test Methods and Techniques

Variation in Mach number.- The Mach number  $M_0$  approaching an interaction region was varied in several ways. At subsonic speed, the angle of attack was held fixed while adjustment of the diffuser minimum area provided variation in test-section Mach number  $M_\infty$ . At supersonic speed, the angle of attack was changed to provide variation in  $M_0$ , as illustrated in sketch (a), and the flexible nozzle walls occasionally were repositioned to provide additional variation in  $M_\infty$ . Only a few



Sketch (a)

test-section Mach numbers were required to achieve variation in  $M_0$  from values near 1 to about 3.6, inasmuch as the angle of attack for some of the models could be varied by  $\pm 16^\circ$ . Thus a given  $M_0$  could be obtained with either an expansion wave or a shock wave occurring at the model leading edge (see sketch (a)). It was found in most cases that for a given  $M_0$  both types of settings would yield the same pressure distribution over the center-span portion of the model. In several cases, though, detached bow waves at  $\alpha > 0$  resulted from excessive flow deflection over the lower surface, and this caused transition to occur prematurely on the upper surface. Under such conditions, the pressure distribution in transitional-type separations differed from that obtained at the same  $M_0$ , but with an expansion wave at the leading edge. In some cases of laminar separation, small differences in the shape of pressure distribution - but not in the plateau pressure rise or in the pressure rise to separation - were observed at the same  $M_0$  for the two types of settings. These small differences are attributed to known differences in tunnel-empty pressure distribution at the different nozzle settings.

Optical techniques.- One or more shadowgraphs were taken for each pressure distribution in order to determine the location of transition. Relatively long exposure times were used (1/25 to 1/100 sec) since the mean position of transition was desired rather than an instantaneous position. In the first two phases of experimentation, film was placed next to a side window which intercepted near-parallel light passing through the test section. Polaroid-Land film was used. In the third phase of experimentation, the film was placed on a parallel-motion mechanism surrounded by light-proof bellows (see fig. 3). This enabled the distance from the model to the film to be adjusted in order to take advantage of focusing effects induced by the refraction of parallel light as it passes through the boundary layer (for an explanation of the focusing effects, see ref. 18). Comparison of figures 4(b) with 4(a) reveals the improvement achieved by increasing the distance between the film and the flat-plate model. The white line, indicating the nature of boundary-layer flow, is displaced from the surface where it can be better observed. Comparison of figures 4(d) with 4(c) reveals the improvement achieved in visualizing the separated flow over a curved surface model by increasing the film-to-model distance; for example, a double boundary-layer image indicating spanwise nonuniformity is evident in figure 4(d), but not in figure 4(c).

High-speed motion pictures (Fastax) were taken of the shadowgraph field in order to ascertain the relative steadiness of various separated flows. The parallel light was of sufficient intensity to permit pictures of several thousand frames per second to be taken from the shadowgraph pattern cast on a ground-glass screen. Runs at various frame speeds up to 6000 frames per second showed that flow unsteadiness could be detected readily at speeds near 2000 frames per second.

Transition determination from shadowgraphs.- Two methods, depending upon tunnel pressure, were used to detect transition from the shadowgraphs. At low tunnel static pressures, with small film-to-model distances, transition location appeared as the "end" of the laminar (white) line on the shadowgraphs. At high tunnel static pressures, with small film-to-model distances, or at arbitrary pressure with large film-to-model distances, optical refraction effects are large, and a technique used by Pearcey (ref. 18) was employed to locate transition. Under these conditions the white laminar line appears displaced from the surface by a distance large compared to the boundary-layer thickness. For flow over a flat plate, the apparent displacement is nearly constant from the surface as long as the layer remains laminar, since the density profiles are nearly similar along the plate length. An example is illustrated in figure 5(a). When the Reynolds number is increased so that transition occurs on the plate, the white line converges to the surface in the transition region. Examples of this are illustrated in figures 5(b) and 5(c). The beginning of convergence represents the beginning of transition effects on the density profile and is taken as the beginning of transition itself. The end of convergence, where the white line practically meets the surface, represents the first position where the density profile has its maximum

gradient close to the surface (compared to a laminar profile) and is taken as the end of transition. Under high refraction conditions, therefore, both the beginning and end of transition often could be ascertained approximately. As an example, the results of transition determinations by this method for the flow over a flat plate (leading-edge thickness 0.005 in.) are presented in figure 6. The transition Reynolds number is plotted as a function of the Reynolds number per unit length, inasmuch as this variable appears to be more significant than the Mach number. For example, at stream Mach numbers above 2.0, the curves for both beginning and end of transition are independent of Mach number when plotted in this fashion. These curves will be used later in comparison with other data.

Boundary-layer trips.- A common experience in supersonic wind-tunnel operation is that larger and more severe trips are required as the supersonic Mach number is increased. This trend is reported in detail by Winter, Scott-Wilson, and Davies (ref. 19) who find that the required wire diameter for tripping the boundary layer increases roughly exponentially with Mach number (an interpretation of this trend is given later as it involves a result from the present research). Moreover, merely placing a disturbance at some streamwise position on a model does not insure a fixed transition location. For example, in the present investigation, at Mach numbers near 3 the wire trips often did not effect transition until a short distance before the separation position. Under these conditions the effective origin of the turbulent layer varied with tunnel pressure in an unknown manner over the plate length between the wire and the separation position. Data obtained on the effects of Reynolds number variation are uncertain under such conditions.

In the course of experimentation various full-span boundary-layer trips were used depending primarily on the Mach number. At subsonic and moderate supersonic Mach numbers a 0.015-inch-diameter wire (trip 1) placed 0.13 inch from the leading edge, as sketched in figure 2(f), was adequate to effect transition near the wire. At the higher supersonic Mach numbers a trip more severe than a small wire was needed. On several models tested in this higher Mach number range during the second phase of experiments, the upstream portion of the model plate was corrugated by saw-toothed machining (see trip 2 in fig. 2(f)) and on one model a section of wire screen also was added (trip 3). During the third phase of research a "base trip," consisting of a small wedgelike attachment to the leading edge, was employed (see trip 4 in fig. 2(f) and photograph in fig. 1(e)). A pressure orifice was installed in this base in order to determine when the trip fixed transition. A plot of the base pressure as a function of tunnel pressure revealed the tunnel pressure above which transition was fixed near the trip.

Surface oil-film technique.- A useful technique employed in the course of research was an oil-film method for determining quantitatively the location of separation and hence the pressure rise to a separation point. It is known that liquids coated on a surface will accumulate

along a line of separation. The flow upstream of separation washes liquid downstream, whereas reverse flow downstream of separation washes liquid upstream. In order to make this technique quantitative and to minimize interference, very small amounts of liquid are required. To detect minute accumulations of liquid, light at glancing incidence was employed. This enabled an accumulation to be detected of height much smaller, for example, than the mouth of a pitot tube. Silicone oil (Dow Corning DC 200-10) was employed, sometimes mixed with regular hydrocarbon oil. Thin films of this oil were mobile yet would not evaporate even after four or five hours of continuous tunnel operation. It was found possible either to coat portions of a model before a run or to emit oil from an orifice during a run. The minute, threadlike lines of accumulation, which were observed readily, could not be photographed well during tunnel operation. For photographic purposes, the surface oil film for the model in figure 1(a) (possibly not visible in half-tone reproduction), was allowed to accumulate in larger amounts than for most quantitative measurements. A typical accumulation pattern is sketched in figure 1(b).

The oil-film technique for determining the separation point is believed to be more sensitive than the pitot-probe technique. Using a Stanton tube 0.005-inch high, for example, Gadd, et al., (ref. 15) could determine only roughly the laminar separation point and, hence, were unable to detect any Reynolds number dependence on the pressure rise to separation. As will be seen later, the oil-film technique readily enables the Reynolds number dependence to be determined as well as quantitative values of rather good accuracy for the pressure rise.

Extensive use of the oil-film technique revealed, under certain test conditions, an anomalous, double-accumulation pattern which was difficult to interpret. Some details of the research conducted to resolve this anomalous behavior are described in Appendix A.

## RESULTS AND DISCUSSION PERTAINING TO RELATIVE TRANSITION LOCATION

### General Survey Illustrating Dominant Importance of Relative Transition Location

Results of initial experiments.- As noted previously, the initial experiments were conducted on step models in a two-dimensional-channel apparatus; they clearly revealed the basic importance of transition location relative to a reattachment position. Transition location was found to correlate closely with an abrupt rise in pressure when transition was between separation and reattachment. A typical example of this is illustrated in figure 7(a). The pressure distribution in this type of separation was affected markedly by variations in Reynolds number. In contradistinction, no abrupt rise in pressure was observed when transition

was downstream of the reattachment point (step shoulder); figure 7(b) represents a typical example of this. The step height in figure 7(b) is smaller than that in figure 7(a) and is sufficiently small so as not to bring about transition. The pressure distribution for this pure laminar type of separation was affected only slightly by variations in Reynolds number. These contrasting characteristics show that the location of transition relative to reattachment is of critical importance at least to the separated flow ahead of a step.

The results of the initial experiments revealed some intriguing similarities between various results of experiments on separated flow from several other sources involving entirely different object shapes. The trend observed, of a slight influence of Reynolds number on pure laminar separations, was the same as the trend which could be interpreted from the base-pressure experiments of Reller and Hamaker (ref. 20). Also, the trend of large influences of Reynolds number for transitional separations was the same as that which could be interpreted from many previous measurements of base pressure. Crocco and Lees (ref. 9) make essentially this interpretation, only with reference to transition upstream of a "critical" location in the wake rather than upstream of reattachment. Consequently, it seemed possible that transition location relative to reattachment might be generally important to separated flows and that there might be some characteristics common to a variety of separated flows having the same relative transition location. The second phase of experiments was conducted with various model shapes in order to investigate this possibility. Some of the more salient results are surveyed below; they relate to the correlation between transition and abrupt pressure rise, to the relationship between type of pressure distribution and relative transition location, and to the effects of Reynolds number variation on separated flows.

Correlation between transition and occurrence of abrupt pressure rise.- Transition was determined from shadowgraphs in two different ways (described in the section APPARATUS AND TEST METHODS). Under conditions of low pressure and low optical refraction, the mean location of transition was taken as the end of the familiar white line adjacent to a surface. Altogether about 170 cases of this type were examined corresponding to different combinations of Mach number, Reynolds number, and model shape. Figure 7(a) represents one example, and various others are shown in figure 8<sup>2</sup> for subsonic as well as supersonic flow. The terminal location of the white line is near an abrupt pressure rise in each case. There is sufficiently close coincidence of the two locations to associate the location of transition with that of a rapid rise in pressure. Emphasis is placed on the fact that the correlation for subsonic flow (figs. 8(a) and 8(b)) is much the same as that for supersonic flow. This attests to the fundamental importance of transition for separated flows.

---

<sup>2</sup>In these and other figures, a separation point determined from an oil film observation is represented by a filled symbol. Separation pressure rises determined from a correlation (presented later) of measurements on a variety of model shapes are represented by a short line.

As explained previously, both the beginning and the end of transition could often be determined, when optical refraction was high, by the beginning and end of convergence of the white line toward a solid surface. Altogether, about 95 cases of this type were examined for various combinations of Mach number, Reynolds number, and model shape. Some typical examples are shown in figure 9. In most of these examples transition occurs in an adverse pressure gradient, and the streamwise extent of the transition region is much shorter than on a flat plate. In all cases the abrupt pressure rise occurs near the transition region, so that a marked pressure rise again is associated with transition.

It is interesting that, in subsonic flow over step models, separation bubbles often were observed on the flat surface well upstream of the step. An example is illustrated in figure 8(b). In such cases, oil film accumulated at two streamwise locations; the upstream separation is that of a laminar layer and locates the upstream portion of the bubble; the downstream separation (not evident in shadowgraph) is that of a turbulent layer as it approaches the step. Turbulent reattachment presumably occurs somewhere between the two experimentally determined positions of separation.

The correlation of the location of transition with that of an abrupt pressure rise has been observed previously in many isolated cases. Experiments at low subsonic speeds conducted on circular cylinders, spheres, and airfoils, as reported by Fage (ref. 21), showed similar close correlation of transition location (determined by surface shear data from a Stanton tube) with an inflection point in pressure distribution which just preceded an abrupt pressure rise.<sup>3</sup> Analogous correlation also was noticed in transonic flow by Ackeret, Feldmann, and Rott (ref. 4), in supersonic shock-induced separations by Gadd, Holder, and Regan (ref. 15), and in subsonic separation bubbles on airfoils by Gault (ref. 8).

In spite of the many observations of correlation between transition location and abrupt pressure rise - as evidenced in figures 7 to 9 and in previous experiments - it is not necessary that transition in a separated layer be accompanied by a rapid pressure rise, or that abrupt rises in pressure necessarily indicate transition. If transition is far upstream of reattachment, and only slightly downstream of separation, then transition can occur in the mixing layer under conditions of nearly constant

---

<sup>3</sup>In retrospect, it would be expected that for such correlation to have existed, transition would have occurred within a small "separation bubble" in these early experiments. This expectation was indicated by Bursnall and Loftin (ref. 22). Such bubbles have been observed frequently on airfoils but rarely on a sphere or circular cylinder. A direct confirmation of the existence, not often appreciated, of a small separation bubble on the upstream half of a circular cylinder in the supercritical Reynolds number range is reported by Gault (ref. 8) who used a liquid film to detect separation.

---



pressure. An example of this is shown in figure 10(a) in which transition is completed well upstream of reattachment and the pressure rise is brought about by a fully turbulent layer as it reattaches. If a reattaching layer is laminar and very thin, it also can bring about an apparent rapid rise in pressure and not be indicative of transition. An example of this is presented in figure 10(b) for which transition is downstream of the field of view. (A theory for the pressure rise of a thin, pure laminar, reattaching layer is given later.) In view of these observations, the pertinent conclusions drawn from the close correlation often observed between transition and an abrupt pressure rise is as follows: Once transition is between separation and reattachment - and is relatively close to reattachment - there is an abrupt pressure rise associated with transition; hence, any change in a parameter which experience has shown to affect transition (such as Reynolds number, surface roughness, turbulence level, etc.) can also change pressure distribution directly through its change in the location and magnitude of the steep pressure rise.

Representative pressure distributions for the three regimes and results of high-speed motion picture studies.- As the importance of transition location relative to reattachment is now manifest, and the importance of transition location relative to separation has long been known, it is clear that distinction should be made for any given object shape between the three regimes of flow separation; "pure laminar" where transition is downstream of reattachment, "transitional" where transition is between reattachment and separation, and "turbulent" where transition is upstream of separation. Within the scope of this study, all three regimes were observed for most of the model shapes, as the following table illustrates:

Regimes observed in present study			
Model	Pure laminar	Transitional	Turbulent
Step	$M > 1, M < 1$	$M > 1, M < 1$	$M > 1, M < 1$
Compression corner	$M > 1, M < 1$	$M > 1, M < 1$	$M > 1, M < 1$
Base	$M > 1$	$M > 1$	$M > 1$
Curved surface	$M > 1$	$M > 1$	$M > 1$
Oblique shock	$M > 1$	$M > 1$	
Leading-edge separation	$M > 1$	$M > 1$	

Studies were not conducted with the turbulent regime for leading-edge separation, or with the turbulent regime for oblique-shock-induced separation. Much data are available for this latter case in references 14 and 15.

Shadowgraphs and corresponding pressure distributions for the three regimes, at both supersonic and subsonic speeds, are illustrated in figures 11 through 17 for various models and various Mach numbers. Figure 11, which shows the step in supersonic flow, reveals as well as any the basic differences between the three regimes. The pure laminar regime (fig. 11(a))

has a plateau region of nearly constant pressure representing a dead-air region. The separation-point pressure,  $p_s$ , and the plateau pressure,  $p_p$ , are of the order of 15 and 30 percent greater, respectively, than the pressure  $p_0$  just upstream of the separated region. For some step models, pressures were measured at a few points on the step face and were usually found - for the pure laminar regime - to be the same as the dead-air pressure (see fig. 7(b) for example). In a few cases, a very small pressure rise was observed in the corner and on the step face. It is thought that there always is a small region near the step shoulder where pressures on the face locally are higher than the dead-air pressure, since a portion of the separated layer presumably must be brought to rest on the step face. If the separated layer at separation is thick, then the expected magnitude of pressure increase would be small, and if it is very thin, then the area over which the pressure increase would occur would be confined to a small area near the shoulder. This may explain why a significant pressure variation over the step face is not often measured. High-speed motion pictures (taken at  $M_0 = 2.3$  with 2000 to 6000 frames per sec) indicated the pure laminar separation over a step to be steady.

Most of these characteristics for pure laminar separation over a step differ from those for transitional separation illustrated in figure 11(b). In the transitional regime the boundary layer is still laminar at separation so the pressure rise to separation remains about the same as for pure laminar separation, but the role of transition is to bring about much greater pressure rises before reattachment occurs at the step. Pressure variation on the step face, now easily measurable, amounts to the order of  $0.1 p_0$  (see fig. 7(a) for example). As Lange (ref. 23) has noticed previously, this variation implies that sizable subsonic velocities exist within the reverse flow region just upstream of the step. High-speed motion pictures indicated the flow to be unsteady in the region between transition and reattachment on the step. Such unsteadiness might be expected since transition itself is fundamentally a nonstationary phenomenon. In spite of this unsteadiness, the white line indicative of laminar flow appeared reasonably steady over most of its length whenever transition was relatively far from separation and relatively close to reattachment. At higher Reynolds number, though, where transition was close to separation, the angle of separation appeared unsteady in the motion pictures as did the flow downstream of transition.

These qualitative flow conditions again alter on passing to the turbulent regime illustrated in figure 11(c). The pressure rise to separation now is much larger (about five times larger), as should be expected. A plateau in pressure (characteristic of dead air) does not occur since the eddying motion of the turbulent layer energizes the air. Pressures on the step face were found to vary in much the same manner as for the transitional regime. The flow field observed in high-speed motion pictures was not perfectly steady like the laminar separation was, but, compared to the transitional separation, the turbulent separation was relatively steady. Shock waves occasionally appeared to move slightly

but no appreciable movement of the separated layer could be detected. This degree of steadiness of turbulent separation upstream of a step appears much the same as that observed by Bogdonoff and Kepler (ref. 14).

The data in figures 12 through 17 for steps, compression corners, bases, and curved surfaces show several similarities within a given regime to the characteristics just described for a step at  $M_0 = 2.3$ . It is emphasized that certain qualitative similarities exist irrespective of model shape or Mach number, or whether the flow is subsonic or supersonic (cf., e.g., figs. 11 and 13). Pure laminar separations ((a) portions of figs. 11 through 17) usually involve small pressure changes and relatively gradual pressure gradients. They are steady when observed in motion pictures at several thousand frames per second.<sup>4</sup> The transitional separations for the different configurations ((b) portions of figs. 11 to 17) involve severe pressure gradients near transition and usually were observed to be unsteady. The only transitional-type separation of those investigated which appeared steady was that over the base (e.g., fig. 16(b)). The various turbulent separations (figs. 11(c) to 17(c)) are associated with abrupt pressure variation near both separation and reattachment. They were observed to be relatively steady flows except for the compression corners, which were rather unsteady in several cases at Mach numbers near shock detachment.

A general feature worth noting concerns the proximity of shock waves to the boundary layer in the various types of separated flow. For pure laminar separations the shock wave associated with separation, as well as the shock wave associated with reattachment on a flat surface, does not enter or originate within the boundary layer (see figs. 14(a), 16(a), and 18(a)). The coalescence of compression wavelets into a shock wave occurs at a considerable distance from the boundary layer. In these cases, there obviously is no direct interaction of shock wave and boundary layer; there is, however, strong interaction of the supersonic external flow and the boundary layer. When pure laminar separation is induced by the reflection of an incident shock wave from a laminar boundary layer, the incident wave necessarily enters and locally interacts with the viscous layer near the station of impingement, but the shock waves formed near separation and reattachment do not originate within the viscous layer (see fig. 18(a)). It is only after transition moves upstream of a reattachment position, thereby bringing about a steep pressure rise, that a shock wave originates partially within the boundary-layer flow near reattachment on a surface (see figs. 11(b) through 18(b)). Similarly, only after transition moves upstream of separation does a shock wave originate partially within the boundary-layer flow near separation.

In the process of varying tunnel pressure, the conversion from transitional-type to turbulent-type separation often was observed to be

---

<sup>4</sup>Obviously, not all pure laminar separations are steady in subsonic flow. It is well known that the separated flow behind a cylinder develops into an unsteady vortex trail even at Reynolds numbers near 100 where the separated flow is entirely laminar.

irregular and unsteady. During such conversion, shadowgraphs were blurred since relatively long exposure times were used. The pressure distribution was not smooth since the various orifice-tube connections were not identical, and thus responded differently to the fluctuating pressure. An example illustrating these characteristics is shown in figure 19(a) in comparison to an example of steady turbulent flow (fig. 19(b)). Also, during such conversion between transitional and turbulent regimes, oil film did not accumulate along a threadlike line as it otherwise did. Instead, oil wandered irregularly over the plate in a jagged, random fashion. It is interesting, perhaps, to note that similar unsteady conversions have long been observed. In the fundamental paper on spheres by Prandtl (ref. 1) wherein smoke was used to determine the line of separation, the same type of unsteady flow with jagged separation line was observed during the conversion from the transitional regime to the turbulent regime. It is possible that certain of the unsteady flow phenomena sometimes found on various practical devices are intimately related to the unsteadiness found on these models of simple shape when conditions were such that the flow was on the verge of conversion between transitional-type and turbulent-type separation.

Representative Reynolds number effects for the three regimes.- As previously remarked, a variation in Reynolds number was found to have only a minor effect on pure laminar separations. This is illustrated in figure 20(a). The ordinate is the pressure rise  $|p' - p|$  across the reattachment region divided by the pressure  $p'$  just downstream of reattachment. The quantity  $p$  is measured at an arbitrary fixed point in the separated region. Some of the pure laminar separations are seen to be affected to a negligible extent by variation in Reynolds number. This is consistent with a theory to be developed shortly which indicates that the lack of dependence on Reynolds number is a characteristic of pure laminar separations for which the boundary-layer thickness at separation is zero or negligible. Other curves in figure 20(a) show a small Reynolds number effect which amounts at the most to about a  $1/4$ -power variation. In these cases the boundary-layer thickness at separation is not negligible. Generally speaking, though, the pure laminar separations investigated are affected only to a small extent by variation in Reynolds number.

As might be anticipated, transitional-type separations behave differently than the pure laminar separations when subjected to variation in the Reynolds number. The effect of Reynolds number on various transitional-type separations is shown in figure 20(b). Some of these flows are affected markedly by variation in Reynolds number. When such large variations were found, it was observed that transition was relatively near reattachment. For example, the lower Reynolds number portion of the filled-circle data points shows large effects and corresponds to transition relatively near reattachment, whereas the higher Reynolds number portion corresponds to transition relatively near separation and shows much less effect. In most cases, a movement of transition upstream of reattachment (brought about by an increase in Reynolds number) increases the pressure rise through the reattachment region.

Turning now to turbulent flows for which transition is upstream of separation, the characteristic influence of Reynolds number again changes rather strikingly. The effect of the variation in Reynolds number on various turbulent separations is shown in figure 20(c). For this type of separation, the effects of Reynolds number are either small or negligible.

The typical effects of Reynolds number variation for the three separation regimes also can be clearly seen from complete pressure distributions. Some example pressure distributions for pure laminar separations over a compression corner at various Reynolds numbers are shown in figure 21(a). These pressure distributions are only slightly affected by variation in Reynolds number, as would be anticipated from the trend illustrated in figure 20(a). Some example pressure distributions for transitional separations over a curved surface at various Reynolds numbers are shown in figure 21(b). These data show a large effect of variation in Reynolds number just as do the data in figure 20(b). For example, the pressure drag coefficient of the curved surface would change by a factor of about 4 over the range of Reynolds numbers ( $0.16$  to  $0.81 \times 10^6$ ) represented. Also in agreement with the trend of figure 20(b) for transitional separations, it is seen from figure 21(b) that the changes in final pressure rise with Reynolds number are larger when transition is relatively near reattachment (Reynolds numbers from  $0.16$  to  $0.36 \times 10^6$ ) than when transition is relatively near separation (Reynolds numbers from  $0.36$  to  $0.81 \times 10^6$ ). Some example pressure distributions in turbulent separation at various Reynolds numbers are shown in figure 21(c). As previously noted in figure 20(c), the observed dependence on Reynolds number is small.

The characteristic influences of Reynolds number variation as illustrated for these different models also can be illustrated by a single model. A special model consisting of three bases in series was investigated on which all three separation regimes were found to occur simultaneously at 21 psia tunnel pressure, as may be deduced from study of figure 22. Although the results obtained with this special model are instructive, they do not reveal any new feature over and above those already illustrated in figures 11 through 17.

Representative Mach number effects for the three regimes.- Pressure-distribution curves for pure laminar separation over a step in the Mach number range between 1.3 and 3.1 are presented in figure 23(a). These curves are for  $R_L = 0.13 \times 10^6$ . The various curves qualitatively are similar, and exhibit only a small effect of Mach number on the streamwise length of dead-air region.

Pressure-distribution curves for transitional separation over a step in the Mach number range between 1.3 and 3.3 are presented in figure 23(b) for  $R_L \approx 0.6 \times 10^6$ . These curves show that transition moves downstream as the Mach number is increased. At  $M_0 = 1.3$  the separated laminar layer is relatively unstable, resulting in transition near separation and a large

pressure rise above the plateau pressure; at  $M_0 = 3.3$  the separated laminar layer is much more stable, resulting in transition near reattachment and only a small pressure rise above the plateau.

The effect of Mach number on the pressure distribution over a step in turbulent flow at Mach numbers between 2.0 and 3.4 is presented in figure 23(c). These data correspond to  $R_L \approx 2.6 \times 10^6$ . The streamwise extent of the interaction region is seen to be not significantly affected by variations in Mach number over the range investigated. The peak pressures, though, are strongly dependent on Mach number.

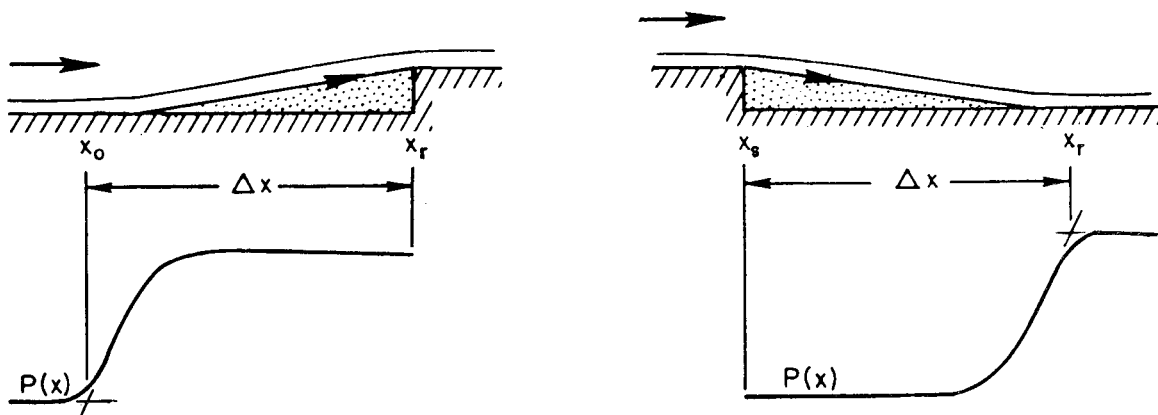
Significance to wind-tunnel testing.- From one viewpoint it is fortunate that a variety of separated flows, such as supersonic flow behind a base, or subsonic flow in a corner, or the flow induced by a strong shock wave impinging on a boundary layer, turn out actually to be dominated largely by a single variable, namely, the location of transition relative to reattachment and separation positions. On the other hand, from the viewpoint of wind-tunnel testing of prototype models, it is unfortunate that a variable like transition, which is so elusive to control and difficult to predict, turns out to be so important. Nevertheless, merely an understanding of the dominating influence of transition on separated flows can be helpful. For example, it is clear that the proper simulation in a wind tunnel of any flow involving separation in flight, such as large-deflection control effectiveness, buffeting, or high angle-of-attack force characteristics, would require the relative transition location to be duplicated between wind tunnel and flight. If the relative transition location is either downstream of reattachment (pure laminar separation) or upstream of separation (turbulent separation), then the precise position of transition does not critically affect the pressure distribution provided the relative location is duplicated; but, if transition is between separation and reattachment (transitional-type separation), then the precise position is important.

The requirement of matching relative transition location between wind tunnel and flight appears particularly important at hypersonic speeds. Inasmuch as a separated laminar mixing layer is relatively stable at hypersonic Mach numbers (see next section), transition can often occur near reattachment in this speed range. Under such conditions, the type of separation could be transitional in the wind tunnel yet pure laminar in flight, or vice versa. Even if a separation is transitional both in wind tunnel and in flight, the type of flow field can be sensitive to variations in Reynolds number when transition is near reattachment, as was illustrated by figures 20(b) and 21(b). In the past, interest has focused more on flow at lower Mach numbers where transition is relatively near separation, under which conditions a close matching of relative transition location for transitional separations is not so important.

## REYNOLDS NUMBER RANGE FOR PURE LAMINAR SEPARATIONS

As the investigation progressed, it became evident that the prevalence of pure laminar-type separations increased as the Mach number was increased. In order to put these qualitative observations on a quantitative basis, data from various models were examined to determine the maximum Reynolds number up to which pure laminar separation was found at each Mach number. Such determinations from shadowgraphs agreed well with corresponding determinations from a break in the curves of dead-air pressure plotted against  $u_0L/v_0$ . The values so obtained for  $(u_0L/v_0)_{\max}$  were different for various models, but for each model they consistently showed strong dependence on Mach number as illustrated in figure 24(a) for various step and base models. Also included in this figure are two data points (at  $M_0 = 4$  and  $M_0 = 4.5$ ) determined from an examination of various unpublished spark photographs obtained by Reller and Hamaker during their investigation (ref. 20) of base pressure on bodies of revolution, and one data point determined from Kavanau's experiments on base pressure (ref. 24). The close agreement of data from bodies of revolution with that from two-dimensional models is regarded as accidental. Also shown in figure 24(a) for purposes of comparison are two curves representing the Reynolds number for the beginning and the end of transition on an attached boundary layer over a flat plate. These two curves correspond to a Reynolds number per inch of  $0.3 \times 10^6$ , as obtained from a cross plot of the data of figure 6.

Since models of different geometry have different lengths of separated layer relative to the model length, it would seem more significant to consider a Reynolds number based on some typical length of separated layer, rather than on model length. A pertinent length easy to determine from pressure distributions is the length  $\Delta x$  as sketched. The maximum



Sketch (b)

Reynolds number for the pure laminar regime  $(u_0 \Delta x / \nu_0)_{\max}$  is plotted as a function of Mach number in figure 24(b).<sup>5</sup> It is evident from figure 24(b) that the stability of a laminar mixing layer increases markedly with an increase in Mach number. In subsonic flow the separated laminar layer is stable only to about a Reynolds number  $u_0 \Delta x / \nu_0$  of 60,000, whereas at Mach numbers near 4 it is stable to a Reynolds number of about a million.

For purposes of comparison in figure 24(b), the two curves are shown which represent the Reynolds numbers for beginning and end of transition on a flat plate. These transition data are directly comparable to the separated-flow data from the present experiments, inasmuch as they were obtained in the same wind tunnel, with essentially the same model leading-edge thickness, at approximately the same tunnel pressures, and under identical conditions of essentially constant pressure and zero heat transfer. The data are not comparable, however, to flight conditions. Flight conditions involve different rates of heat transfer, and different levels of external disturbance. Consequently, the quantitative values for Reynolds number in figure 24(b) are not of central importance. Instead the important item is that, compared to an attached laminar boundary layer, the stability of a separated laminar mixing layer increases markedly with an increase in Mach number.

It is noted that the data of figure 24 correspond to models having relatively extensive regions of separated flow; that is, they represent separated flows wherein the length of separated layer  $\Delta x$  is roughly 0.5 to 0.7 of the model length  $L$ . If a separated flow extends over only a small portion of the model length, then the data in figure 24 might not be closely applicable. An example illustrating this is presented in figure 25. Here the step height is  $0.009L$  and  $\Delta x$  is the order of  $0.3L$ . Over the Mach number range investigated, these pure laminar separations extend to higher Reynolds numbers than for the main body of data representing relatively extensive separated regions.

Although the conventional neutral stability theory - which considers only infinitesimal two-dimensional disturbances - is not a theory for transition, it has indicated certain trends which transition also follows in some cases. For example, surface cooling stabilizes a laminar boundary layer according to both neutral stability calculations and transition experiments. Neutral stability calculations for the laminar mixing layer in compressible flow have been made by Lin (ref. 25) who finds complete stability at Mach numbers above 2.5 for conditions of zero heat transfer. It can be said then that neutral stability theory for certain restricted types of disturbances indicates a strong stabilizing effect of Mach number on laminar mixing layers in accordance with the present experiments.

---

<sup>5</sup>In a preliminary report of this research (ref. 12) a slightly different length,  $x_r - x_s$ , between the reattachment location,  $x_r$ , and separation location,  $x_s$ , was used in place of  $\Delta x$ . The length  $\Delta x$  can be precisely determined; the length  $x_r - x_s$  was only approximate.

---



The experimental result that the stability of a separated laminar mixing layer increases markedly with an increase in Mach number provides an explanation of an experimental characteristic commonly encountered in conducting wind-tunnel tests. In attempting to trip the laminar boundary layer for certain wind-tunnel tests, it has been found that the diameter of wire required increases markedly at the higher Mach numbers. This can be attributed directly to the increase in stability of separated laminar mixing layers. If a given wire does not effectively trip the boundary layer, then the baselike separated flow downstream of the wire, as well as the steplike separated region upstream of the wire, are of the pure laminar type. As soon as transition moves upstream of reattachment in the baselike separation downstream of the wire, then the wire trip has effectively promoted transition. Thus, the maximum Reynolds number for pure laminar-type separation downstream of the wire corresponds precisely to the minimum Reynolds number required to fix transition. Winter, Scott-Wilson, and Davies (ref. 19) have determined quantitatively from experiments with different wire diameters the critical Reynolds number (based on wire diameter) which will fix transition for various Mach numbers. If their data are converted to a Reynolds number based on  $\Delta x$ , the length of separated laminar layer upstream and downstream of the wire ( $\Delta x$  is roughly  $20d$  for conditions of their experiments), then a direct comparison can be made with the data shown in figure 24. Their data have the same trend as the data in figure 24, but fall about a factor of 4 below. This situation is consistent with observations from the present experiments, inasmuch as the data in figure 24 represent only certain configurations and the data for other configurations are different (as in fig. 25). A wire trip represents one configuration which is not conducive to the promotion of extensive laminar separation.

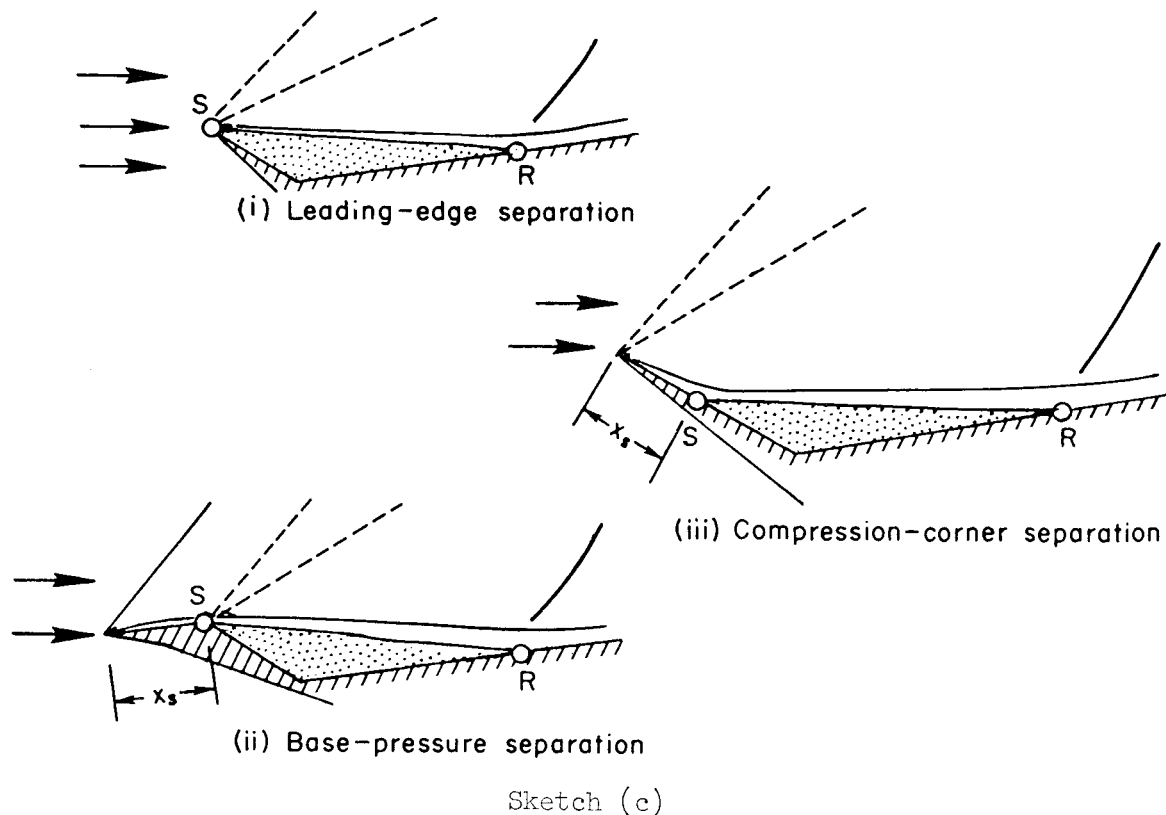
The trend of increasing stability of separated laminar layers with increasing Mach number may be practically significant inasmuch as separated laminar flows have certain uncommon characteristics which might be advantageous. After the trend evident in figure 24 was observed, it appeared desirable to investigate theoretically the heat-transfer and skin-friction characteristics of certain simple pure laminar separations. Such analysis is presented in a separate report (ref. 26) which indicates that the heat transfer and skin friction are less than those of a comparable attached laminar boundary layer.

MECHANISM DETERMINING PRESSURE IN SEPARATED REGIONS  
AND THEORETICAL EXPLANATION FOR IMPORTANCE OF  
TRANSITION LOCATION RELATIVE TO REATTACHMENT

Prior to further discussion of experimental results, a digression is made here in order to develop a theory of the mechanism which determines the dead-air pressure in a separated region. This theory is used subsequently to provide an explanation of the principal experimental result of the preceding section; namely, that transition location relative to a reattachment position is of crucial importance to separated flows.

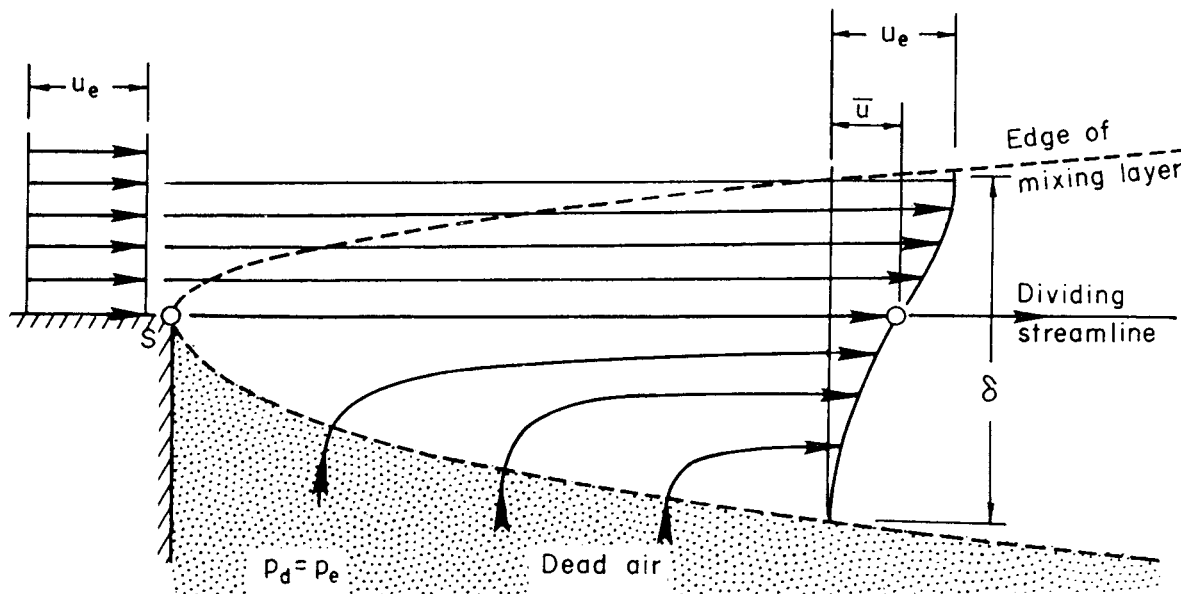
## Theoretical Analysis of Leading-Edge Separation

In order to establish a separated flow amenable to a simple theoretical calculation which requires no empirical knowledge, and which would thereby be helpful in analyzing the mechanism governing pressure in separated regions, a special type of model was investigated which produced leading-edge separation. The flow field is illustrated as (i) in sketch (c). This type of separation actually represents a limiting case both of separations behind a base (case (ii) in sketch (c)) and of separations in a compression corner (case (iii)), the limit being taken in each case as the distance  $x_s$ , from leading edge to separation, approaches zero. Leading-edge separation is relatively easy to analyze



because the complicated course of boundary-layer development in the region of pressure variation between the boundary-layer origin and its position of separation need not be considered. Also, calculations of the laminar mixing layer (SR in case (i)) already are available (ref. 27) for flows of this type wherein the boundary-layer thickness at separation,  $\delta_s$ , is zero, and the pressure is essentially constant. These theoretical calculations would apply directly, provided that transition is excluded from consideration.

Before developing the basic idea for calculating dead-air pressure, it is advantageous to outline the results of the laminar-mixing-layer theory which forms the basis for such calculations. Typical streamlines in the viscous mixing region and a representative velocity profile are depicted in sketch (d). A uniform stream of velocity  $u_e$ , Mach number  $M_e$ , and pressure  $p_e$  mixes with a dead-air region (of pressure  $p_d = p_e$ ) having dimensions large compared to the thickness  $\delta$  of the mixing layer.



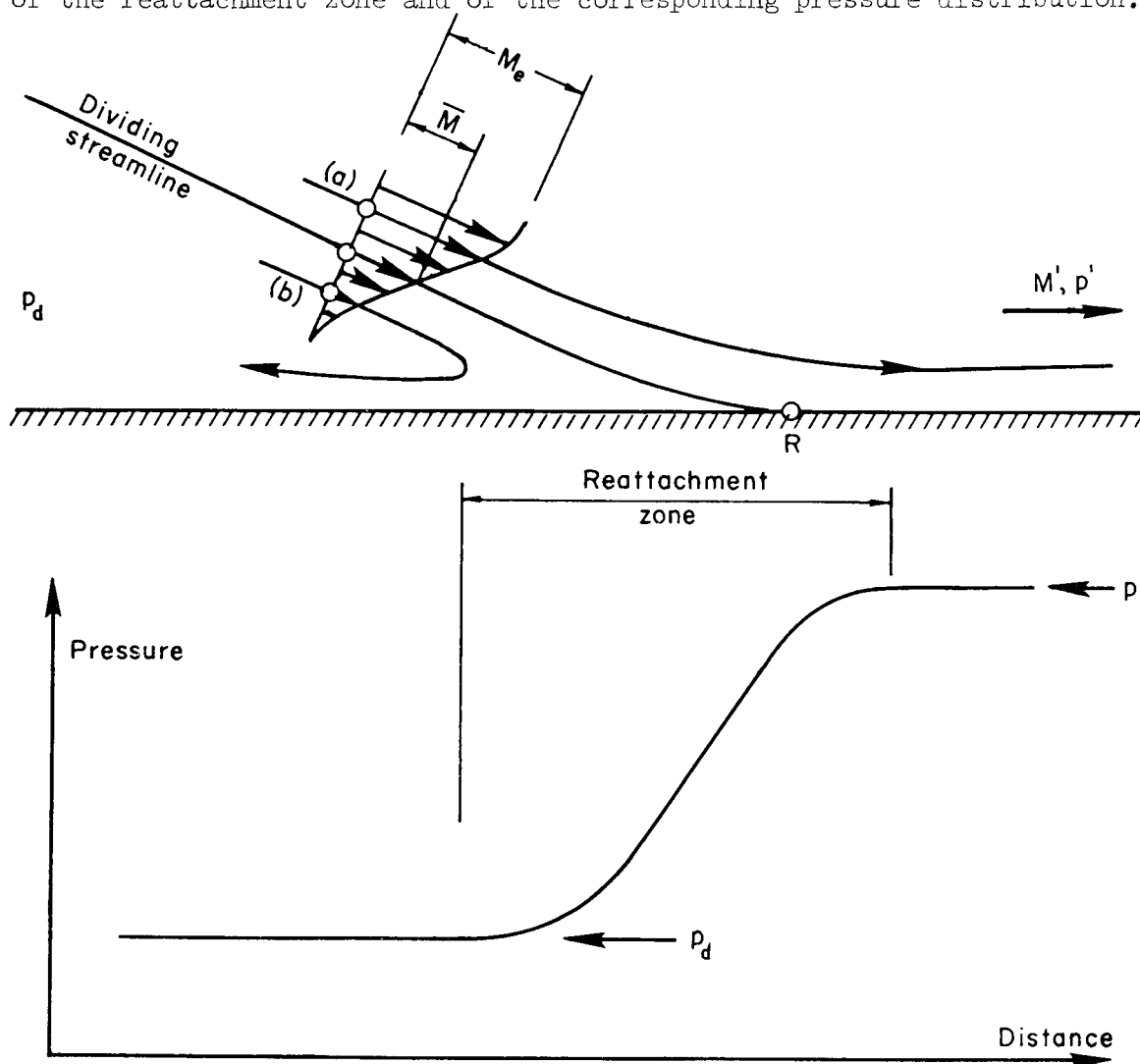
Sketch (d)

The mixing-layer thickness grows parabolically with distance from the origin of mixing just as a laminar boundary layer grows, but the rate of growth is roughly three times that of a corresponding boundary layer. The velocity profiles at different streamwise stations are similar; hence, the velocity ratio  $\bar{u}/u_e$  along the dividing streamline (see sketch (d)) does not change with Reynolds number or with distance from separation. An important consequence of this fact soon will appear. Moreover, this velocity ratio changes only slightly with variation in Mach number and in temperature-viscosity relationship. Computed values, reference 27, of  $\bar{u}/u_e$  are obtained by solving the familiar nonlinear differential equation of Blasius with unfamiliar boundary conditions. Some values are tabulated as follows:

Computed values of $\bar{u}_* \equiv \bar{u}/u_e$ (ref. 27)		
Mach number, $M_e$	for $\mu_* \sim T_*$	for $\mu_* = T_*^{0.76}$
0	0.587	0.587
1	.587	.588
2	.587	.591
3	.587	.593
5	.587	.597

In subsequent calculations, the ratio  $\bar{u}/u_e \equiv \bar{u}_*$  appears often. From the table, it is clear that the single value  $\bar{u}_* = 0.587$ , corresponding to the linear temperature-viscosity relationship, is a reasonable approximation for all conditions. It is noted that the tabulated values of  $\bar{u}_*$  involve no empirical constants and are exact within the framework of the boundary-layer equations.

In the calculation of dead-air pressure, the essential mechanism is considered to be a balance between mass flow scavenged from the dead-air region by the mixing layer and mass flow reversed back into the dead-air region by the pressure rise through the reattachment zone. For steady flow the dividing streamline at separation as calculated from mixing-layer theory must also be a dividing streamline at reattachment. If this were not the case air would be either continually removed from or continually injected into the dead-air region, and the scavenged mass flux would not balance the reversed mass flux. The pertinent conditions are illustrated by sketch (e) of the reattachment zone and of the corresponding pressure distribution.



Sketch (e)

In order for a particle along a streamline within the mixing layer to be able to overcome the pressure rise through the reattachment zone and to pass downstream, its total pressure  $p_t$  must be greater than the terminal static pressure  $p'$  at the end of the reattachment zone. In the sketch, particle (a) passes downstream in this manner. Particle (b), however, has a low velocity with corresponding low total pressure and is reversed before the pressure rises from  $p_d$  to  $p'$ . The dead-air pressure is determined by requiring<sup>6</sup> that the total pressure along the dividing streamline as it approaches the reattachment zone

$$\begin{aligned}\bar{p}_t &\equiv p_e \left( 1 + \frac{\gamma - 1}{2} \bar{M}^2 \right)^{\gamma/(\gamma-1)} \\ &= p_d \left( 1 + \frac{\gamma - 1}{2} \bar{M}^2 \right)^{\gamma/(\gamma-1)}\end{aligned}\quad (1)$$

be equal to the terminal static pressure  $p'$ . Thus the flow is divided into two regions: a viscous layer wherein the pressure is assumed to be constant, and a reattachment zone wherein the compression is assumed to be such that not much total pressure is lost along the dividing streamline. This yields

$$p_d = \frac{p'}{\left( 1 + \frac{\gamma - 1}{2} \bar{M}^2 \right)^{\gamma/(\gamma-1)}}\quad (2)$$

To cast this equation into a convenient form, it is necessary to relate  $\bar{M}$  to the terminal Mach number  $M'$ , or to the Mach number  $M_e$  along the outer edge of the mixing layer. From the mixing-layer calculations in which the Prandtl number is assumed to be unity,<sup>7</sup> the Mach number  $\bar{M}$  along the dividing streamline is related to the corresponding velocity  $\bar{u}$  by the Busemann isoenergetic integral of the energy equation if the dead-air temperature  $T_d$  is equal to the outer stream total temperature

<sup>6</sup>As is discussed later, essentially the same idea also has been employed effectively to calculate base pressure for turbulent boundary layers in a recent paper by Korst, Page, and Childs (ref. 16).

<sup>7</sup>As long as temperature profiles or heat-transfer characteristics are not considered, the assumption  $Pr = 1$  provides a satisfactory approximation for air. For example, at  $M' = 2$  the calculated value of  $p_d/p'$  for  $Pr = 0.72$  (the approximate value for air) is only 0.025 below that for  $Pr = 1$ . Consequently, the analysis for  $Pr = 0.72$  is not presented here as it is much more complex, and does not yield a final equation in closed form.

$$T_{te} \equiv T_e \left( 1 + \frac{\gamma - 1}{2} M_e^2 \right) \quad (3)$$

and by the Crocco integral if  $T_d$  differs from  $T_{te}$ . (See ref. 27.) At present, the dead-air temperature is considered equal to the recovery temperature ( $T_{te}$  for  $Pr = 1$ ), so that Busemann's integral for a perfect gas yields

$$\bar{M}^2 = \frac{(\bar{u}/u_e)^2 M_e^2}{1 + \frac{\gamma - 1}{2} M_e^2 \left( 1 - \frac{\bar{u}^2}{u_e^2} \right)} \quad (4)$$

Combining the above two equations gives an equation for dead-air pressure

$$\frac{p_d}{p'} = \left[ \frac{1 + (1 - \bar{u}_*^2) \frac{\gamma - 1}{2} M_e^2}{1 + \frac{\gamma - 1}{2} M_e^2} \right]^{\gamma/(\gamma-1)} \quad (5)$$

where  $\bar{u}_* = 0.587$ . Since  $\bar{u}_*$  is independent of Reynolds number,  $p_d$  also is independent of Reynolds number. Body shape affects  $p_d$  only through its effect on  $p'$ , the reference pressure.

A more convenient equation for  $p_d/p'$  can be obtained by expressing  $M_e$  in terms of the Mach number  $M'$  which exists just downstream of the reattachment zone. Because the outer edge of the laminar viscous layer curves smoothly, the trailing shock wave does not form within or near this viscous layer, and the flow along this outer edge is isentropic. Hence the values of  $M'$  and  $p'$  for two-dimensional flow are, in the terminology of reference 28, the same as the "equivalent free-stream conditions" approaching separation. For isentropic flow along the outer edge of the viscous layer

$$\frac{p'}{p_d} = \frac{p'}{p_e} = \left( \frac{1 + \frac{\gamma - 1}{2} M_e^2}{1 + \frac{\gamma - 1}{2} M'^2} \right)^{\gamma/(\gamma-1)} \quad (6)$$

By combining this with equation (5), there results

$$M'^2 = (1 - \bar{u}_*^2) M_e^2 \quad (7)$$

which yields the simple physical interpretation that the Mach number ratio across the laminar reattachment zone  $M'/M_e$  is a constant equal to  $(1 - \bar{u}_*^2)^{1/2} = 0.81$ . Equations (5) and (7) provide an explicit equation for dead-air pressure.

$$\frac{p_d}{p'} = \left[ \frac{1 + \frac{\gamma - 1}{2} M'^2}{1 + \frac{\gamma - 1}{2} \frac{M'^2}{(1 - \bar{u}_*^2)}} \right]^{\gamma/(\gamma-1)} \quad (8)$$

This equation was presented in reference 12 without derivation.

The foregoing theory also would apply to low-speed flow. By taking the limit of equation (8) as  $M' \rightarrow 0$ , there results

$$\begin{aligned} \frac{p_d - p'}{q'} &= \frac{p_d - p'}{\frac{\gamma}{2} p' M'^2} = \lim_{M' \rightarrow 0} \frac{2}{\gamma M'^2} \left\{ \left[ \frac{1 + \frac{\gamma - 1}{2} M'^2}{1 + \frac{\gamma - 1}{2} \frac{M'^2}{(1 - \bar{u}_*^2)}} \right]^{\gamma/(\gamma-1)} - 1 \right\} \\ &= - \frac{\bar{u}_*^2}{1 - \bar{u}_*^2} \quad (9) \end{aligned}$$

or, since  $\bar{u}_* = 0.587$ ,

$$\frac{p_d - p'}{\frac{1}{2} \rho u'^2} = -0.526 \quad (10)$$

Equation (10) for incompressible flow, just like equation (8) for compressible flow, would apply irrespective of the Reynolds number or the shape of the dead-air region.

The chief approximations and restricting assumptions made in the foregoing analysis should be noted. One essential approximation is that the compression is isentropic along the dividing streamline through the reattachment zone. Actually there would be some change in total pressure. Another approximation is that the dividing streamline terminates at a point where the pressure is  $p'$  rather than at the reattachment point where the pressure is  $p_r$ . Considering these two facts, the fundamental equation corresponding to equation (2) would be

$$p_d = \frac{p_r}{\eta \left( 1 + \frac{\gamma - 1}{2} M^2 \right)^{\gamma/(\gamma-1)}}$$

where  $\eta \equiv p_r/\bar{p}_t$  is a factor (not necessarily less than unity) representing the "efficiency" of compression relative to that of an isentropic process. It is evident that the use of  $p'$  in equation (2) - rather than the use of  $p_r/\eta$  - entails the disregard of two factors: the pressure rise downstream of reattachment and the viscous effects on the compression along the dividing streamline. Aside from these approximations it is to be remembered that the substitution  $\bar{u}_* = 0.587$  in equation (8) is restricted to steady, two-dimensional, pure laminar, separated flows having zero boundary-layer thickness at the separation point. If the boundary-layer thickness at separation were sizable, equation (8) would still apply, but the velocity profiles at different stations along the mixing layer would not be similar and  $\bar{u}_*$  would not be 0.587. The value of  $\bar{u}_*$  would have to be calculated by solving the partial differential equations of viscous flow for each case.

#### Experimental Results for Flows With Negligible Boundary-Layer Thickness at Separation

There are two features of the theory which can be tested quantitatively by present experiments: the absence of a dependence on Reynolds number, and the calculated dependence on Mach number. Three typical shadowgraphs from the experiments on leading-edge separation are shown in figure 26. Unless specified otherwise, the measurements correspond to an attached bow wave as in figures 26(a) and 26(c) rather than to a detached wave as in figure 26(b). In principle, equation (8) should apply equally well to both types of bow wave, as long as  $M'$  and  $p'$  are known. In figure 27 the measured variation of  $p_d/p'$  with Reynolds numbers at  $M' = 1.8$ , where the bow wave is detached, is compared with the value calculated from equation (8). There is seen to be no marked variation with Reynolds number. A similar absence of such variation also was observed at other Mach numbers investigated (1.3 to 2.0). It is apparent also from figure 27 that the calculated and experimental values agree rather well. Agreement of this nature extends to the other Mach numbers investigated, as is shown in figure 28 where the various data points plotted at each Mach number represent measurements at different Reynolds numbers. The several data points corresponding to a detached bow wave fall somewhat below the general trend, but not far below. Considering the simple nature of the theory and the fact that the calculation involves no empirical information or adjustable constants, the observed correspondence of theory and experiment is quite satisfactory. This establishes considerable confidence in the mechanism postulated for the calculations.



Although the present experiments did not include cases of pure laminar leading-edge separation at low speeds, some recent experiments of Roshko (ref. 29) approximate such conditions and provide further test of the theory. In order largely to avoid the usual unsteadiness of subsonic wakes, Roshko employed the splitter-plate technique. His data for cylinders and a flat plate normal to the flow are shown in figure 29. These data do not show any significant dependence either on body shape or Reynolds number. This lack of dependence is in accord with the theory. For quantitative comparison with the theory, it is assumed that  $p' = p_\infty$  which is indicated to be closely the case by several streamwise wake pressure distributions presented by Roshko. The agreement exhibited in figure 29 is quite good. The close agreement should be viewed with reservation inasmuch as the splitter plates did not always render the flow perfectly steady, and the mixing layer may not be entirely laminar. The Reynolds numbers are low enough though (5,000 to 17,000), so that extensive laminar flow would be expected along the mixing layer.

For incompressible flow, a comparison of the present theory can be made with the numerical solution to the full Navier-Stokes equations obtained by Kawaguti (ref. 30) for the steady flow over a circular cylinder at Reynolds number 40. His solution yields a value of -0.55 for the pressure coefficient at the rear of the cylinder. The corresponding experimental value (ref. 30) is about the same. This is surprisingly close to the value -0.526 obtained from the present theory.

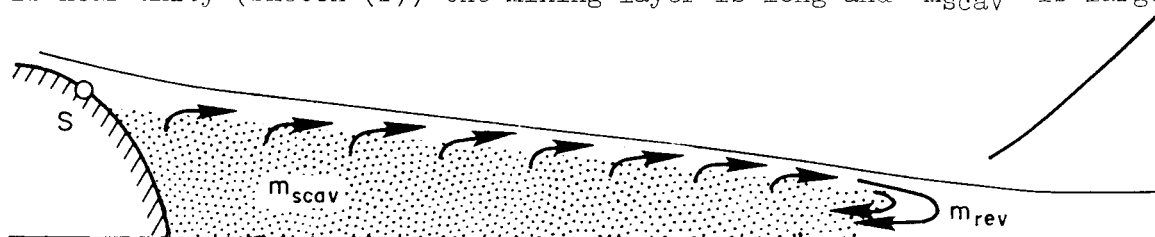
Additional evidence as to the soundness of the basic calculation method is provided by an independent theoretical analysis of Korst, Page, and Childs (ref. 31), which became available during preparation of reference 12. In their analysis, the same basic method is used for calculating dead-air pressure. Since they were concerned with fully turbulent flow rather than with pure laminar flow, their results complement the results of the present research. A direct comparison of their equations with equation (8) cannot be made since they did not present an explicit equation for dead-air pressure, but a comparison can be made of the various assumptions employed in the two analyses. Such comparison indicated only small, relatively unimportant differences in the two calculation methods. For calculating the velocity ratio  $\bar{u}_*$  along the dividing streamline they employed a simplified equation since the rigorous equations for turbulent flow are unsolvable. They obtain values of  $\bar{u}_*$  for turbulent flow ranging between 0.62 at zero Mach number to apparently 1.00 at infinite Mach number, whereas the corresponding value for laminar flow is 0.59, as noted earlier. They used the oblique shock equations across the reattachment region, whereas the isentropic equations are applied above for pure laminar flow. The dead-air pressure was calculated by equating the total pressure along the dividing streamline to the static pressure downstream; this is the essential idea common to both analyses. They obtain very close agreement with base pressure measurements for turbulent flow over a wide range of conditions, and this strengthens further the simple idea common to the two calculations.

It is noted that the values of  $p_d/p'$  in figure 28 for pure laminar separations with  $\delta_s \approx 0$  are not much greater than for turbulent base pressure measurements (ref. 17) with  $\delta_s \approx 0$ . From the theoretical viewpoint, this arises because the corresponding values of  $\bar{u}_x$  are not greatly different. Thus, a thin reattaching laminar layer can undergo a pressure rise comparable to that of a thin reattaching turbulent layer. Hence, with  $\delta_s \approx 0$ , the movement of transition from downstream to upstream of reattachment would not markedly alter such flows. Experiments confirm this. For example, at Reynolds numbers beyond those shown in figure 27, at which the separations on both CC35<sup>0</sup>-1 and CC35<sup>0</sup>-2 were transitional, the values of  $p_d/p'$  were only slightly smaller. On the other hand, when  $\delta_s$  is relatively large and  $\bar{u}_x$  for laminar flow is much less than 0.587 (corresponding to  $\delta_s = 0$ ), then the movement of transition from downstream to upstream of reattachment can markedly alter flow conditions.

In regard to theoretical methods for calculating dead-air pressure in a separated flow, it is noted that there is one aspect of the Crocco-Lees theory (ref. 9) which appears to be at variance with both the present theory and with certain experiments. This aspect is discussed in Appendix B.

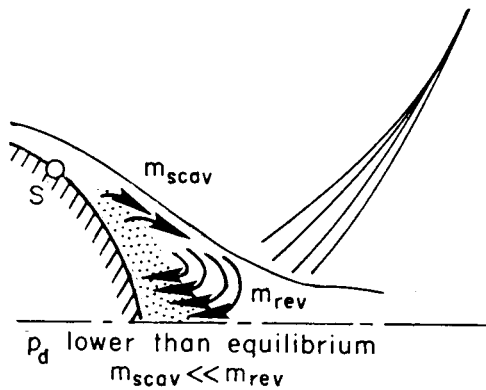
#### An Explanation of the Importance of Transition Location Relative to Reattachment

The basic mechanism assumed in the calculations of dead-air pressure appears well confirmed and thus can be used now to provide an explanation of one of the main experimental results described earlier, namely, an explanation of why a separated flow changes markedly when transition moves upstream of the reattachment position. For equilibrium, the basic requirement is that the mass flow scavenged ( $m_{scav}$ ) from the dead-air region by the mixing layer balance the mass flow reversed ( $m_{rev}$ ) by the pressure rise through the reattachment zone. This can be made clear by considering the variation of  $m_{scav}$  and  $m_{rev}$  with dead-air pressure for conditions removed from equilibrium. It is assumed temporarily that transition is slightly downstream of reattachment. For simplicity the external flow is assumed to be supersonic and two-dimensional. If  $p_d/p'$  is near unity (sketch (f)) the mixing layer is long and  $m_{scav}$  is large

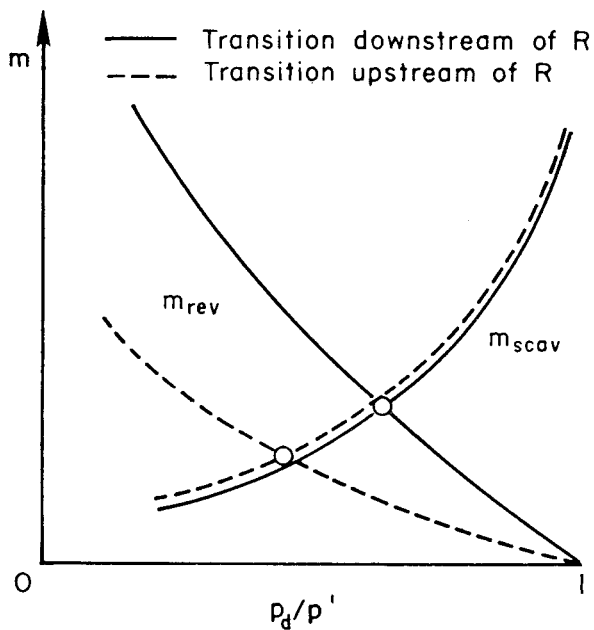


$p_d$  higher than equilibrium;  $m_{scav} \gg m_{rev}$

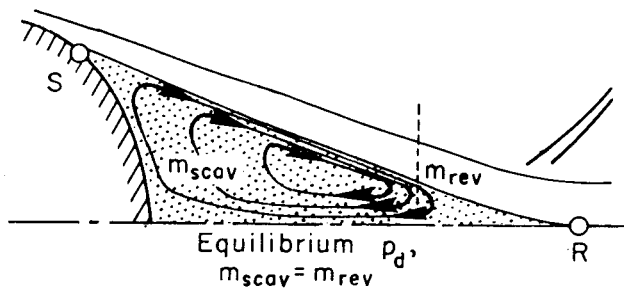
Sketch (f)



Sketch (g)



Sketch (h)



Sketch (i)

since it depends on the product  $\rho_e u_e$  as well as the length of mixing; but if  $p_d/p'$  is near zero (sketch (g)), the mixing layer is short,  $\rho_e u_e$  is small, and  $m_{scav}$  is small. Thus the scavenged air increases as  $p_d$  increases, as illustrated in sketch (h). The reversed flow, however, follows an opposite trend: if  $p_d/p'$  is near unity, the pressure rise  $p' - p_d$  is small and  $m_{rev}$  is small, but if  $p_d/p'$  is near zero the pressure rise is large and  $m_{rev}$  is large; hence,  $m_{rev}$  decreases as  $p_d$  increases, as illustrated in sketch (h). Intersection of the curves determines  $p_d$  for equilibrium (provided no mass flow is injected or removed by external means). If transition were now to move suddenly to a new position slightly upstream of reattachment, say, to the position of the dotted line in the lower right portion of sketch (i), then  $m_{scav}$  would be affected only negligibly since the distance between transition and reattachment is negligible compared to the distance between separation and transition. The new  $m_{scav}$  curve (dotted line in sketch (h)) would be close to the corresponding  $m_{scav}$  representing transition slightly downstream of reattachment (solid line in sketch (h)). Because of the turbulence, however, the  $m_{rev}$  curve would be much lower. The energy imparted to the low-velocity portion of the mixing layer would be much increased by the transport of eddies from the outer stream and this energizing process would greatly reduce the amount of air reversed for a given

pressure ratio  $p_d/p'$ . The new equilibrium dead-air pressure would be represented by the intersection of dotted curves in sketch (h). As transition moves upstream of reattachment, therefore, the ratio  $p_d/p'$  would be expected to decrease substantially. This agrees with the experimental observations described earlier, irrespective of whether the separation is induced by a base, compression corner, curved surface, step, or an incident shock wave.

Transition actually should begin to affect a separated flow as soon as it occurs in the small recompression region downstream of the reattachment point, even if negligible turbulence exists upstream of the reattachment point. In this region, where the pressure is between  $p_r$  and  $p'$ , the introduction of turbulence would permit a greater pressure rise  $p' - p_r$  to occur after the reattachment point, and this would change the dead-air pressure. Obviously transition is not a steady, point phenomenon, but is spread over some distance. Strictly speaking then, the pure laminar regime would end as soon as appreciable turbulence occurs in the downstream portion of a reattachment zone. A separated flow that is laminar only to the reattachment point could be quite different from the pure laminar type, which is defined as being laminar through the reattachment zone.

#### CHARACTERISTICS INDEPENDENT OF THE MODE OF INDUCING SEPARATION (FREE INTERACTIONS)

During the course of experimentation, it was observed that certain characteristics of separated flows did not depend on the object shape or on the mode of inducing separation. Similar observations previously have been made in the researches of Gadd, Holder, and Regan (ref. 15) and of Bogdonoff and Kepler (ref. 14). Any phenomenon near separation which is independent of object shape would not depend on geometric boundary conditions which describe the flow downstream, but would depend only on the simultaneous solution of the equations for flow in the boundary layer together with the equations for flow external to the boundary layer. Such flows that are free from direct influences of downstream geometry, and are free from complicating influences of the mode of inducing separation, arbitrarily will be termed "free interactions" for brevity. In the present section, some pressure distributions are compared first for a given body in supersonic and in subsonic flow. Free interaction is observed in supersonic separation, though not in subsonic separation on this body. A simple analysis is then made of the Reynolds number dependence of free interactions in supersonic flow. Subsequent to this analysis, various experimental results are presented and compared with the analysis where possible.

## Results for Various Separated Flows

Difference between subsonic and supersonic separations.- A fundamental difference between subsonic and supersonic separations can be seen from pressure distributions obtained at various Reynolds numbers in subsonic and in supersonic flow for a given model geometry. Measured distributions for laminar separation ahead of a  $10^\circ$  compression corner in subsonic flow are shown in figure 30(a) together with the calculated distribution that would exist in an incompressible, inviscid fluid (dotted line).<sup>8</sup> At these subsonic speeds ( $0.4 \leq M_\infty \leq 0.8$ ) variation in Reynolds number brings about only small changes in pressure distribution and no measurable change in pressure rise to separation ( $(p_s - p_o)/q_o$  is equal to  $0.08 \pm 0.005$  for all  $R$ ). Moreover, the distribution is roughly that which would exist in an inviscid flow, as represented by the dotted line. In contrast, the pressure distributions shown in figure 30(b), which also were obtained on a  $10^\circ$  compression corner, in the same wind tunnel, and over the same Reynolds number range, exhibit relatively large changes in pressure distribution as well as easily measurable changes in the position of and the pressure rise to separation. Further contrast is exhibited by the disparity between the measured distributions at supersonic speed and the calculated distribution for inviscid flow (a constant pressure with discontinuous jump as indicated by the dotted line). These data illustrate how the pressure distribution in subsonic flow near and upstream of separation is determined primarily by the inviscid flow pressure distribution about the object shape, and only secondarily by the Reynolds number dependent interaction between boundary layer and external flow; whereas, in supersonic flow, the pressure distribution near separation is determined primarily by a Reynolds number dependent interaction (free interaction) and only secondarily by the inviscid flow pressure distribution.

Only in supersonic flow were free interactions commonly observed in the present experiments. The fact that they were not observed at subsonic speed does not necessarily mean that free interactions cannot occur at such speeds. Lighthill (ref. 32) has made an analysis of the incompressible flow upstream of a step, which, in effect, assumes that the pressure distribution is determined by interaction of boundary layer and external flow. In the present experiments, relatively small steps were employed and the pressure distribution was determined primarily by the geometry of the model, and only secondarily by interaction phenomena. Consequently, the present experiments and Lighthill's theory for incompressible flow upstream of a step are not comparable. It would appear

---

<sup>8</sup>These calculations were made with small-disturbance theory by superimposing the appropriate thickness pressure distributions for wedges with the appropriate lift pressure distribution for an inclined flat plate.

---

possible, by using a step with larger ratio of step height to plate length, and a model with smaller leading-edge angle, that the pressure distribution in subsonic flow might be determined primarily by interaction phenomena and only secondarily by external constraints imposed through model geometry.

Simplified analysis for free-interaction regions.- If a pressure distribution is determined locally by free interaction of boundary layer and external supersonic flow, then the applicable equations are the momentum equation for steady flow in the viscous layer coupled with the following equation for external supersonic flow:

$$p = p_{\text{inviscid}} + \frac{\rho_e u_e^2}{\sqrt{M_e^2 - 1}} \frac{d\delta^*}{dx} \quad (11)$$

This equation would apply for both laminar and turbulent flow. For the special case of free interaction in regions where the inviscid pressure distribution (first term in eq. (11)) is constant or is small compared to the interaction term, certain information about the effects of Reynolds number can be extracted from order-of-magnitude arguments alone. Since the rate of boundary-layer growth is small, equation (11) for a free interaction is written as

$$\frac{p - p_o}{q_o} = \frac{2}{\sqrt{M_o^2 - 1}} \frac{d\delta^*}{dx} \quad (12)$$

The subscript  $o$  designates conditions at the beginning of interaction, that is, at the downstream-most point upstream of which the pressure is sensibly the same as the inviscid flow. If  $l_i$  is a length characteristic of the streamwise extent of free interaction, then order-of-magnitude considerations applied to equation (12) yield

$$\frac{p - p_o}{q_o} \sim \frac{\delta^*}{l_i \sqrt{M_o^2 - 1}} \quad (13)$$

Turning now to the equation for viscous flow, the usual boundary-layer momentum equation

$$\rho u \frac{\partial u}{\partial x} + \rho v \frac{\partial u}{\partial y} = - \frac{dp}{dx} + \frac{\partial \tau}{\partial y} \quad (14)$$

would apply provided the transverse pressure gradients within the layer are small compared to the streamwise gradients. This would be the case for laminar flow but is questionable for turbulent flow, since the detailed surveys of Bogdonoff and Kepler (ref. 14) at  $M_0 = 2.9$  reveal the average transverse gradient near separation to be larger, in fact, than the streamwise gradient. Since large curvature of streamlines is required for large transverse pressure gradients, and since the streamlines must approach straight lines in the immediate vicinity of a straight wall, it follows that only in the outer part of a boundary layer is the streamline curvature large near separation and the turbulent boundary-layer equations locally questionable. For this reason, the boundary-layer equation is applied at the wall where it becomes

$$\frac{dp}{dx} = \left( \frac{\partial \tau}{\partial y} \right)_w \quad (15)$$

This application places emphasis on the low-velocity part of the boundary layer, which appears desirable in analyzing the flow approaching separation. By applying order-of-magnitude considerations to equation (15) there results for constant Mach number  $M_0$ ,

$$\frac{p - p_0}{l_i} \sim \frac{\tau_w}{\delta} \sim \frac{\tau_{w0}}{\delta^*} \quad (16)$$

In this last step, the wall shear  $\tau_{w0}$  at the beginning of interaction has been taken as a measure of the variable wall shear  $\tau_w$ . What this and the previous steps amount to is the consideration of a family of similar flows having a fixed Mach number, but differing in the Reynolds number.

Mach number dependent factors have been omitted from equation (16) since they arise from density variations across the boundary layer and would be smoothly varying functions of  $M_0$ . In contrast, the factor  $(\sqrt{M_0^2 - 1})^{-1}$  arising from density variations along the edge of the boundary layer was retained in equation (13) since it is a singular function at  $M_0 = 1$ , and would be the dominant factor if  $M_0$  is only slightly greater than 1. By multiplying equations (16) and (13) there results

$$\frac{p - p_0}{q_0} \sim \left( \frac{\tau_{w0}}{q_0 \sqrt{M_0^2 - 1}} \right)^{1/2} \sim \frac{\sqrt{c_{f0}}}{(M_0^2 - 1)^{1/4}} \quad (17)$$

and, by dividing them, there results

$$\frac{\lambda_i}{\delta^*} \sim \left( \frac{q_0}{\tau_{w0} \sqrt{M_0^2 - 1}} \right)^{1/2} \sim \frac{1}{\sqrt{c_{f0}} (M_0^2 - 1)^{1/4}} \quad (18)$$

For convenience, the ratio  $\tilde{c}_f$  of skin friction at a given Reynolds number to skin friction at a Reynolds number of one million, is introduced

$$\tilde{c}_f \equiv \frac{c_{f0}}{(c_{f0})_{R=10^6}} \quad (19)$$

At constant  $M_0$ , then, equations (17) and (18) become

$$\frac{p - p_0}{p_0} \sim \sqrt{\tilde{c}_f} \quad (17a)$$

$$\frac{\lambda_i}{\delta^*} \sim \frac{1}{\sqrt{\tilde{c}_f}} \quad (18a)$$

Equation (17a) was originally presented in reference 12 without derivation. Curves of  $\sqrt{\tilde{c}_f}$  as a function of Reynolds number are shown in figure 31 for both laminar and turbulent boundary layers. The curves for laminar layers represent a  $(R_{X_0})^{-1/4}$  variation. The curves for turbulent layers represent the variation indicated by the Kármán-Schoenherr equation applicable to incompressible flow. A more accurate variation applicable to compressible turbulent flow is unknown at present.

The above results, as regards variation with Reynolds number, would apply to the pressure rise in either laminar or turbulent flow, provided the flow is determined by free interaction and not complicated by influences of downstream geometry; they would apply to the separation pressure rise  $(p_s - p_0)$ , to the peak or plateau pressure rise  $(p_p - p_0)$ , and to the over-all configuration pressure rise for incipient separation if such rises were determined by free interaction. For the particular case of pressure rise to a laminar separation point, equation (17a) agrees with the first analysis of this problem made by Lees (ref. 33), who obtained a  $R_{X_0}^{-1/4}$  variation. Subsequent analyses have obtained different results (e.g.,  $R_{X_0}^{-2/5}$  variation in ref. 34). It should be noted that the approach used above considers interaction of boundary layer and external flow to be the heart of the problem (as also is considered, though in more detail, in refs. 9, 33, and 35). Other approaches to the problem of boundary-layer separation in supersonic flow have disregarded this interaction (e.g., refs. 36, 37, and 38).



Experiments on effects of geometry, Reynolds number, and Mach number for laminar separation.- Inasmuch as the pressure distribution in laminar separation depends on Reynolds number and Mach number, it is necessary in assessing the effects of model geometry to hold these numbers fixed. Some pressure distributions obtained with four different models - a step, a compression corner, a curved surface, and an incident shock model - are presented in figure 32 for the fixed conditions of  $M_0 = 2.3$  and  $R_{X_0} = 0.20 \times 10^6$ . The dotted lines rising from terminal data points designate the eventual rise in pressure observed as the separated laminar layer either begins to reattach or to be affected by transition. It is evident that the pressure distribution does not depend significantly on the mode of inducing laminar separation (this independence will be further substantiated in subsequent figures). Such pressure distributions represent free interactions.

To assess the influence of Reynolds number, only the Mach number is held fixed. As is illustrated by the data in figure 33 for  $M_0 = 2.3$ , the curves for various Reynolds numbers are qualitatively similar but quantitatively quite different. An analogous spread of the curves was observed at the other supersonic Mach numbers investigated. For quantitative comparison with results from the simple dimensional analysis, the pressure at separation,  $p_s$ , and the plateau pressure,  $p_p$ , are plotted in figure 34 as a function of  $R_{X_0}$ . Common reference lines (dashed) are shown in both figures 34(a) and 34(b), from which it appears that both  $p_s$  and  $p_p$  approximately follow the same curve irrespective of whether transition is upstream or downstream of reattachment. Actually, when the type of separation changes from pure laminar to transitional, the distance  $x_0$  changes, but not the relation between pressure and  $R_{X_0}$ . It is noteworthy that the result from the simple order-of-magnitude analysis of free interactions ( $\Delta p/p_0 \sim \sqrt{c_f} \sim (R_{X_0})^{-1/4}$  for laminar flow) is in good agreement with the experimental data over the wide range of  $R_{X_0}$  investigated ( $1.2 \times 10^4$  to  $1.2 \times 10^6$ ).

Attention is called to several restrictions pertinent to the correlation of the laminar pressure rise data of figure 34. One such restriction is to two-dimensional flow. The oil-film technique revealed readily any flow that was not two-dimensional. Shadowgraphs likewise indicated occasional departures from two-dimensional flow. An example of this, where the shadowgraph indicates multiple separation lines (and the oil film similarly indicated lack of two-dimensionality) is shown in figure 35. The downstream geometry of this particular model was not uniform across the span. Under such conditions the peak-pressure rise was found to be less (up to about 30 percent) than for the correlated data of figure 34. In figure 36 some data are presented which illustrate an additional restriction for correlation of transitional data, namely, that transition not be too close to separation. In this figure the pressure at three different points is plotted for a step model: the pressure at separation  $p_s$ , the plateau pressure  $p_p$ , and the pressure

measured in the step corner  $p_c$ . At Reynolds numbers below  $10^5$  the separation is of the pure laminar type, since  $p_c$  does not differ from  $p_p$ ; both  $p_s - p_o$  and  $p_p - p_o$  are close to the dashed lines representing the correlation of figure 34. Between Reynolds numbers of  $10^5$  and about  $2.5 \times 10^5$ , the separation is of the transitional type since  $p_c$  rises well above  $p_p$ , but both  $p_s - p_o$  and  $p_p - p_o$  still follow the same  $R_{X_0}^{-1/4}$  variation as the correlated data. Above  $R_{X_0} = 2.5 \times 10^5$ , the separation type remains transitional, and the pressure distributions (not shown) reveal transition to be approaching closely the separation point. Both  $p_s$  and  $p_p$  depart from the correlated data above this Reynolds number. When transition is close to separation, the flow in the neighborhood of separation would not be expected to be steady and often was not. Examination of various data obtained in the present experiments revealed two sufficient conditions for correlation: (1) that the pressure distribution have a length of sensibly constant plateau pressure not less than about 1.5 times the length over which it takes the pressure to rise from  $p_o$  to  $p_p$ ; (2) that the disturbance due to transition - as measured by the magnitude of pressure rise above the laminar plateau - not exceed two to three times the pressure rise to the laminar plateau. No necessary conditions for correlation could be observed from the data obtained, but it would be expected from theoretical considerations that the laminar separation should be steady and have at least a short length of plateau. These various restrictions may account for the lack of consistency in some previous measurements of pressure rise in laminar separation.

The fact that  $(p_s - p_o)/p_o$  and  $(p_p - p_o)/p_o$  in laminar flow vary nearly as  $\sqrt{\tilde{c}_f} \sim R_{X_0}^{-1/4}$ , in agreement with the simple dimensional analysis, encourages a further test of the analysis by examination of the entire pressure distribution. In laminar flow  $\delta^* \sim x(R_X)^{-1/2} \sim x\tilde{c}_f$ , so that equation (18a) for the characteristic interaction distance  $l_i$  becomes

$$l_i \sim \frac{\delta^*}{\sqrt{\tilde{c}_f}} \sim \frac{x_0 \tilde{c}_f}{\sqrt{\tilde{c}_f}} \sim x_0 \sqrt{\tilde{c}_f} \quad (19)$$

Since  $\Delta p/p_o \sim \sqrt{\tilde{c}_f}$ , it follows that correlation of the pressure-distribution curves would be expected by plotting  $[(p - p_o)/p_o](\tilde{c}_f)^{-1/2}$  versus  $[(x - x_0)/x_0](\tilde{c}_f)^{-1/2}$ . A plot of the data in figure 33 using these special coordinates is shown in figure 37. Data from a compression corner, a curved surface, two steps, and an incident shock-wave-induced separation are included in this figure. The various pressure distributions in the special coordinate system appear independent of Reynolds number as well as independent of object shape in conformity with the simple analysis of free interactions.

In view of the correlation observed for Reynolds number effects on the pressure distribution in laminar separation, it follows that the essential results pertaining to pressure rises can be obtained from a plot of the quantities  $[(p_s - p_o)/p_o](\tilde{c}_f)^{-1/2}$  and  $[(p_p - p_o)/p_o](\tilde{c}_f)^{-1/2}$  as functions of Mach number. Such a plot is shown in figure 38. Near  $M_o = 1$  the singularity  $(M_o^2 - 1)^{-1/4}$  should dominate in equation (17) and the plateau pressure rise  $(p_p - p_o)/q_o$  should asymptotically follow a  $(M_o^2 - 1)^{-1/4}$  variation as  $M_o$  approaches unity. Hence  $(p_p - p_o)/p_o$  should asymptotically follow a  $M_o^2(M_o^2 - 1)^{-1/4}$  variation. The dotted line in figure 38 represents such a variation. Unfortunately the data do not extend to sufficiently low Mach numbers to test critically the predicted increase in pressure rise near  $M_o = 1$ . Over the range of data obtained, however, there is surprising consistency with the theoretical variation. This consistency accidentally extends to supersonic Mach numbers much higher than could be expected from a knowledge of the assumptions made in the analysis.

Experiments on effects of geometry, Reynolds number, and Mach number for turbulent separation.- The pressure distributions for turbulent separation over a step, a compression corner, and a curved surface are shown in figure 39(a). These distributions are for a constant Mach number of 2.0 and a constant Reynolds number of  $3.1 \times 10^6$ . Only the model shape differs for these three pressure distributions. The three curves are essentially the same up to the separation point, but beyond this they begin to depart from each other. It is evident also from figure 39(a) that the separated flow over a step is the only flow of those investigated which exhibits a definite peak in the pressure distribution within the separated region. Analogous results are presented in figure 39(b) for three similar configurations at a Mach number of 3.0. In this case the three curves practically coincide for a short distance downstream of separation, but do not coincide at the station where the peak in pressure occurs for the step. This result is similar to one of Bogdonoff and Kepler (ref. 14) who compared distributions for a step and a strong incident shock.

It is evident already that there is an essential difference between the qualitative characteristics of laminar separations and turbulent separations. Since turbulent separations follow a single curve only as far downstream as the separation point (or perhaps a little farther), only the flow up to the separation point would represent free interaction; the flow downstream of separation, and hence the peak pressure, would not. A possible exception might be the step which shows a definite peak pressure, but the other configurations investigated definitely do not represent free interaction phenomena downstream of the point of separation. In contrast, for laminar separations the pressure distribution well downstream of separation - including the plateau pressure - represents a free-interaction-type flow for all of the various configurations tested.

In order for the pressure distributions up to separation to represent a free interaction independent of the mode of inducing separation, it is necessary that the flow be steady. Actually, the curved-surface model (represented by diamond symbols) in figure 39(b) shows a little irregularity in pressure distribution which is attributed to a slight unsteadiness of the turbulent separation over this particular model. At Mach numbers lower than that represented in figure 39(b), the turbulent separation on this model was sufficiently unsteady to bring about both irregularities in pressure distribution as well as sizable departures from the mean curves representing steady turbulent separations. An example is illustrated in figure 40(a) which corresponds to a Mach number of 2.4. Since the turbulent separation on the curved-surface model is unsteady, the interaction takes place over a much larger streamwise distance than for the steady turbulent separations (on the step and the compression corner). Evidence of the unsteadiness is provided by the jagged pressure distribution and by the lack of sharpness in the corresponding shadowgraph in figure 40. It should be emphasized that most of the turbulent separations were relatively steady and unsteadiness to the degree illustrated in figure 40 was more an exception than a rule.

In assessing the effects of variation in Reynolds number on turbulent separations it is necessary to keep the model shape and the Mach number fixed. This requirement is unlike the case for laminar separation where only the Mach number needed to be held fixed. Some pressure distributions at various Reynolds numbers are shown in figure 41 for turbulent separation over a step at a Mach number of 2.0. The step model is selected inasmuch as it is the only model of those investigated which exhibits a clearly defined peak in pressure distribution. The data of figure 41 cover a range in Reynolds number corresponding to a variation by a factor of about 7 to 1, and show no large effect of such variation. These particular data do show, however, a small but consistent effect in the direction of decreasing peak pressure with increasing Reynolds number. The trend of decreasing pressure rise with increasing Reynolds number is the same as that predicted by the simple analysis for free interactions which indicates the pressure rise to vary as  $\sqrt{\tilde{c}_f}$ . A quantitative comparison of this theoretical result with the measurements on step model S-10 (trip 4) over the  $M_0$  range between 2.0 and 3.4 is presented in figure 42. The various lines shown represent a variation proportional to  $\sqrt{\tilde{c}_f}$  for turbulent flow. At a Mach number of 2.0 the data indicate somewhat less variation than  $\sqrt{\tilde{c}_f}$ , but at Mach numbers near 3 they indicate somewhat greater variation. Part of the experimental variation, particularly at the higher Mach numbers, is due to the fact that the effective origin of the turbulent boundary layer was not always at the boundary-layer trip. At low tunnel pressures, where the boundary-layer trip was not completely effective, transition could be anywhere between the trip and the beginning of separation. Data points taken under these conditions are represented by filled symbols in figure 42. For such points the Reynolds number plotted is somewhat greater than the effective Reynolds number of the turbulent boundary layer; consequently,

small arrows have been attached to these points, indicating the direction in which they would move if plotted as a function of the true effective Reynolds number. It is noted that these points with arrows correspond to a pure-laminar-type separation behind the base of the trip (as determined by measurements of base pressure on the trip) but to a fully turbulent separation over the step.

Although the data in figures 41 and 42 for model S-10 (trip 4) show a consistent decrease in peak pressure rise with increasing Reynolds number, not all of the data for turbulent separations showed this trend. Model S-5 (trip 2) revealed no appreciable variation in  $p_p - p_o$  with  $R_{x_o}$  over the range of  $M_o$  and  $R_{x_o}$  investigated. Similarly, Love (ref. 39) found no appreciable variation of  $p_p - p_o$  with  $R_{x_o}$  over a wide range of  $M_o$  and  $R_{x_o}$ . On the other hand, the several compression-corner and curved-surface models investigated herein exhibited essentially the same trend of decreasing  $p_p - p_o$  with increasing  $R_{x_o}$  as model S-10 (trip 4). The reason for these different results is not known. These apparent discrepancies, however, are consistent with the interpretation that the flow downstream of supersonic turbulent separation - unlike the flow downstream of supersonic laminar separation - usually is not a free-interaction phenomenon, and, thus should not necessarily follow a variation approximately as  $\sqrt{\tilde{c}_f}$ .

In figure 43 a comparison is made between the measured variation with Reynolds number of the pressure rise to a turbulent separation point and the theoretical variation predicted by the analysis. In this comparison, various model shapes are employed inasmuch as  $p_s - p_o$  (unlike  $p_p - p_o$ ) is regarded as being determined by free interaction. Experimental data of Gadd, Holder, and Regan (ref. 15) are shown in figure 43 by the dashed lines. The calculated trend proportional to  $\sqrt{\tilde{c}_f}$  is seen to be in approximate, though not accurate, agreement with the various measurements.

As a further test of the dimensional analysis for turbulent free interactions, pressure measurements can be plotted in coordinates which should make the pressure distributions - at least up to the separation point - independent of both Reynolds number and object shape. According to equations (17) and (18), the quantity  $[(p - p_o)/p_o]\tilde{c}_f^{-1/2}$  should be plotted against  $(x - x_o)/(\delta^*\tilde{c}_f^{-1/2})$ , just as in the case of laminar separation. In the absence of better information,  $\delta^*/x_o$  for turbulent flow is taken as proportional to  $\tilde{c}_f$ .<sup>9</sup> The appropriate longitudinal

---

<sup>9</sup>Approximate formulae for incompressible turbulent flow with 1/7-power velocity profile are:  $\delta^* \sim \delta \sim x(R_x)^{-1/5}$  and  $\tilde{c}_f \sim R_x^{-1/5}$ . These combine to give  $\delta^*/x \sim \tilde{c}_f$ . If more refined analysis is made, such as by combining the wall law with the velocity defect law for incompressible flow, then  $\delta^*/x$  is proportional to about the 1.2 power of  $\tilde{c}_f$ . At present, appropriate formulae for compressible flow are not accurately known; hence the simplest relation  $\delta^*/x \sim \tilde{c}_f$  is used.

coordinate is then  $[(x - x_0)/x_0]\tilde{c}_f^{-1/2}$ . A replot of the data of figure 41 in these appropriate coordinates is presented in figure 44. By observing that  $p/p_0$  is plotted in figure 41 and  $\Delta p/p_0$  in figure 44, it is seen that the small spread due to variation of Reynolds number is approximately, though not entirely, accounted for by the simple analysis. The same coordinates which correlate the pressure distribution in laminar separation up to the plateau pressure, also correlate reasonably well the turbulent separation data up to at least the separation pressure.

The effect of Mach number on the pressure rise to the turbulent separation point of various models is shown in figure 45. The pressure rise  $(p_s - p_0)/p_0$  is divided by  $\sqrt{\tilde{c}_f}$  as this would roughly account for the influence of Reynolds number. Data from various sources for steps, compression corners, and incident shock reflections are included in this figure. Two different techniques were employed in measuring the separation point as indicated in the figure legend. The Reynolds number range for the data from the present investigation is 0.3 to  $6.0 \times 10^6$ ; whereas for the data of Bogdonoff it is approximately 8 to  $36 \times 10^6$  and for the data of Gadd, Holder, and Regan it is from 2 to  $8 \times 10^6$ . Although there is considerable scatter in the measurements (since the pressure rise to the separation point is a difficult quantity to measure accurately), there is no systematic trend discernible between the various configurations. This is consistent with the view that the pressure rise to a separation point in supersonic turbulent flow is a free-interaction phenomenon and should be independent of the mode of inducing separation.

The effect of Mach number on peak pressure rise for steps in turbulent flow is shown in figure 46. Data from experiments of Bogdonoff (ref. 13) and Love (ref. 39) are included in this figure. Two extremes are represented for Bogdonoff's data at each Mach number; they correspond to the smallest and largest step heights used in his experiments. At Mach numbers above about 2.6 the present measurements for S-6 (trip 1) show considerably higher values of  $p_p - p_0$  than do the measurements of Bogdonoff and Love. The large spread of data, as represented by the the crosshatched area, is attributed primarily to the effect of boundary-layer thickness on  $p_p - p_0$ . Models for which the step height  $h$  is considerably smaller than  $\delta_0$  (e.g., the lower data points of Bogdonoff in fig. 46) yield peak pressure values only slightly greater than the separation pressure, whereas the model with the largest ratio  $h/\delta$  (model S-6 with trip 1 for which  $h/\delta \approx 6$ ) yields the largest values for peak pressure. The upper limit of Bogdonoff's data corresponds to an intermediate case of  $h/\delta \approx 2$ .

## CONCLUSIONS

The conclusions which follow were drawn mainly from experiments with boundary layers of essentially constant pressure preceding a two-dimensional separated region. Sufficiently wide variations in model geometry (steps, bases, compression corners, curved surfaces, shock reflections) were covered to regard the conclusions as rather general, although some of these conclusions may not apply for an initial boundary-layer history of strongly rising or falling pressure.

1. For a given model shape, the location of transition relative to the reattachment and separation positions is dominant in controlling the characteristic features of pressure distribution irrespective of Mach number and Reynolds number. This dominance leads to classification of each separated flow into one of three types: pure laminar, transitional, and turbulent.
2. Pure-laminar separations (transition downstream of reattachment zone) were steady in a supersonic stream and depended only to a relatively small extent on Reynolds number. The dead-air pressure for pure-laminar separations having negligible boundary-layer thickness at separation can be calculated from a simple theory involving no empirical information; the theory is applicable to both subsonic and supersonic flow.
3. Transitional separations (transition between separation and reattachment) generally were unsteady and often depended markedly on Reynolds number. In transitional separations an abrupt pressure rise often occurs at the location of transition, especially when transition is only a short distance upstream of reattachment.
4. Most supersonic turbulent separations (transition upstream of separation) were relatively steady compared to transitional separation; all depended only to a minor extent on Reynolds number.
5. The stability of a separated laminar mixing layer increases markedly with an increase in Mach number. As a result, pure laminar separations, which are uncommon at subsonic speed, may become of some practical interest at hypersonic speeds. Because of this marked increase in stability, laminar separations warrant additional research in hypersonic flow.
6. In a region where boundary-layer and external flow interact freely, a simple analysis indicates that pressure rises vary as the square root of the skin friction. Experiments at supersonic speed substantiated this result accurately for laminar separation, and approximately for turbulent separation.

7. The pressure rise to separation is independent of the mode of inducing separation for either laminar or turbulent separation in supersonic flow. The plateau pressure rise in laminar separation is similarly independent, but the peak pressure rise in turbulent separation depends significantly on model geometry.

Ames Aeronautical Laboratory  
National Advisory Committee for Aeronautics  
Moffett Field, Calif., Nov. 29, 1956



## APPENDIX A

## ANOMALOUS OIL-FILM OBSERVATIONS

When the oil-film technique was used, two threadlike lines of accumulation sometimes occurred simultaneously. They were never observed in laminar separation, but only in turbulent separation, and only over a certain Mach number range. Both lines of accumulation were stable, repeatable, and normal to the stream direction of flow. They were displaced streamwise a distance equivalent to several boundary-layer thicknesses. Depending upon test conditions, the downstream line could appear by itself, the two lines could appear simultaneously, or the upstream line could appear by itself. The upstream line corresponded to a pressure rise of about  $0.3 p_0$ , whereas the downstream line corresponded to between  $0.6 p_0$  and  $1.0 p_0$  rise, depending on the Mach number. Comparable measurements of Bogdonoff and of Gadd, derived from a different technique of location separation (near-surface pitot-pressure surveys) corresponded to the downstream line. To determine directly whether the two techniques inherently produce different results, Professor S. M. Bogdonoff volunteered cooperation by trying the oil-film technique with the Princeton apparatus on which the pitot-pressure surveys previously had been made. He immediately confirmed his earlier result on pressure rise to separation at  $M_0 = 2.9$  (corresponding to the downstream line in the present experiments), and did not find any evidence of a second line. Although this left unexplained the simultaneous occurrence of two lines, it did remove suspicion of excessive probe interference and place suspicion on the physical significance of the upstream line of oil accumulation. It appeared possible that the upstream line did not accumulate at a separation position, but actually represented a second, stable, equilibrium position, due to wind forces acting downstream and buoyancy forces acting upstream. Sizable buoyancy forces arise from the large streamwise pressure gradients near turbulent separation. (The gradients near laminar separation are an order of magnitude smaller.)

By regarding the thread of oil as a cylinder of fixed dimensions in a wind stream of density  $\rho_w$  and velocity proportional to  $(\partial u/\partial y)_w$ , the drag per unit span would be proportional to  $\rho_w (\partial u/\partial y)_w^2$ . The upstream-acting buoyancy force would be proportional to  $(dp/dx) \sim (p_0/\delta_0)$ , so that

$$\hat{r} \equiv \frac{\text{buoyancy forces}}{\text{wind forces}} \sim \frac{p_0}{(\delta_0)\rho_w \left(\frac{\partial u}{\partial y}\right)_w^2} \sim \frac{p_0}{\left(\frac{x_0}{R_{x_0}^{1/5}}\right)\rho_w \left(\frac{c_f \rho_0 u_0^2}{\mu_w}\right)^2}$$

or, since  $\rho_w = \rho_e T_e / T_w \sim \rho_o T_o$  (approximately),

$$\hat{r} \sim \frac{R_{x_o}^{1/5}}{x_o \rho_o^2 c_f^2 u_o^4}$$

For fixed  $M_o$  and  $x_o$ ,  $\hat{r} \sim p_o^{1/5} / p_o^2 (p_o^{-1/5})^2 \sim p_o^{-7/5}$ . From this brief analysis three inferences can be drawn: first, an increase in tunnel pressure for fixed  $M_o$  and  $x$  should decrease the importance of buoyancy forces; second, an increase in model length for fixed  $M_o$  and  $p_o$  should decrease the importance of buoyancy forces since  $\hat{r} \sim x_o^{1/5} / x_o \sim x_o^{-4/5}$ ; third, for fixed  $x_o$  and  $p_o$ , the variation of  $\hat{r}$  with an increase in  $M_o$  is dominated by the decrease in  $\rho_o$  and  $c_f$ ; hence an increase in Mach number should increase the importance of buoyancy forces. In view of these inferred trends, a special model (S-5 with trip 2) having double the length  $x_o$  was constructed. Whereas the regular models exhibited the upstream line above about  $M_o = 1.9$ , the larger model exhibited such lines above about  $M_o = 2.5$ . This is consistent with both the second and third inferences above. It was found also that increasing tunnel pressure caused the upstream line to disappear. This is consistent with the first inference. Consequently, it is deduced that the upstream line, which corresponded to a pressure rise of  $\Delta p / p_o = 0.3 \pm 0.1$ , is not a separation line but represents a second position for stable equilibrium of buoyancy forces and wind forces.

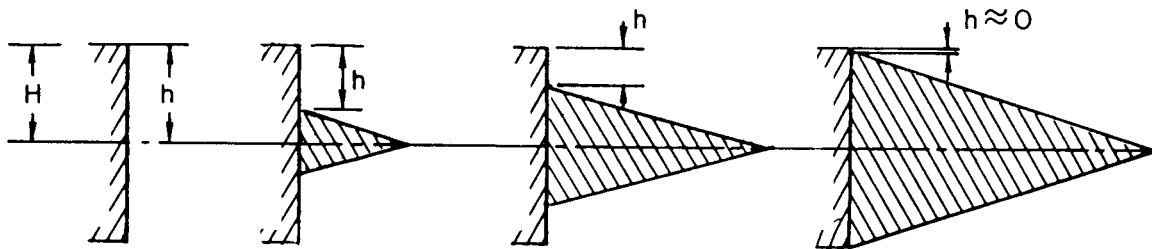
## APPENDIX B

SPECIAL EXPERIMENTS PERTAINING TO  
THE CROCCO-LEES THEORY

The Crocco-Lees theory (ref. 9) is unusually broad in scope, covering laminar-, transitional-, and turbulent-type separations. Because of this extensiveness, many untested approximations are introduced in their analysis where appropriate experimental data are missing and cannot provide a guide. Also, because of the broad scope, it is important to supplement this theory wherever possible with pertinent experimental information. The present experiments suggest a way in which the Crocco-Lees theory for base pressure might be improved. This possible improvement may have no bearing, however, on the Crocco-Lees theory for other types of separation.

In the Crocco-Lees analysis the wake thickness is an important variable appearing throughout their analysis; it determines, among other things, the initial condition for integration of their differential equation which governs the dead-air pressure. On the other hand, the theory of this report indicates that the total wake thickness of a separated region would not influence the dead-air pressure.

The special experiments designed to provide a decisive test of the importance of the thickness of wake were conducted during the initial experiments (1953) on models with triangular inserts as is illustrated in sketch (j). The two-dimensional channel apparatus was employed.



Sketch (j)

The experimental test conditions were especially selected to be in a Reynolds number range wherein the separation was of the transitional type, and wherein the Crocco-Lees theory would indicate the dead-air pressure to be sensitive to changes in the initial wake thickness  $h + \delta$ . If the total thickness of wake were dominant in determining base pressure, then the dead-air pressure for a fixed Reynolds number  $R$  (based on the chord length  $L$  of the airfoil) should correlate roughly as a function of the parameter  $h/\delta$ , or as a function of the equivalent parameter

$L/(h\sqrt{R})$  where  $L$  is the model length. On the other hand, if the thickness of wake is totally unimportant, it would be expected that the dead-air pressure would be unaffected by the triangular-shaped inserts and would correlate much better when plotted as a function of  $H/\delta$ , or of the equivalent parameter  $L/(H\sqrt{R})$ . The experimental data plotted in figure 47 are definitive in showing that  $H$  is the essential characteristic length in the problem; and hence that the total wake thickness is not important in determining base pressure. It is believed that in the Crocco-Lees theory the base height should more appropriately be introduced in a way which determines the length of mixing layer, rather than in a way which determines the initial thickness of the wake.

## REFERENCES

1. Prandtl, L.: Der Luftwiderstand von Kugeln: Nachrichten von der Koniglichen Gessellschaft der Wissenschaften zu Gottingen Math. Phys. Klass, 1914, pp. 177-190.
2. Eiffel, G.: Sur la resistance des spheres dans l'air en mouvement. Comptes Rendus de l'Academie de Sciences, vol. 155, 1912, pp. 1597-1599.
3. Liepmann, H. W.: The Interaction Between Boundary Layer and Shock Waves in Transonic Flow. Jour. Aero. Sci., vol. 13, no. 12, Dec. 1946, pp. 623-637.
4. Ackeret, J., Feldmann, F., and Rott, N.: Investigations of Compression Shocks and Boundary Layers in Gases Moving at High Speed. NACA TM 1113, 1947.
5. Chapman, Dean R., and Perkins, Edward W.: Experimental Investigation of the Effects of Viscosity on the Drag of Bodies of Revolution at a Mach Number of 1.5. NACA RM A7A31a, 1947. (Also available as NACA Rep. 1036)
6. Hankins, G. A.: Experiments of Reynolds Number Effect on Projectiles at Supersonic Speeds. Rep. Engr. Div. N.P.L. No. 221/46, as reported in: Howarth, L., ed., Modern Developments in Fluid Mechanics, High Speed Flow, vol. II, p. 702, Oxford Press, 1953.
7. Schiller, L., and Linke, W.: Pressure and Frictional Resistance of a Cylinder at Reynolds Numbers 5,000 to 40,000. NACA TM 715, 1933.
8. Gault, Donald E.: An Experimental Investigation of Regions of Separated Laminar Flow. NACA TN 3505, 1955.
9. Crocco, Luigi, and Lees, Lester: A Mixing Theory for the Interaction Between Dissipative Flows and Nearly Isentropic Streams. Jour. Aero. Sci., vol. 19, no. 10, Oct. 1952, pp. 649-676.
10. Liepmann, Hans W., and Fila, Gertrude H.: Investigations of Effects of Surface Temperature and Single Roughness Elements on Boundary-Layer Transition. NACA Rep. 890, 1947.
11. Oswatitsch, K., and Wieghardt, K.: Theoretical Analysis of Stationary Potential Flows and Boundary Layers at High Speed. NACA TM 1189, 1948.
12. Chapman, Dean R., Kuehn, Donald M., and Larson, Howard K.: Preliminary Report on a Study of Separated Flows in Supersonic and Subsonic Streams. NACA RM A55L14, 1956.

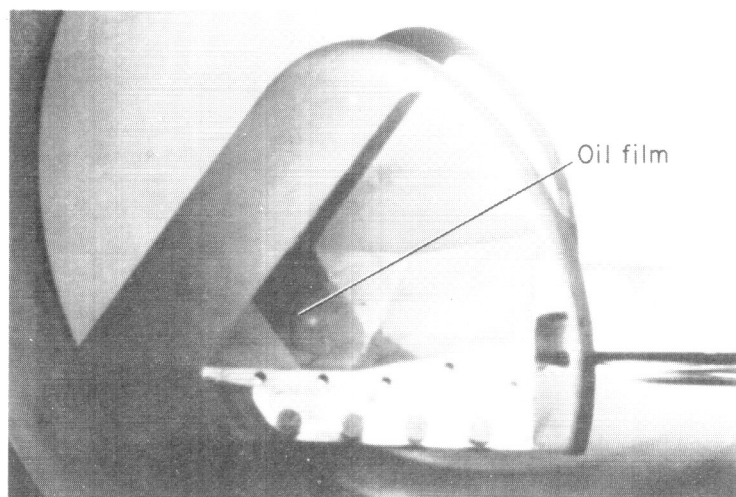
13. Bogdonoff, Seymour M.: Some Experimental Studies of the Separation of Supersonic Turbulent Boundary Layers. Papers presented at the Heat Transfer and Fluid Mechanics Institute, Univ. of Calif. at Los Angeles, June 23-25, 1955, sec. V, pp. 1-23.
14. Bogdonoff, S. M., and Kepler, C. E.: Separation of a Supersonic Turbulent Boundary Layer. Rep. 249, Princeton Univ., Dept. Aero. Engr., Jan. 1954.
15. Gadd, G. E., Holder, D. W., and Regan, J. D.: An Experimental Investigation of the Interaction Between Shock Waves and Boundary Layers. Proc. Roy. Soc. of London, ser. A, vol. 226, 1954, pp. 227-253.
16. Korst, H. H., Page, R. H., and Childs, M. E.: Compressible Two-Dimensional Jet Mixing at Constant Pressure. TN 392-1, Univ. of Ill., Engr. Exp. Sta., Mech. Engr. Dept., 1954.
17. Chapman, Dean R., Wimbrow, William R., and Kester, Robert H.: Experimental Investigation of Base Pressure on Blunt-Trailing-Edge Wings at Supersonic Velocities. NACA TN 2611, 1952.
18. Pearcey, H. H.: The Indication of Boundary-Layer Transition on Aerofoils in the N.P.L. 20 in. x 8 in. High Speed Wind Tunnel. British A.R.C. 11,991, Dec. 14, 1948.
19. Winter, K. G., Scott-Wilson, J. B., and Davies, F. V.: Methods of Determination and of Fixing Boundary Layer Transition on Wind Tunnel Models at Supersonic Speeds. British R.A.E. TN Aero 2341, Sept. 1954.
20. Reller, John O., Jr., and Hamaker, Frank M.: An Experimental Investigation of the Base Pressure Characteristics of Nonlifting Bodies of Revolution at Mach Numbers From 2.73 to 4.98. NACA TN 3393, 1955. (Formerly NACA RM A52E20)
21. Fage, A.: On Reynolds Numbers of Transition. R.&M. 1765, British A.R.C., June 6, 1936.
22. Bursnall, William J., and Loftin, Laurence K.: Experimental Investigation of the Pressure Distribution About a Yawed Circular Cylinder in the Critical Reynolds Number Range. NACA TN 2463, 1951.
23. Lange, Roy H.: Present Status of Information Relative to the Prediction of Shock-Induced Boundary-Layer Separation. NACA TN 3065, 1954.

24. Kavanau, L. L.: Results of Some Base Pressure Experiments at Intermediate Reynolds Numbers with  $M = 2.84$ . TR No. HE-150-117, Univ. of Calif., Inst. of Engr. Res., Oct. 22, 1953.
25. Lin, C. C.: On the Stability of the Laminar Mixing Region Between Two Parallel Streams in a Gas. NACA TN 2887, 1953.
26. Chapman, Dean R.: A Theoretical Analysis of Heat Transfer in Regions of Separated Flow. NACA TN 3792, 1956.
27. Chapman, Dean R.: Laminar Mixing of a Compressible Fluid. NACA Rep. 958, 1950. (Formerly NACA TN 1800)
28. Chapman, Dean R.: An Analysis of Base Pressure at Supersonic Velocities and Comparison With Experiment. NACA Rep. 1051, 1951.
29. Roshko, Anatol: On the Drag and Shedding Frequency of Two-Dimensional Bluff Bodies. NACA TN 3169, 1954.
30. Kawaguti, Mitutosi: Numerical Solution of the Navier-Stokes Equations for the Flow Around a Circular Cylinder at Reynolds Number 40. Phys. Soc. of Japan Journal, vol. 8, no. 6, Nov.-Dec. 1953, pp. 747-757.
31. Korst, H. H., Page, R. H., and Childs, M. E.: A Theory for Base Pressures in Transonic and Supersonic Flow. TN 392-2, Univ. of Ill., Engr. Exp. Sta., Mech. Engr. Dept., Mar. 1955.
32. Lighthill, M. J.: On Boundary Layers and Upstream Influence. I. A Comparison Between Subsonic and Supersonic Flows. Proc. Roy. Soc. of London, ser. A., vol. 217, no. 1130, 1953.
33. Lees, Lester: Interaction Between the Laminar Boundary Layer Over a Plane Surface and an Incident Oblique Shock Wave. Rep. 143, Princeton Univ., Aero. Engr. Lab., Jan. 24, 1949.
34. Stewartson, K.: On the Interaction Between Shock Waves and Boundary Layers. Proc. Camb. Phil. Soc., vol. 47, pt. 3, July 1951, pp. 545-553.
35. Gadd, G. E. Interactions Between Wholly Laminar or Wholly Turbulent Boundary Layers and Shock Waves Strong Enough to Cause Separation. Jour. Aero. Sci., vol. 20, no. 11, Nov. 1953, pp. 729-739.
36. Tyler, Robert D., and Shapiro, Ascher H.: Pressure Rise Required for Separation in Interaction Between Turbulent Boundary Layer and Shock Wave. Jour. Aero. Sci., vol. 20, no. 12, Dec. 1953, pp. 858-860.

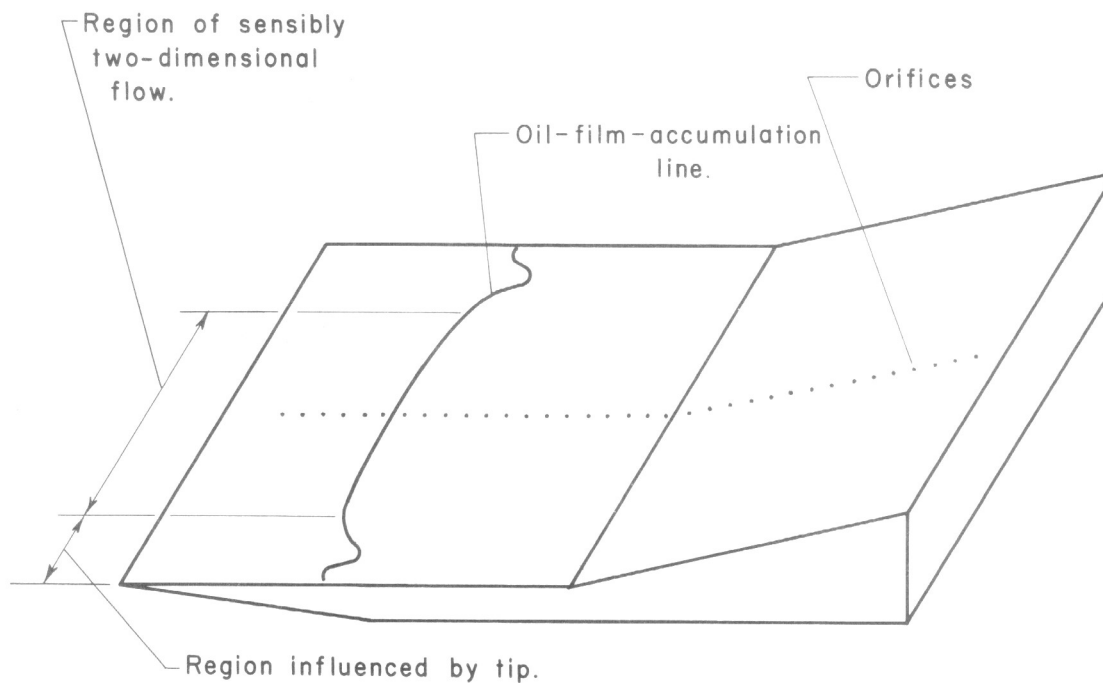
37. Mager, Artur: Prediction of Shock-Induced Turbulent Boundary-Layer Separation. Jour. Aero. Sci., vol. 22, no. 3, Mar. 1955, pp. 201-202.
38. Schuh, H.: On Determining Turbulent Boundary-Layer Separation in Incompressible and Compressible Flow. Jour. Aero. Sci., vol. 22, no. 5, May 1955, pp. 343-345.
39. Love, Eugene S.: Pressure Rise Associated With Shock-Induced Boundary-Layer Separation. NACA TN 3601, 1955.





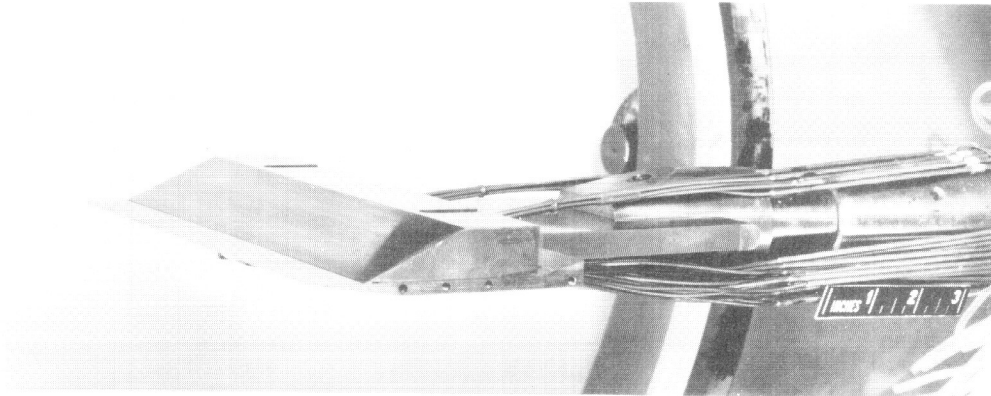


(a) Photograph showing oil film accumulation taken during a run of model CCIO<sup>o</sup>-2 with end plates



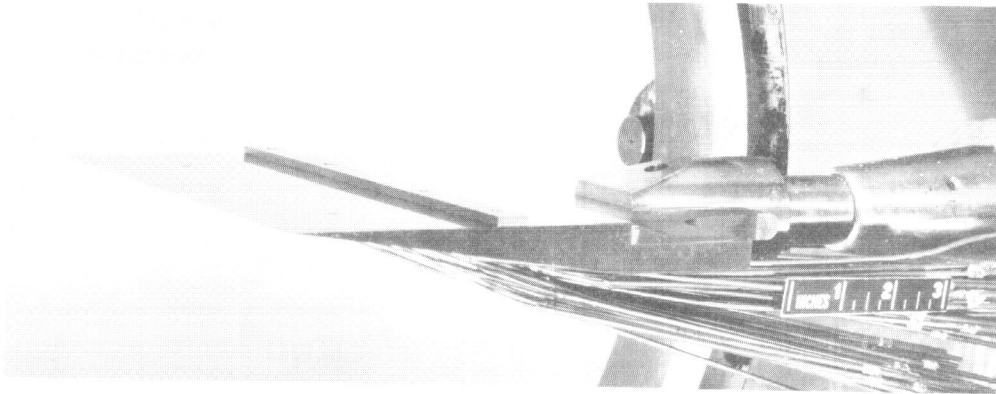
(b) Sketch of typical oil-film-accumulation line.

Figure 1.- Typical model installations.



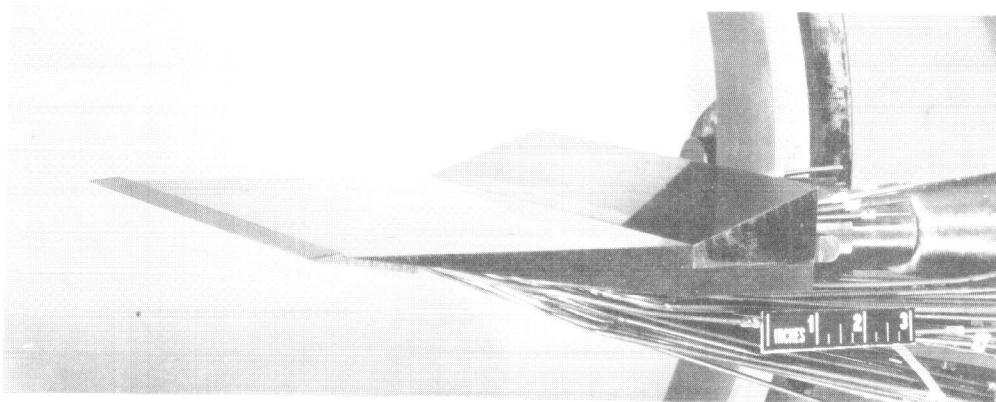
(c) Model CC25°-2

A-21256



(d) Model S-4

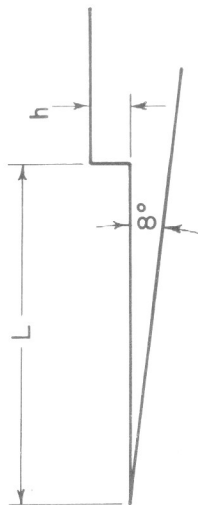
A-21255



(e) Model CC25°-5 (trip 4)

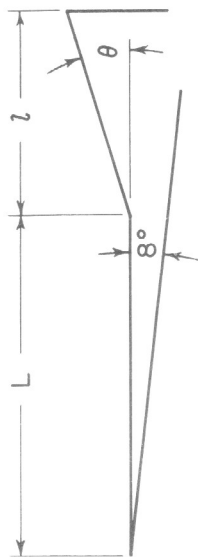
A-21252

Figure 1. — Concluded.



Model designation	L (inches)	h (inches)	$\frac{L}{h}$
S-1	1.14	0.041	27.8
S-2	6.55	0.237	27.7
S-3	2.60	0.094	27.7
S-4	2.73	0.150	18.2
S-5	5.14	0.150	34.3
S-6	2.73	0.300	9.1
S-7	4.70	0.100	47.0
S-8	4.43	0.040	110.8
S-9	3.30	0.150	22.0
S-10	6.05	0.200	30.3

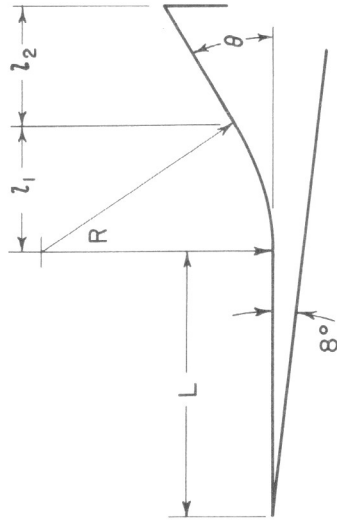
(a) Step models



Model designation	$\theta$ (degrees)	L (inches)	l (inches)
CC10°-1	10	0.75	2.50
CC10°-2	10	2.25	1.75
CC10°-3	10	2.60	1.50
CC10°-4	10	5.00	2.00
CC15°-1	15	0.35	1.10
CC15°-2	15	0.76	1.10
CC15°-3	15	1.72	1.10
CC20°-1	20	0.34	0.80
CC20°-2	20	5.50	2.00
CC25°-1	25	0.28	1.40
CC25°-2	25	0.76	1.40
CC25°-3	25	3.34	0.66
CC25°-4	25	5.00	2.00
CC25°-5	25	5.50	2.00
CC35°-1	35	0.056	2.70
CC35°-2	35	0.166	2.70

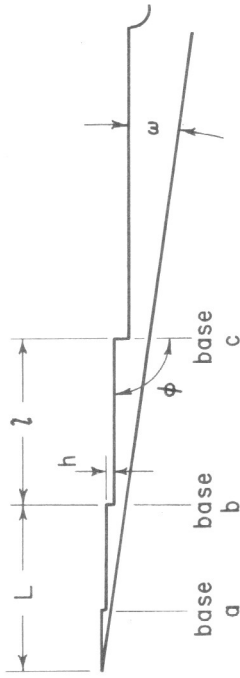
(b) Compression corners

Figure 2.-Model configurations and dimensions.



Model designation (degrees)	$\theta$ (degrees)	L (inches)	R (inches)	$z_1$ (inches)	$z_2$ (inches)
CS15°-1	15	5.00	3.25	0.84	1.16
CS20°-1	20	5.50	2.00	0.68	1.32
CS25°-1	25	2.63	3.25	1.37	0
CS30°-1	30	5.50	1.00	0.50	1.50

(c) Curved surfaces

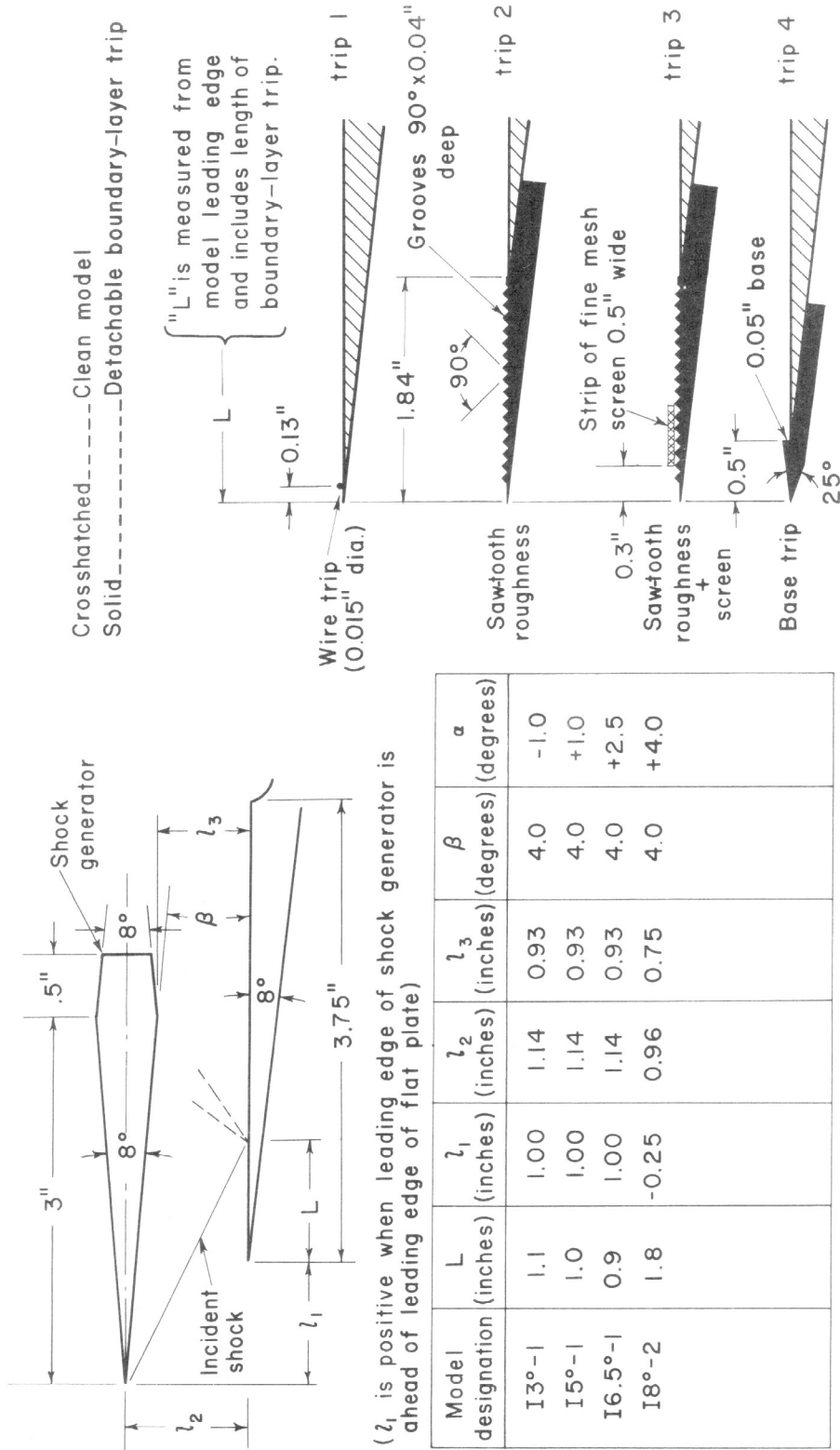


One model has 3 bases in series--others have only a single base. "L" is always measured from the model leading edge to the particular base; "z" is always the length of the unbroken surface downstream of the particular base.

Model designation	L (inches)	h (inches)	z (inches)	$\omega$ (degrees)	$\phi$ (degrees)
B-1-a	0.20	0.01	0.47	8	90
-b	0.67	0.03	1.61	8	90
-c	2.28	0.10	2.22	8	90
B-2	2.00	0.10	2.22	8	90
B-3	0.20	0.09	3.30	35	145

(d) Base models

Figure 2.—Continued.



(e) Incident shock models

(f) Boundary-layer trips

Figure 2.—Concluded.

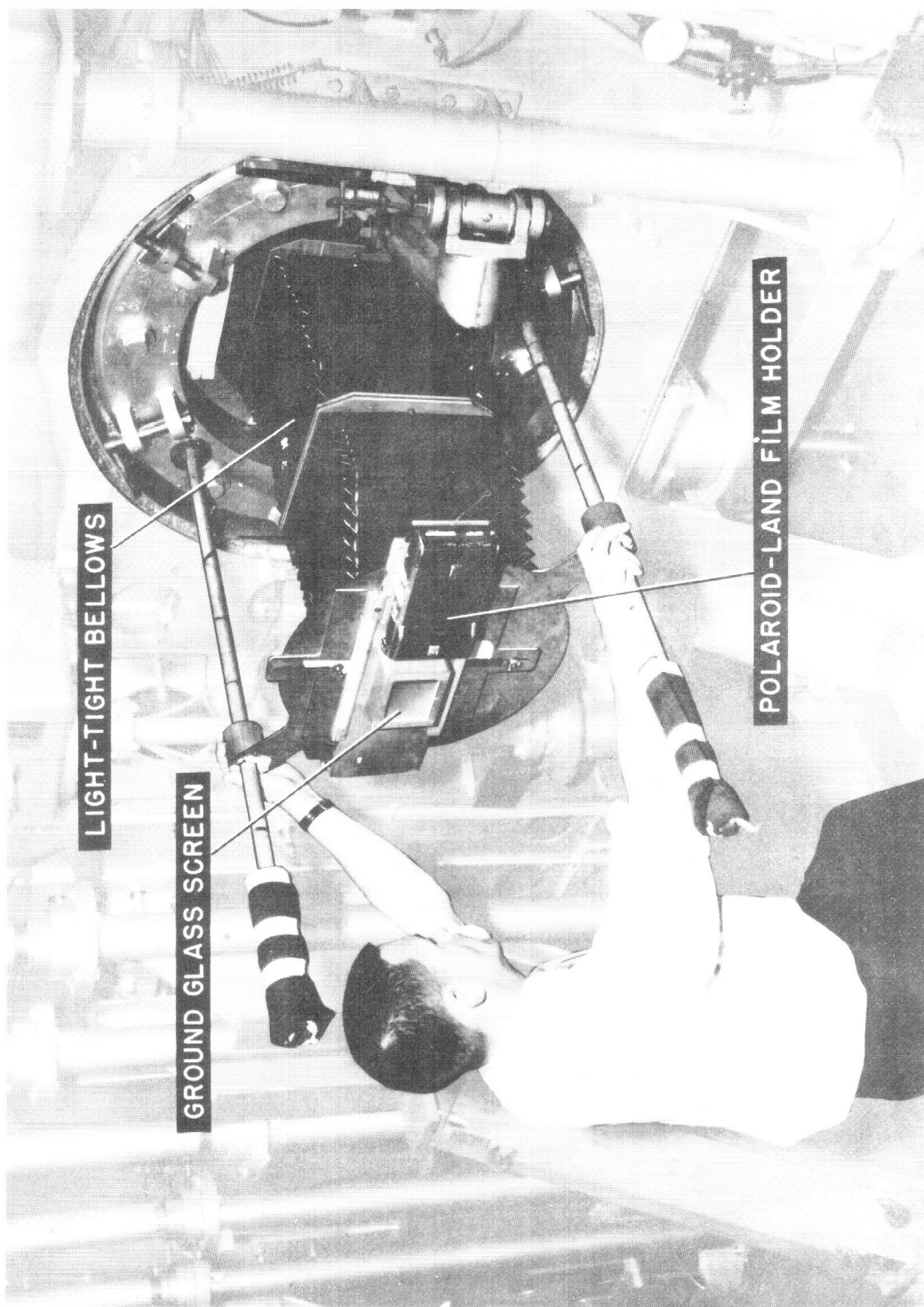
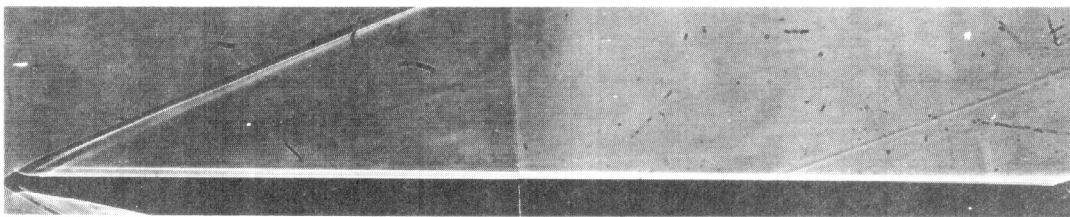
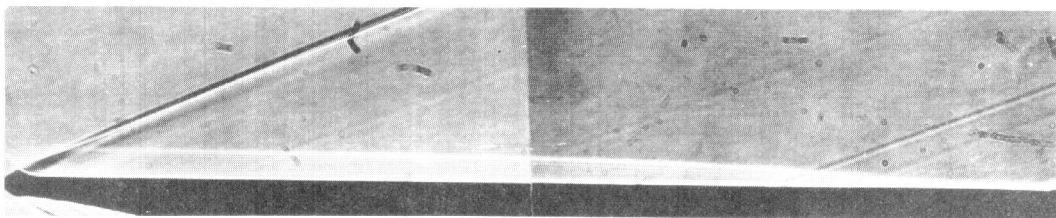


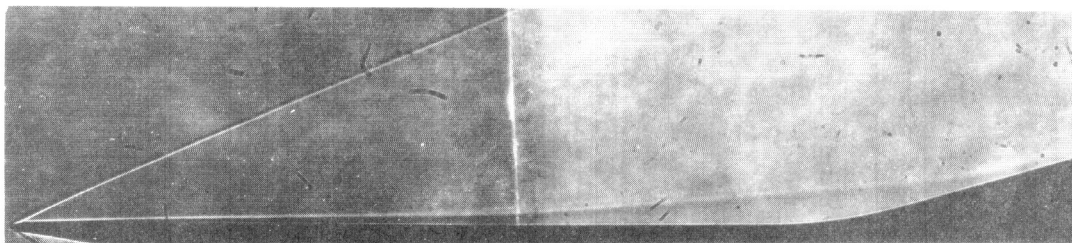
Figure 3.- Adjustable shadowgraph mount with light-tight bellows



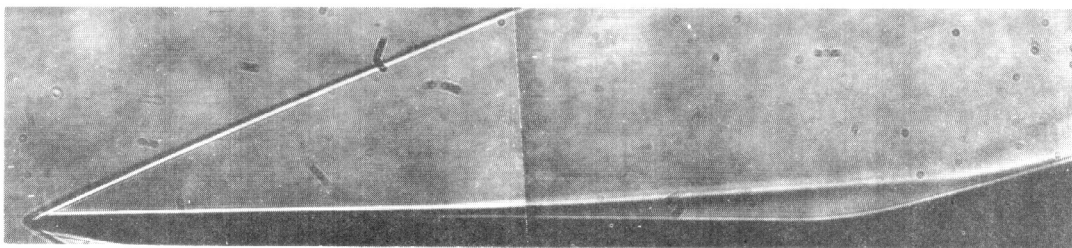
(a) Shadowgraph next to tunnel window. Flat plate model;  $M_0=3.0$ ;  
 $p_t=24.5$  psia.



(b) Shadowgraph 30 inches from tunnel window. Flat plate model;  
 $M_0=3.0$ ;  $p_t=24.5$  psia.



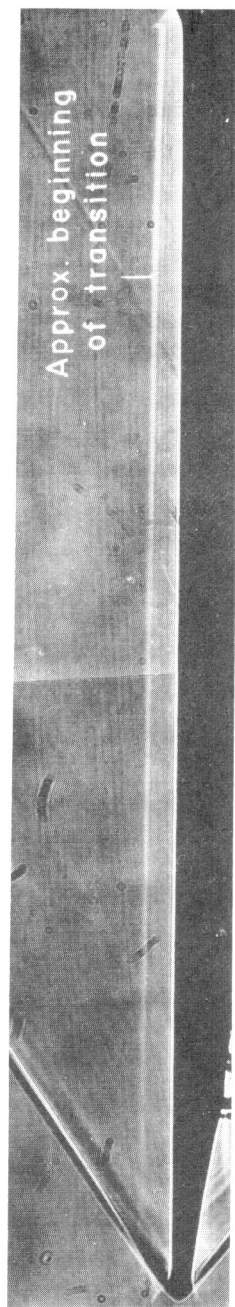
(c) Shadowgraph next to tunnel window. CS15°-1;  $M_0=3.0$ ;  $p_t=3$  psia.



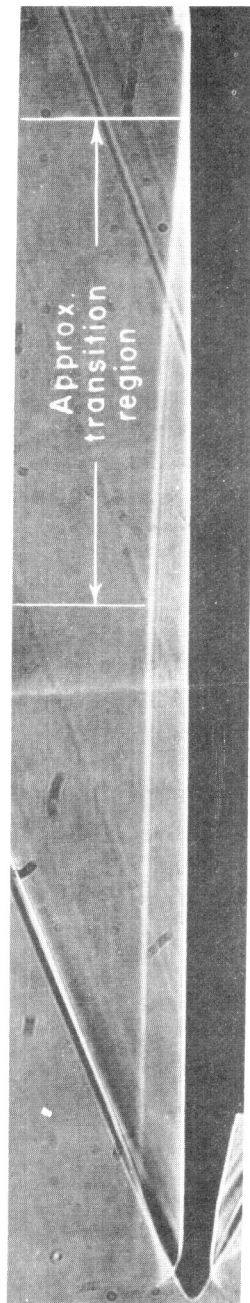
(d) Shadowgraph 42 inches from tunnel window. CS15°-1;  $M_0=3.0$ ;  
 $p_t=3$  psia.

Figure 4.—Effect on shadowgraph appearance of variation in distance between model and shadowgraph film.

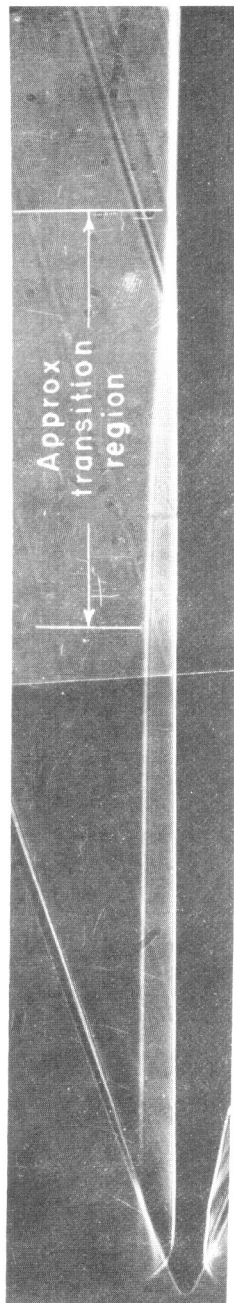




(a) Transition beginning near rear of plate.  $M_0=2.0$ ;  $R_L=1.9 \times 10^6$ .

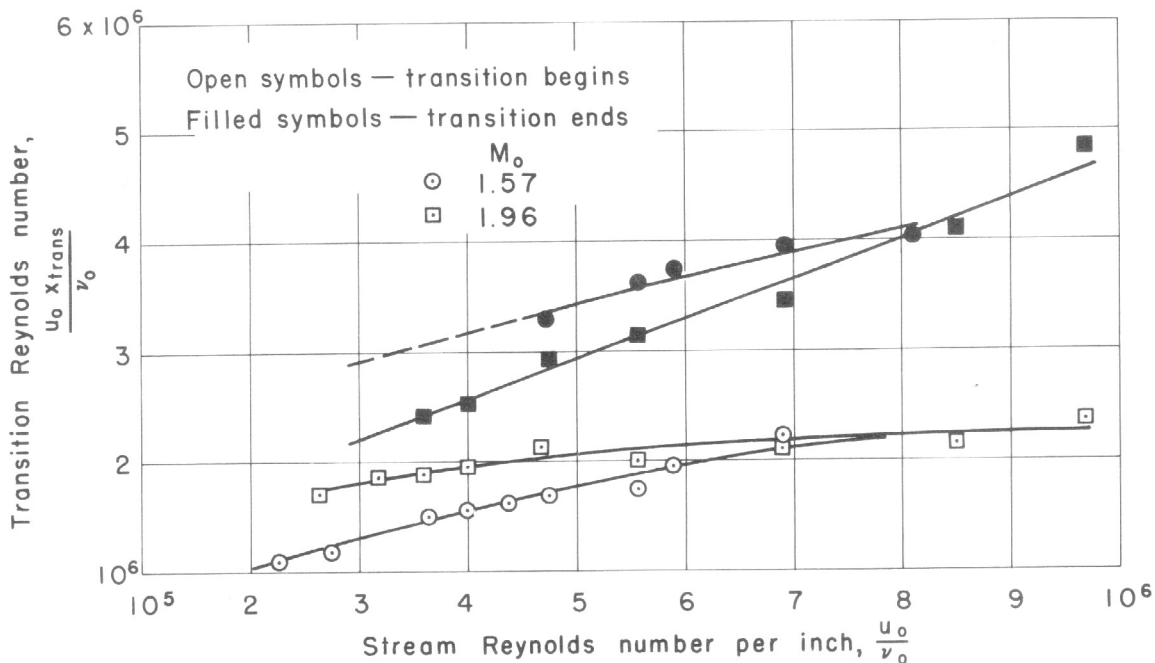


(b) Transition region on plate.  $M_0=3.0$ ;  $R_L=2.3 \times 10^6$ .

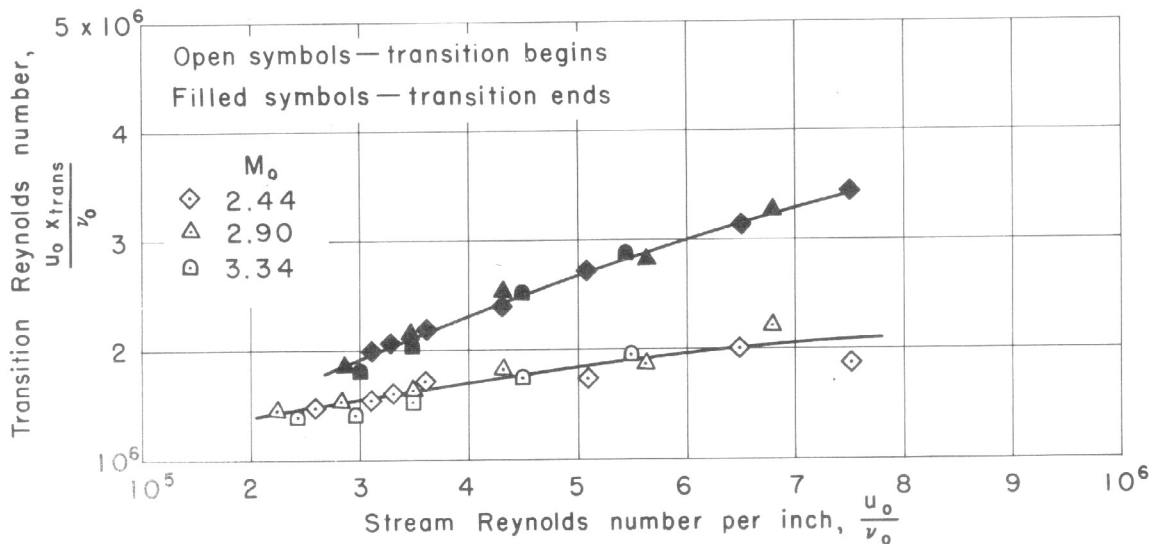


(c) Transition region on plate.  $M_0=3.5$ ;  $R_L=2.8 \times 10^6$ .

Figure 5.—Shadowgraphs indicating type of boundary-layer flow and location of transition on the flat plate model.

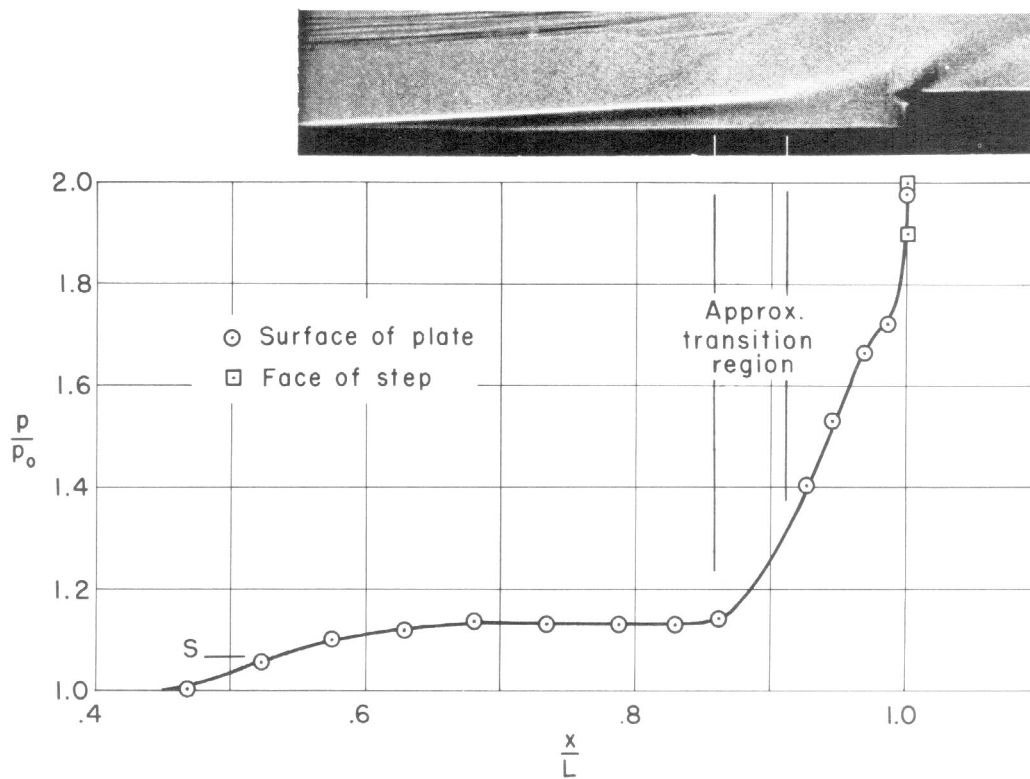


(a) Lower supersonic Mach number range.

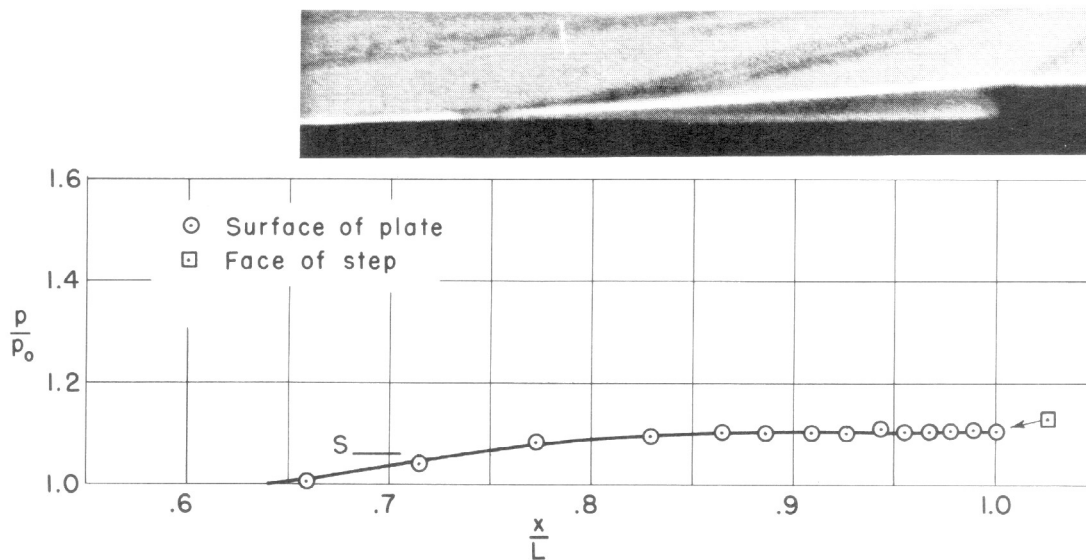


(b) High supersonic Mach number range.

Figure 6.—Reynolds number of transition on a flat plate in the Ames 1-by 3-foot wind tunnel No. 1. (Leading edge approximately 0.005 inch thick.)

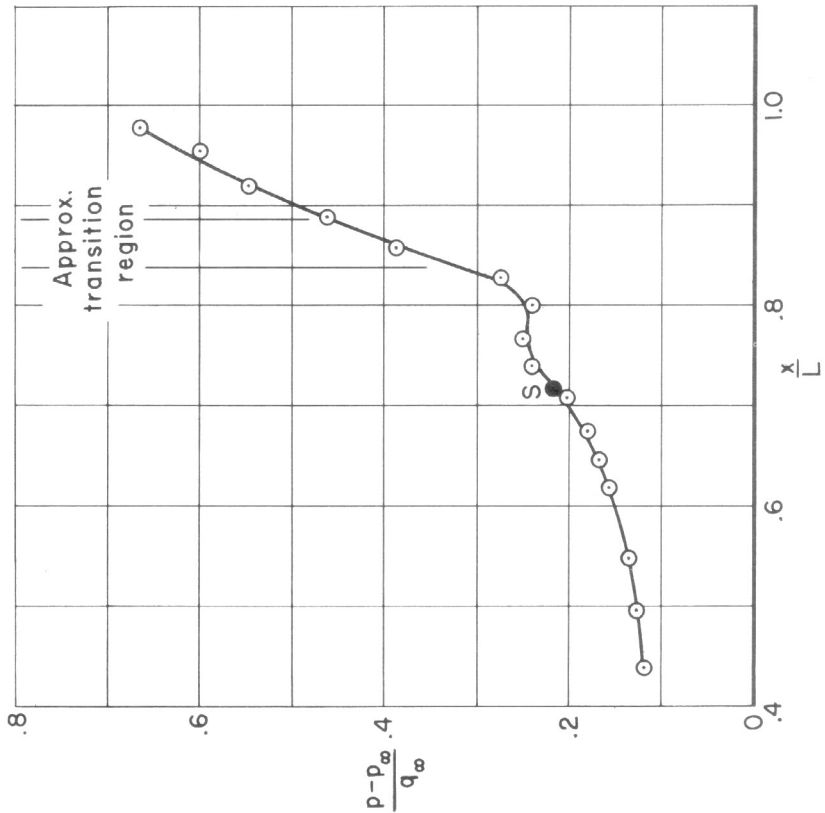
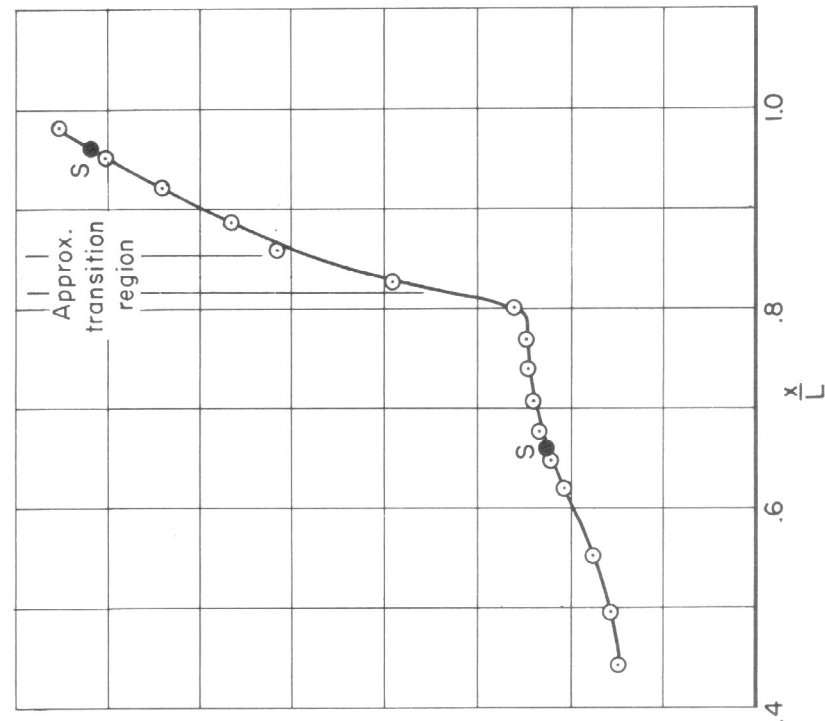
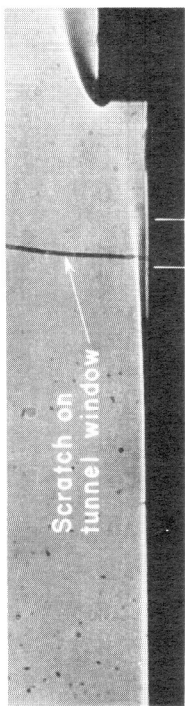
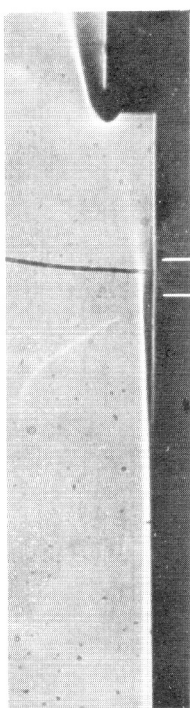


(a) Transition upstream of reattachment; S-7;  $M_0=1.9$ ;  $R_L=0.92 \times 10^6$ .



(b) Transition downstream of reattachment; S-8;  $M_0=1.9$ ;  $R_L=0.87 \times 10^6$ .

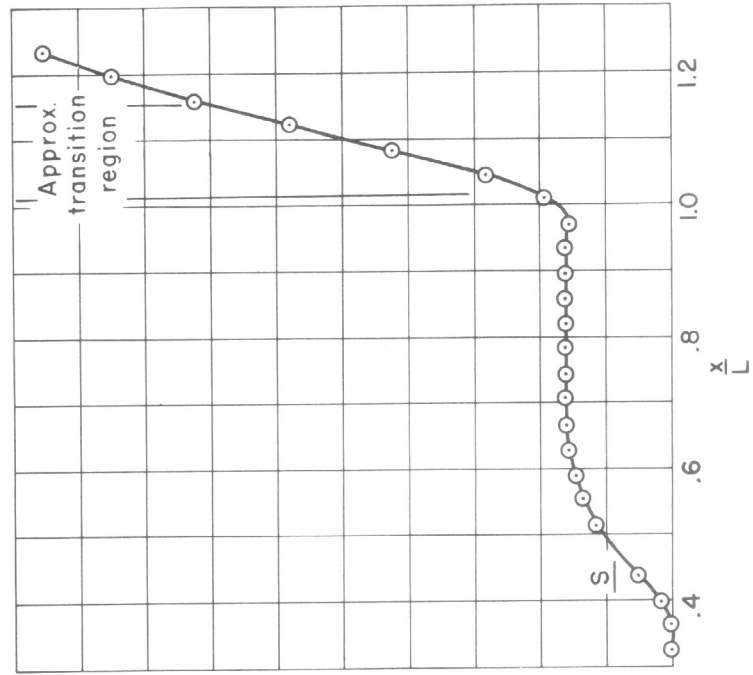
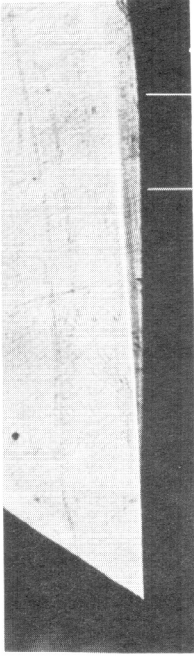
Figure 7.—Typical results from two-dimensional channel illustrating importance of transition location relative to reattachment.



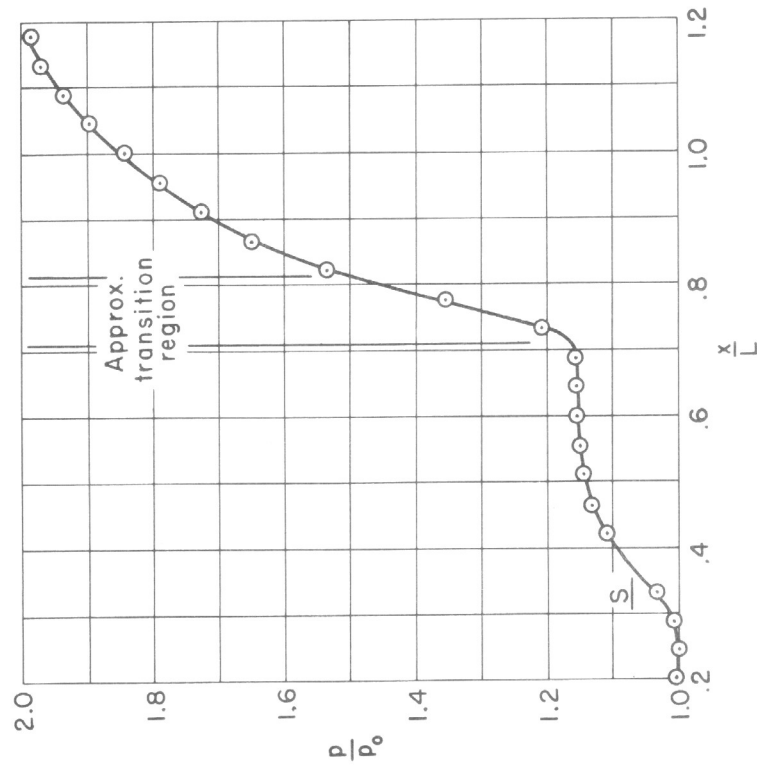
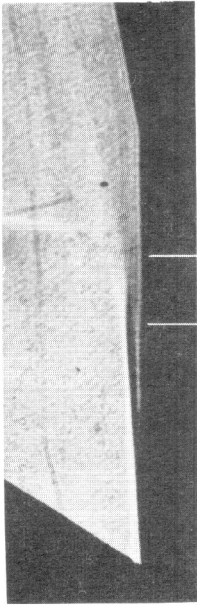
(b) S-9;  $M_\infty=0.76$ ;  $\alpha=-4^\circ$ ;  $R_L=0.50 \times 10^6$

(a) S-9;  $M_\infty=0.47$ ,  $\alpha=-4^\circ$ ;  $R_L=0.47 \times 10^6$

Figure 8.-Correlation of transition with abrupt pressure rise; low tunnel pressures.

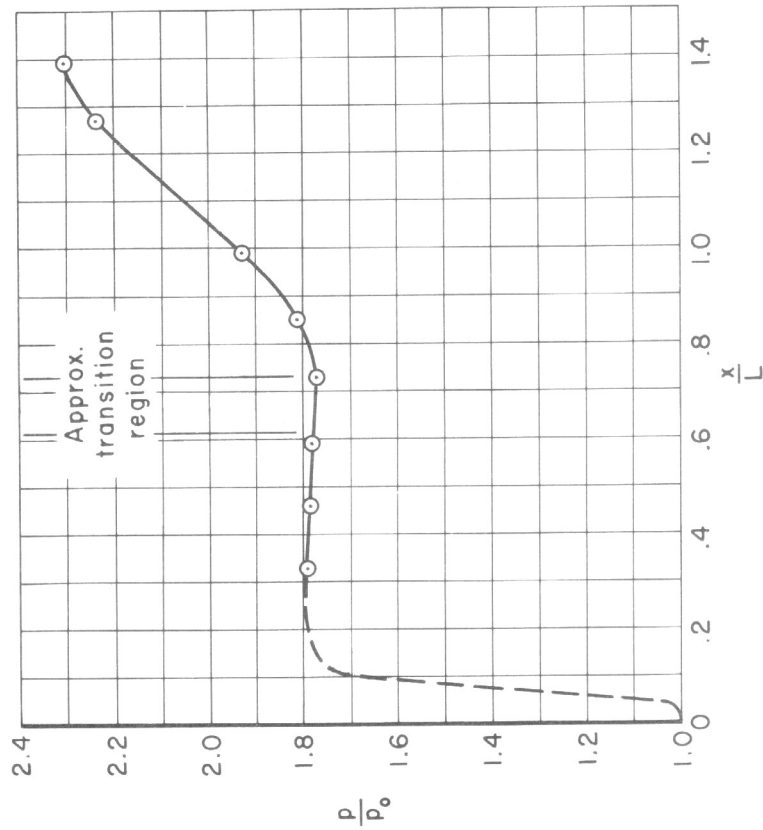
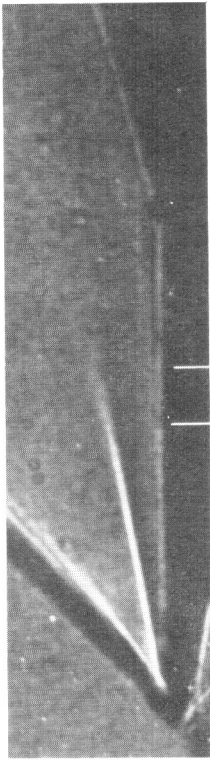
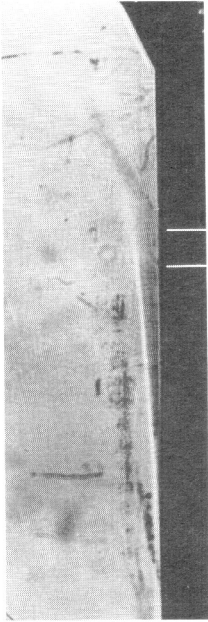


(d)  $CC25^\circ-1$ ;  $M_0=1.7$ ;  $R_L=0.26 \times 10^6$

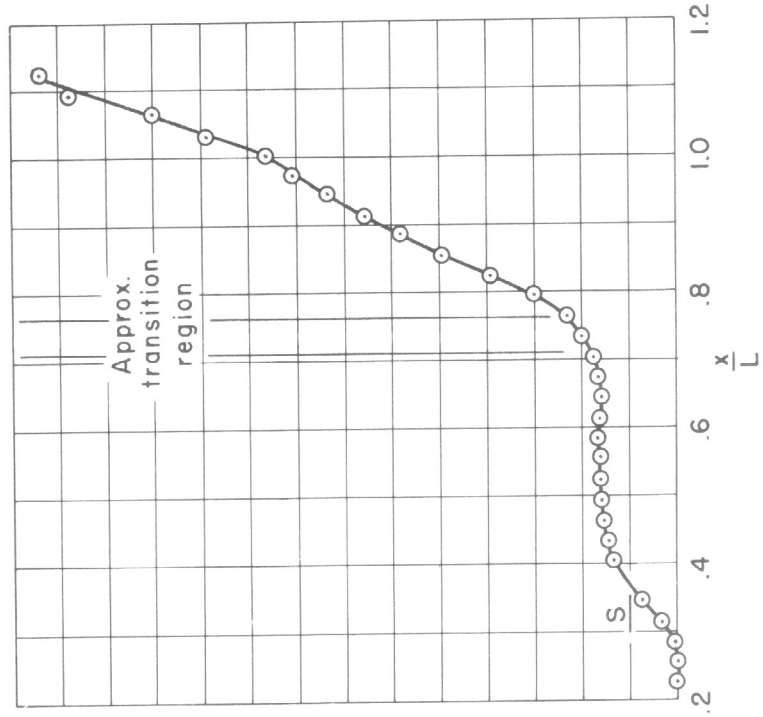


(c)  $CC10^\circ-2$ ;  $M_0=1.4$ ;  $R_L=0.33 \times 10^6$

Figure 8.—Continued.



(e) CC15°-2;  $M_0=1.7$ ;  $R_L=0.058 \times 10^6$



(f) CC25°-3;  $M_0=2.0$ ;  $R_L=0.44 \times 10^6$

Figure 8.—Concluded.

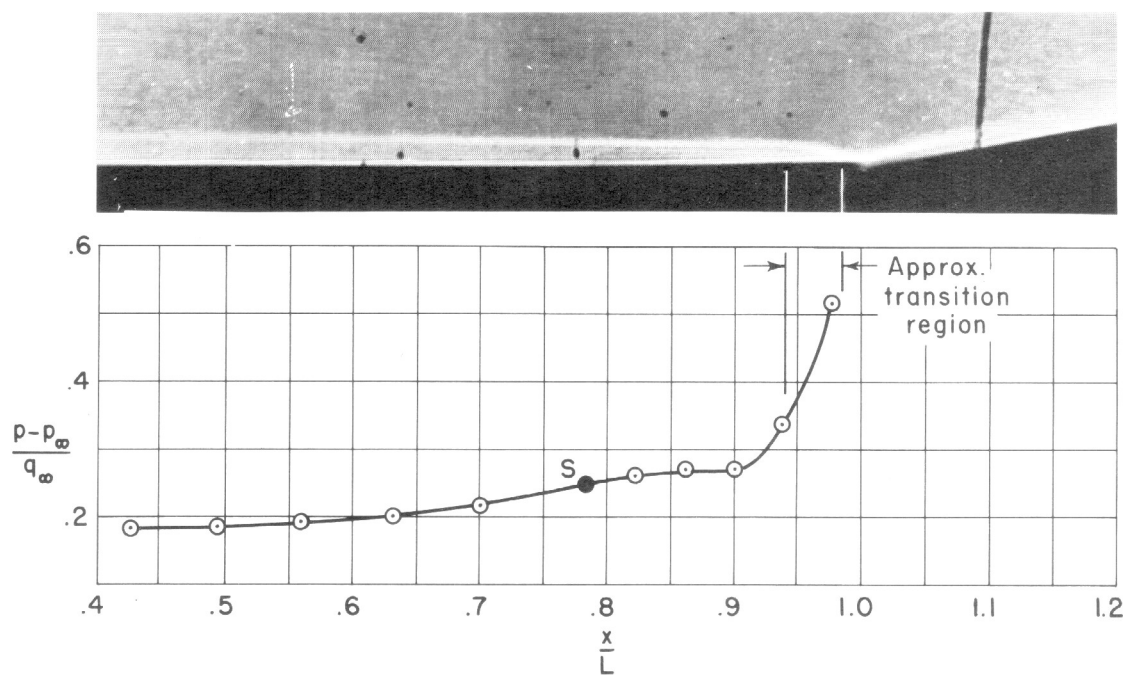
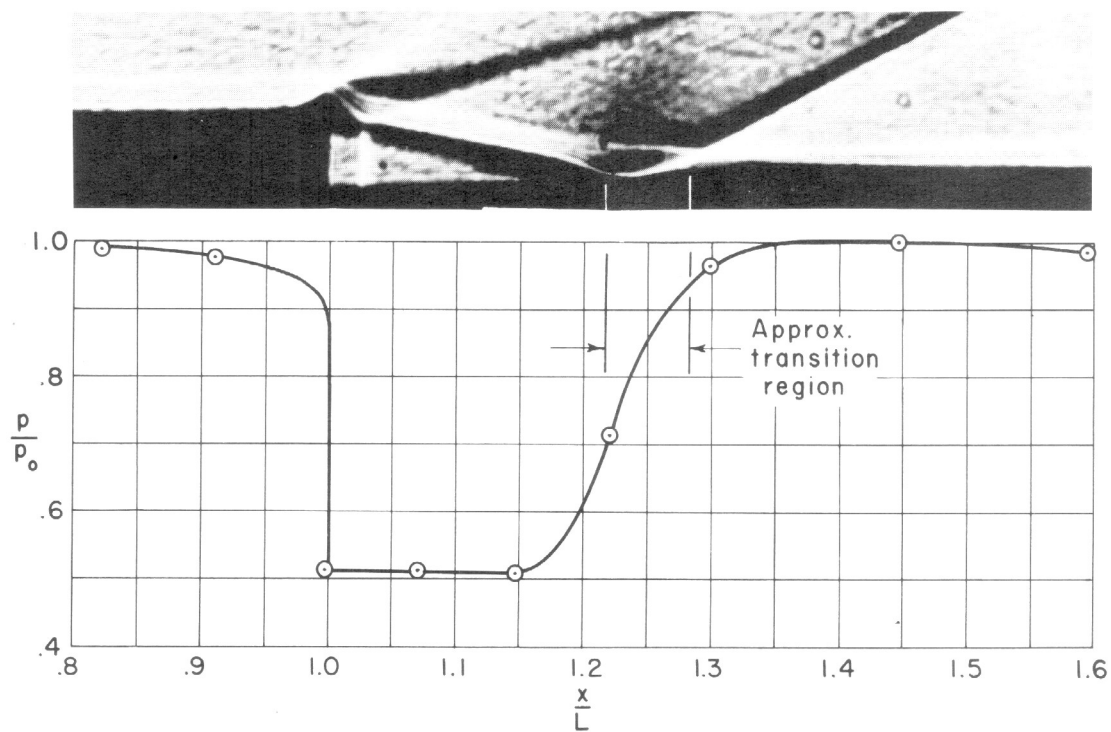
(a) CCI0°-3;  $M_\infty=0.78$ ;  $\alpha=-4^\circ$ ;  $R_L=0.75 \times 10^6$ (b) B-2;  $M_\infty=1.7$ ;  $R_L=0.57 \times 10^6$ 

Figure 9.—Correlation of transition with abrupt pressure rise; high tunnel pressures.

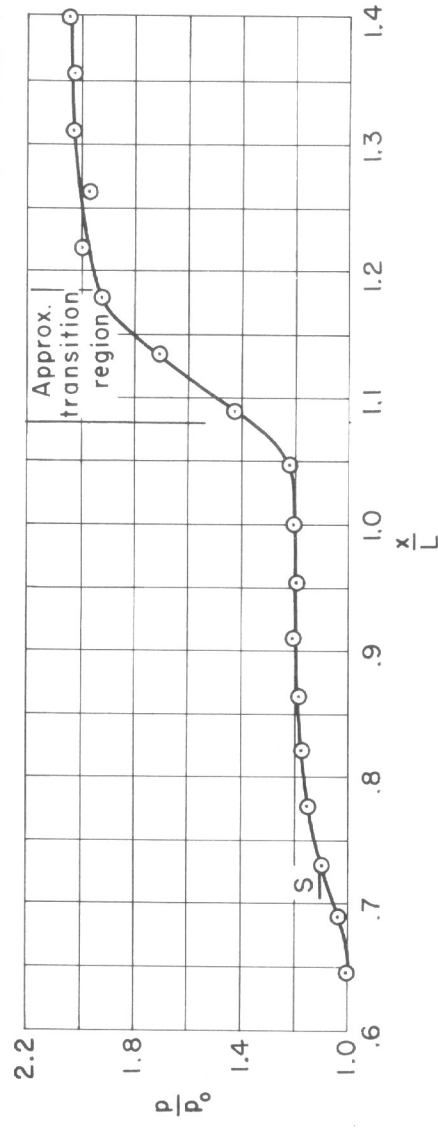
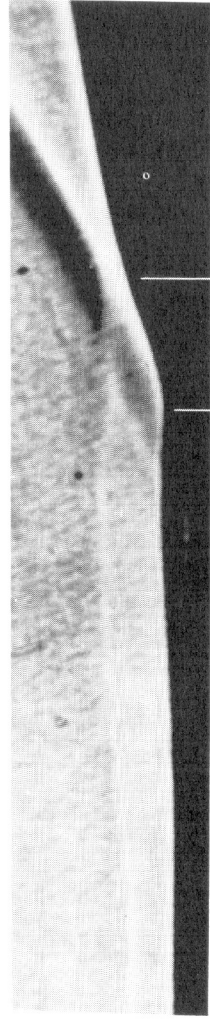
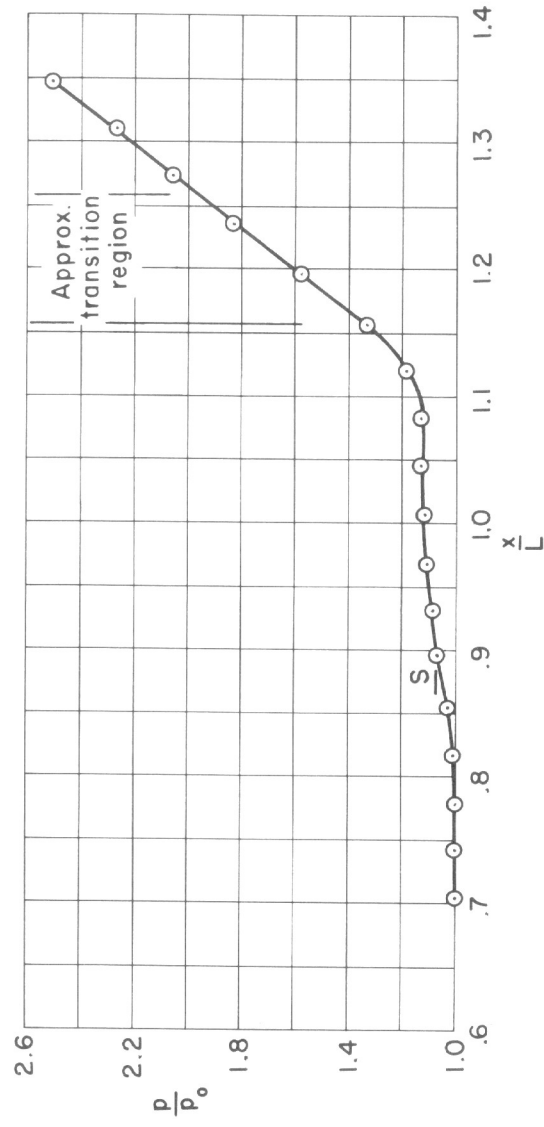
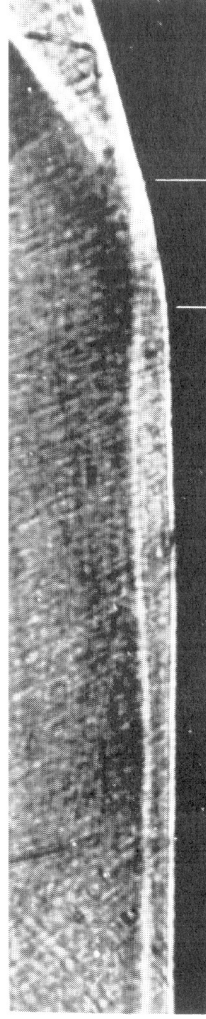
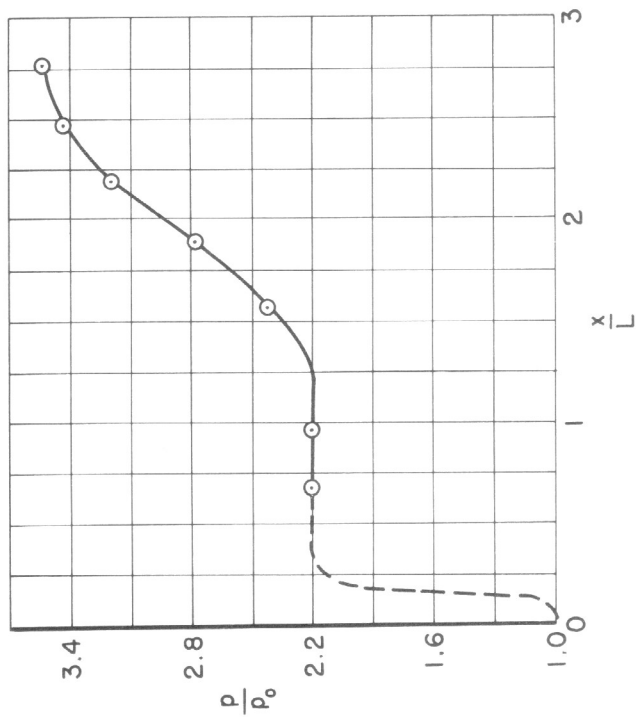
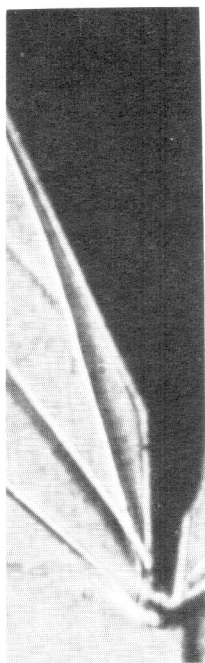
(c) CC10°-2;  $M_0=2.7$ ;  $R_L=1.05 \times 10^6$ (d) CS25°-1;  $M_0=2.1$ ;  $R_L=1.13 \times 10^6$ 

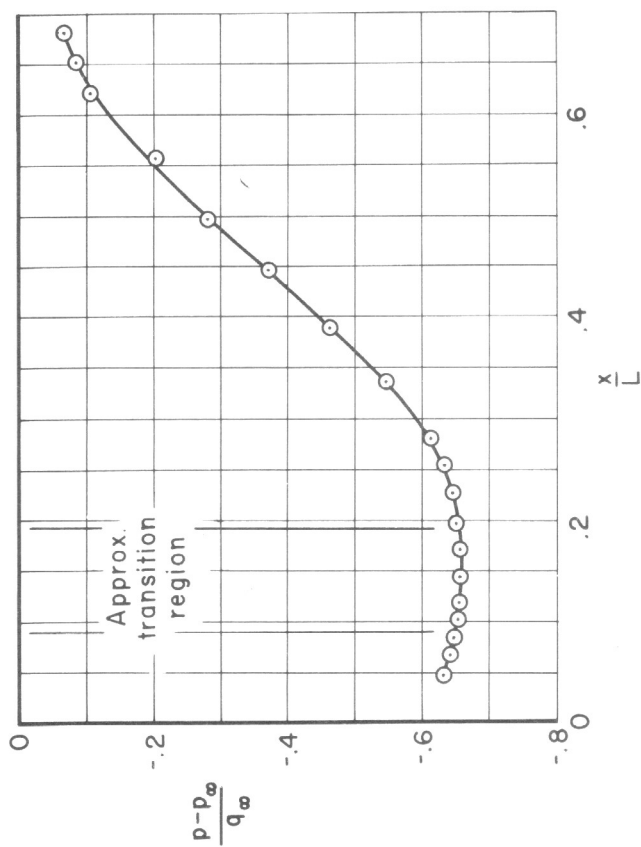
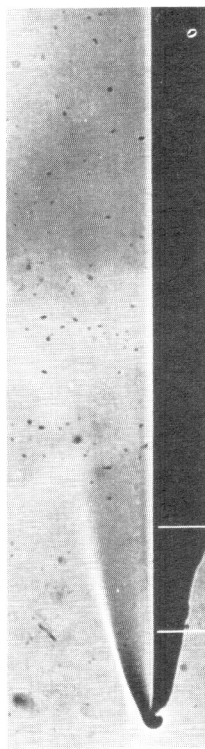
Figure 9.—Concluded.





(b) Abrupt rise near reattachment of thin laminar layer.

CC20°-1;  $M_\infty=3.0$ ;  $R_L=0.018 \times 10^6$



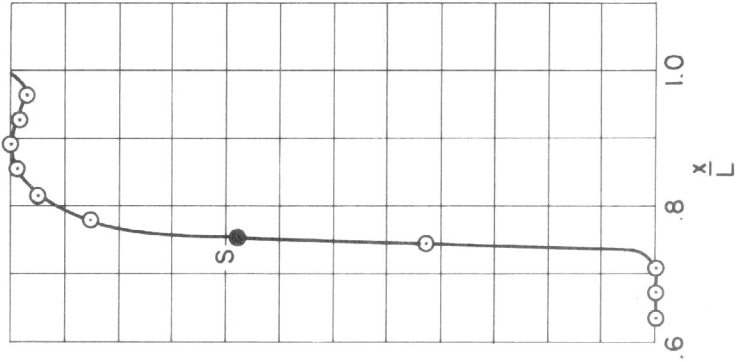
(a) Abrupt rise near reattachment of turbulent layer.

S-9;  $M_\infty=0.47$ ;  $\alpha=+3^\circ$ ;  $R_L=0.68 \times 10^6$

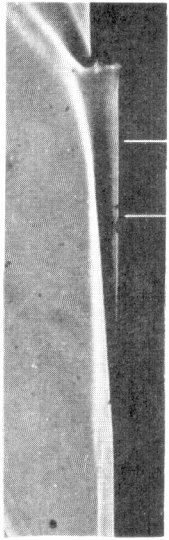
Figure 10.—Examples of abrupt pressure rise not correlated with the location of transition.



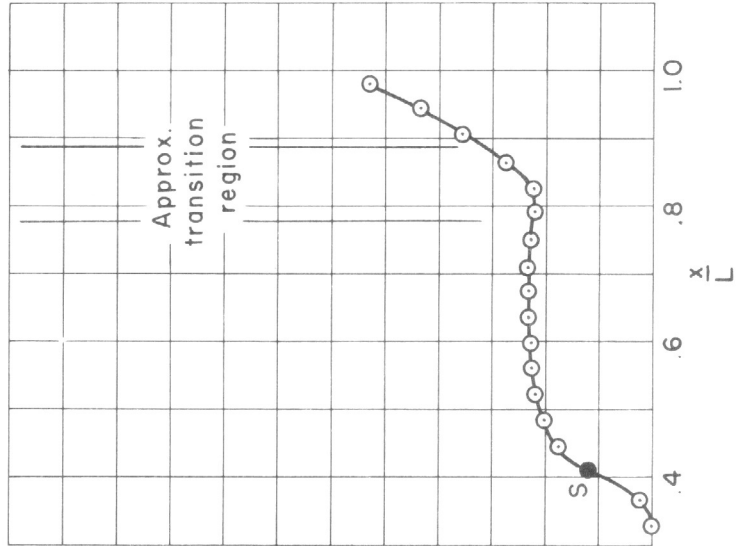
Turbulent



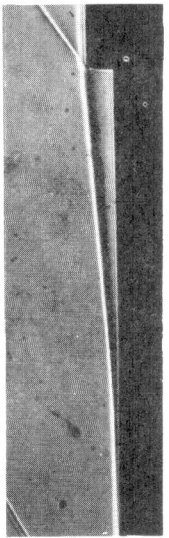
(c) S-4 (trip l);  $M_0 = 2.3$ ;  
 $R_L = 1.52 \times 10^6$



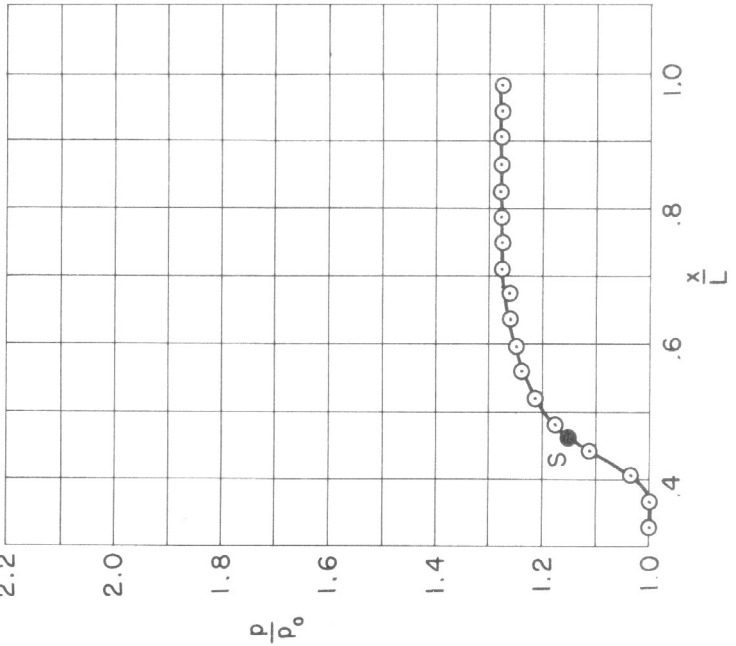
Transitional



(b) S-3;  $M_0 = 2.3$ ;  $R_L = 0.46 \times 10^6$

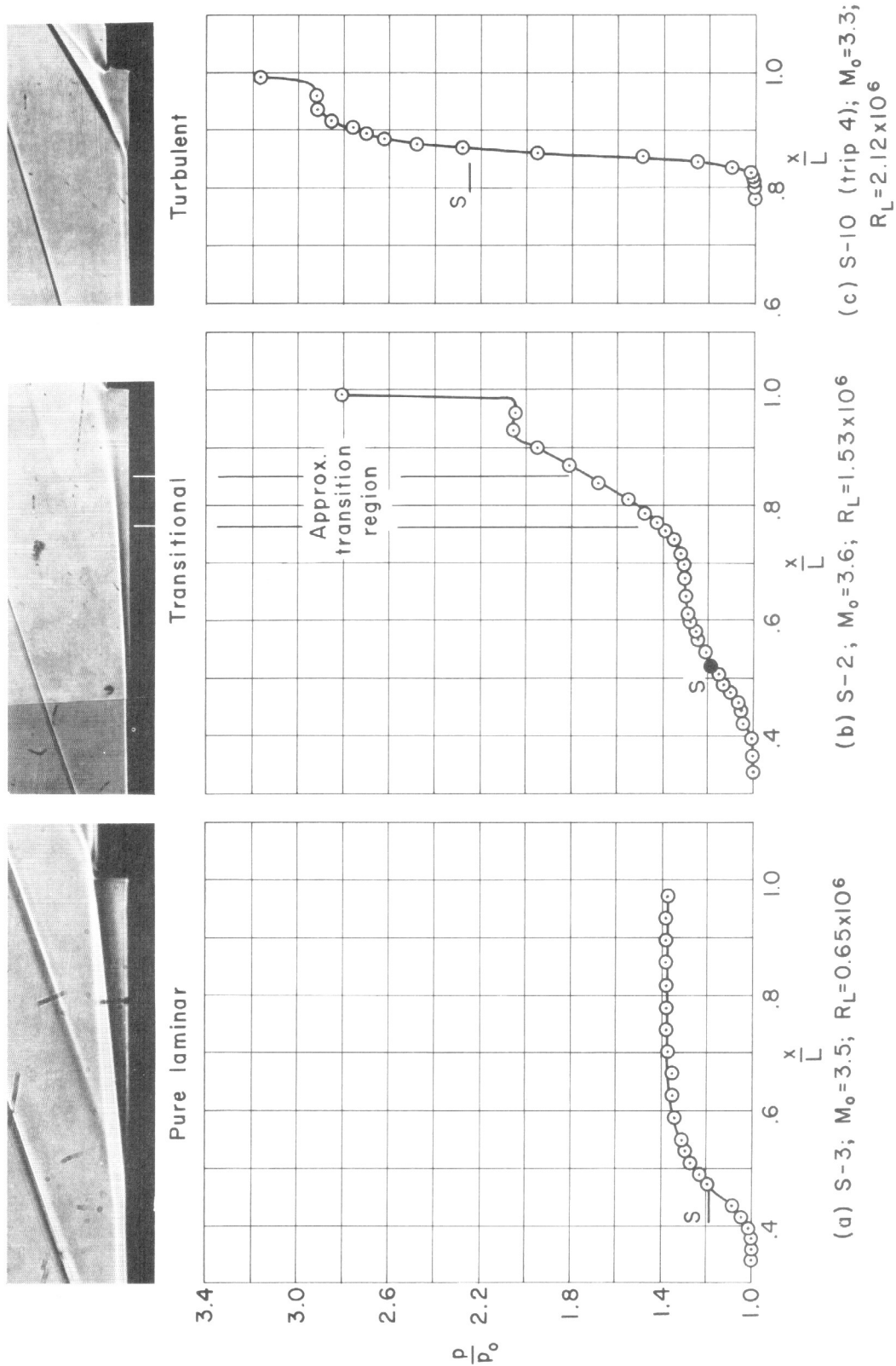


Pure laminar



(a) S-3;  $M_0 = 2.3$ ;  $R_L = 0.20 \times 10^6$

Figure 11.—The three-regimes for a step;  $M_0 = 2.3$

Figure 12.—The three regimes for a step;  $M_0 \approx 3.5$

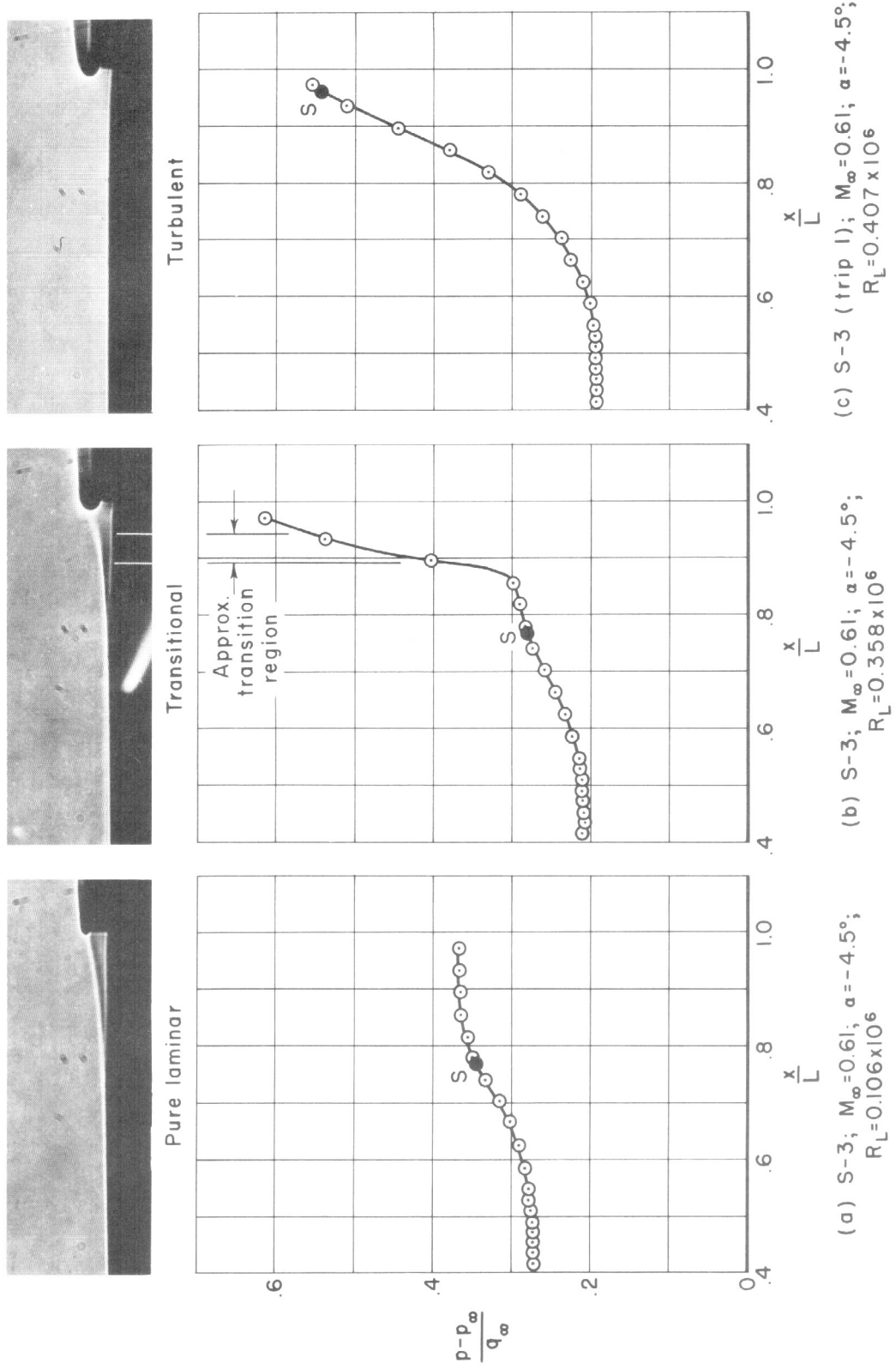
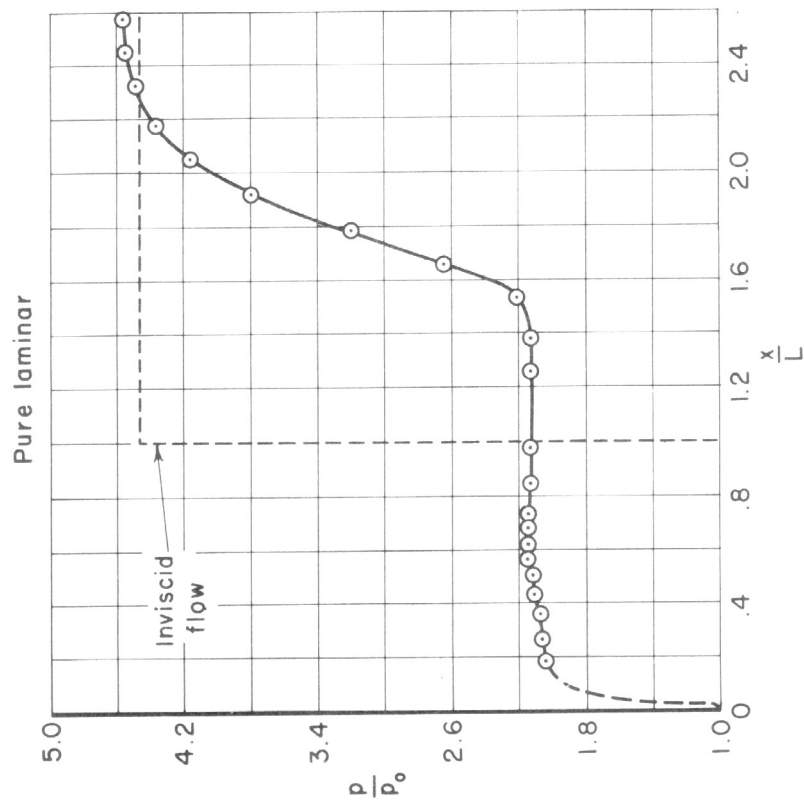
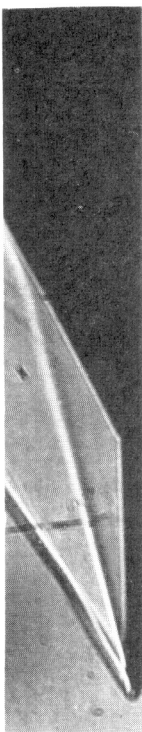
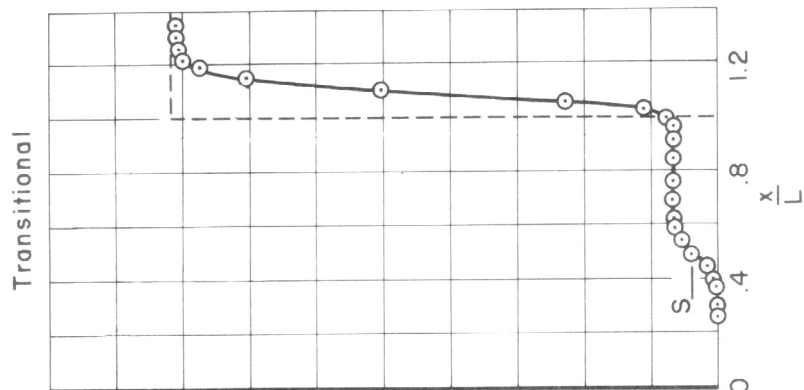
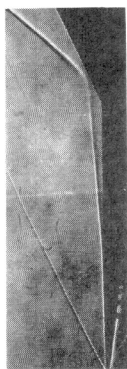


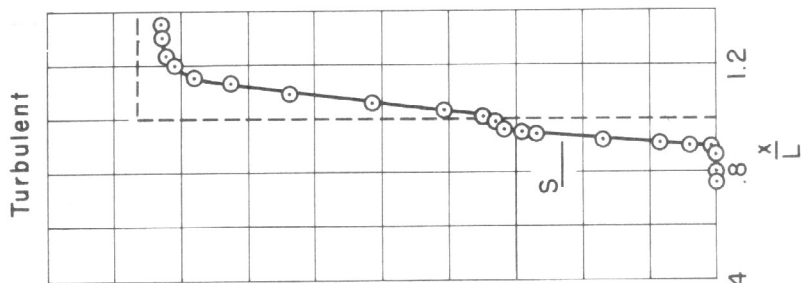
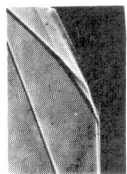
Figure 13.—The three regimes for a step in subsonic flow;  $M_\infty = 0.61$



(a) CC25°-2;  $M_0=2.7$ ;  $R_L=0.033 \times 10^6$

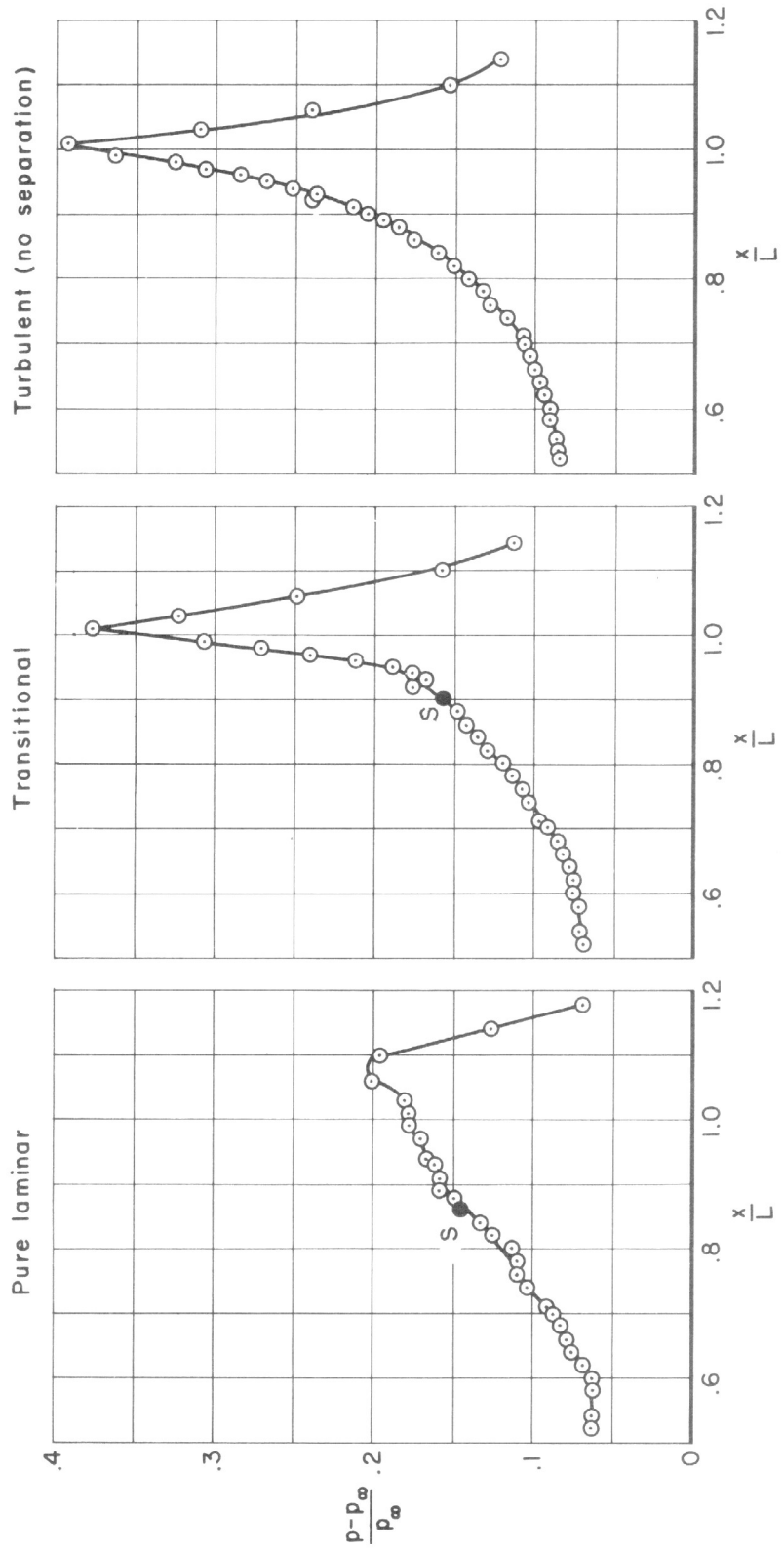
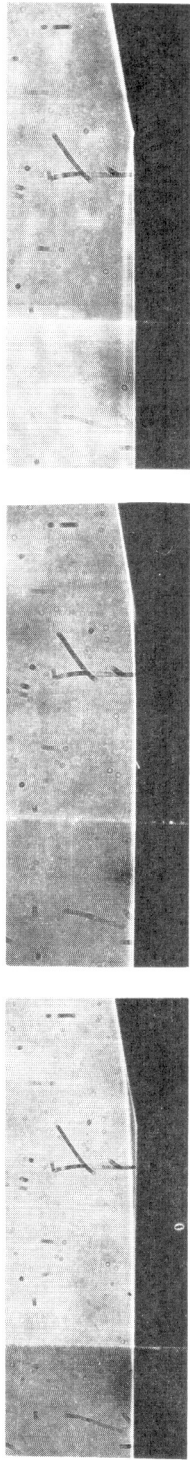


(b) CC25°-4;  $M_0=2.6$ ;  
 $R_L=0.33 \times 10^6$



(c) CC25°-5; (trip 4);  
 $M_0=2.7$ ;  $R_L=1.65 \times 10^6$

Figure 14.—The three regimes for a compression corner;  $M_0 \approx 2.7$

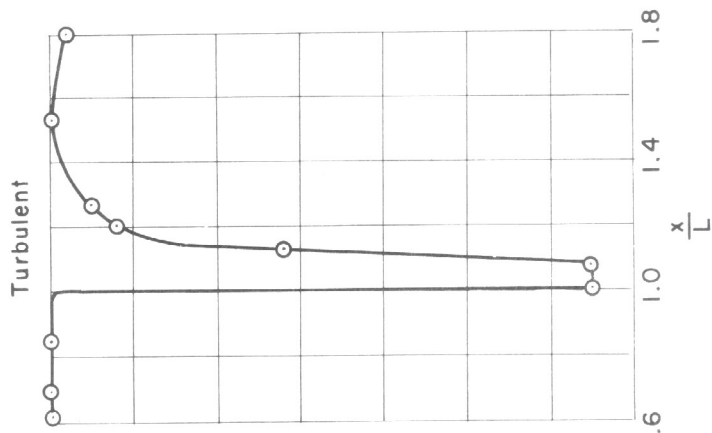


(a) CC10°-4;  $M_\infty=0.5$ ;  $\alpha=-4^\circ$ ;  
 $R_L=0.17 \times 10^6$

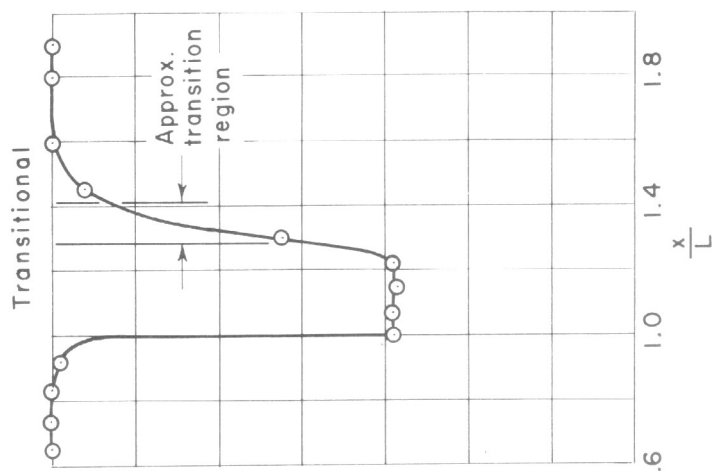
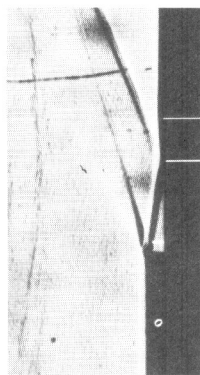
(b) CC10°-4;  $M_\infty=0.5$ ;  $\alpha=-4^\circ$ ;  
 $R_L=0.43 \times 10^6$

(c) CC10°-4;  $M_\infty=0.5$ ;  $\alpha=-4^\circ$ ;  
 $R_L=1.22 \times 10^6$

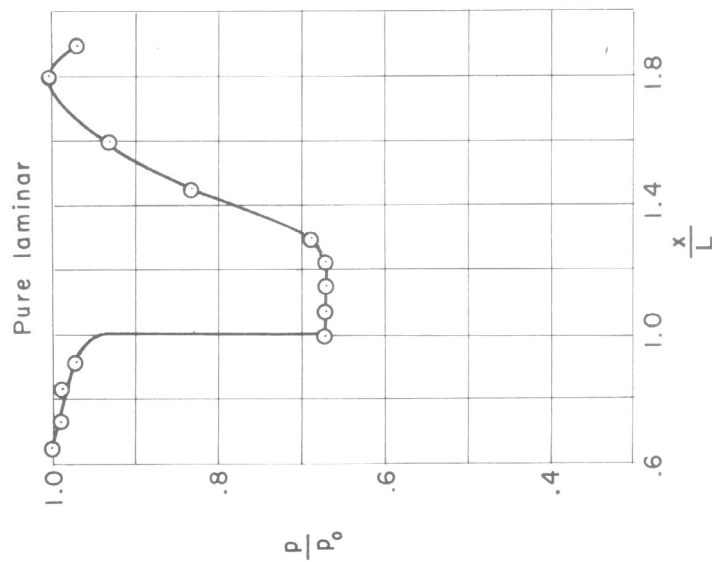
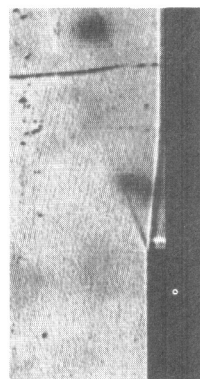
Figure 15.—The three regimes for a compression corner in subsonic flow;  $M_\infty=0.5$



(c) B-1-c(trip l);  $M_0 = 2.0$ ;  
 $R_L = 0.39 \times 10^6$

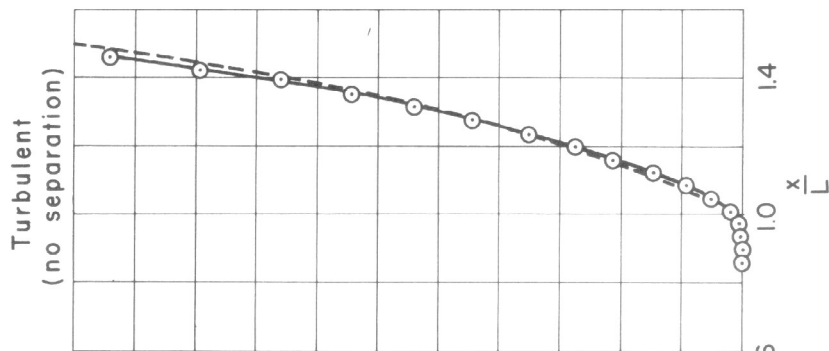
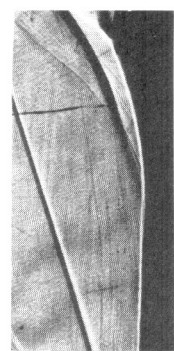


(b) B-2;  $M_0 = 2.0$ ;  $R_L = 0.50 \times 10^6$

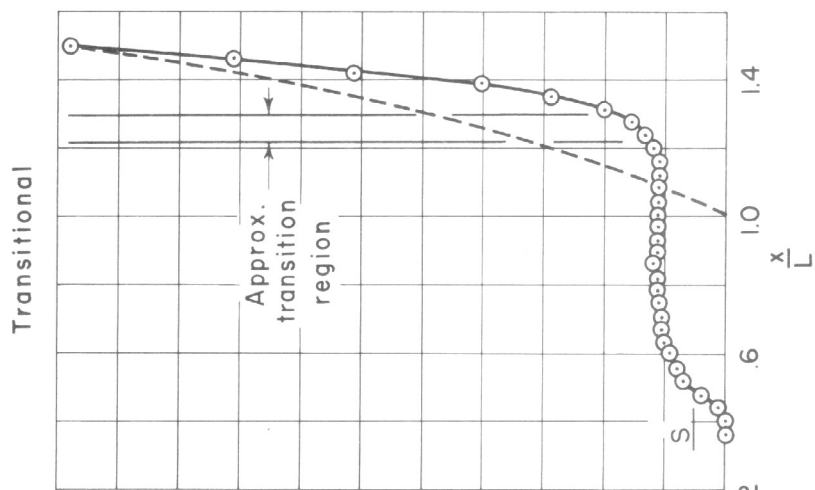
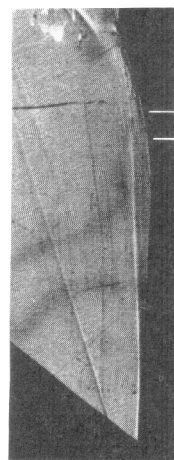


(a) B-2;  $M_0 = 2.0$ ;  $R_L = 0.17 \times 10^6$

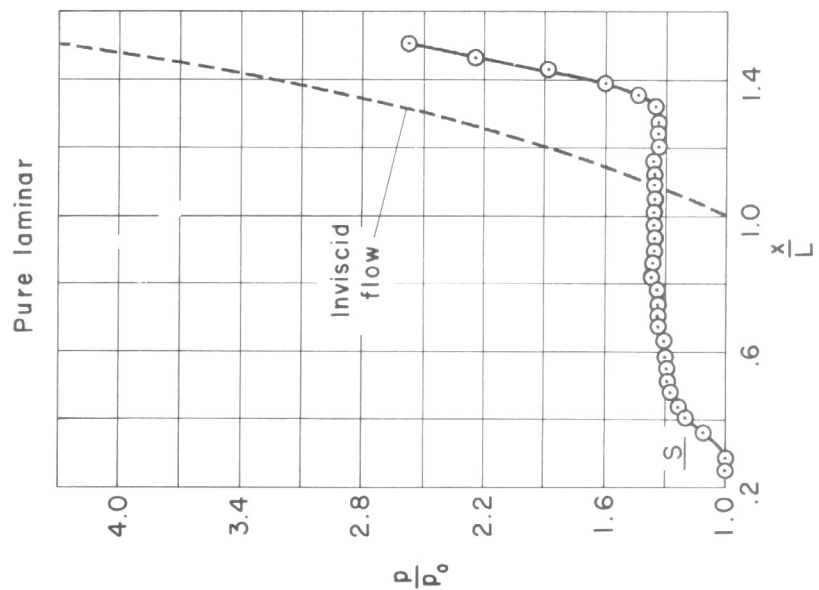
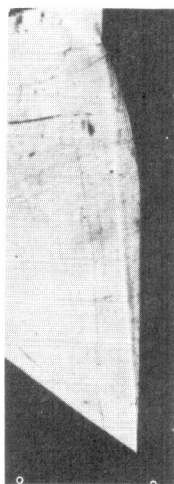
Figure 16.—The three regimes for a base;  $M_0 = 2.0$



(c) CS25°-1 (trip 1);  
 $M_0=2.7$ ;  $R_L=0.96 \times 10^6$



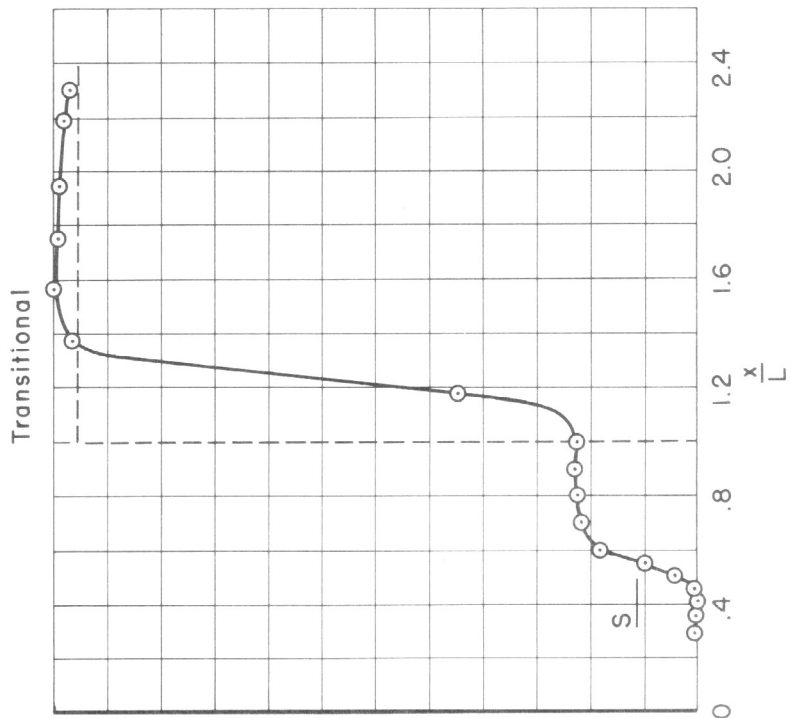
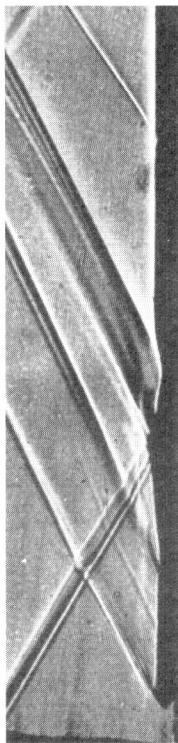
(b) CS25°-1 (trip 1);  $M_0=2.7$ ;  
 $R_L=0.21 \times 10^6$



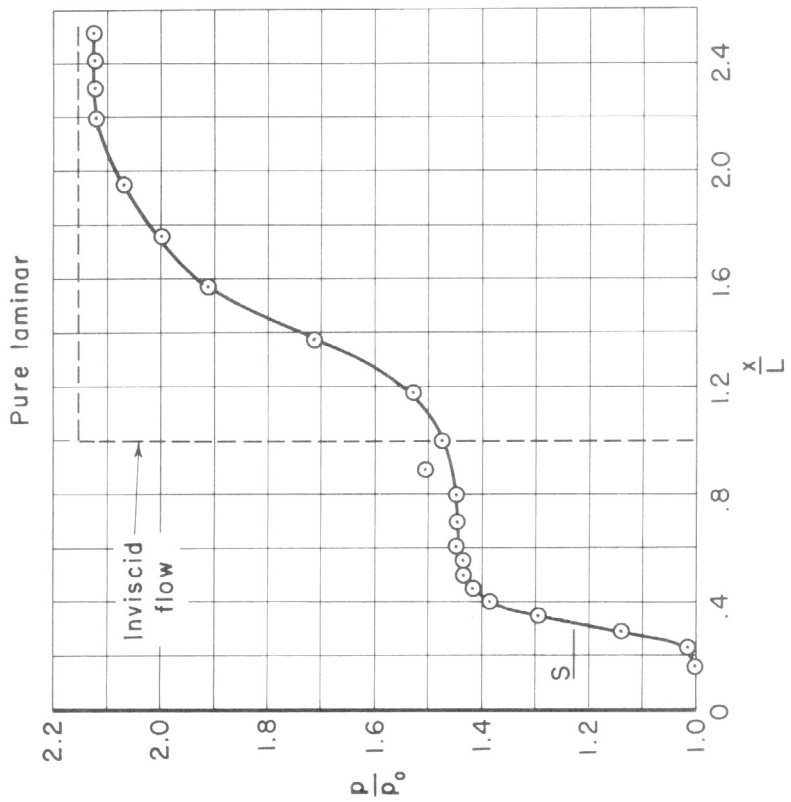
(a) CS25°-1;  $M_0=2.7$ ;  $R_L=0.16 \times 10^6$

Figure 17.—The three regimes for a curved surface;  $M_0=2.7$



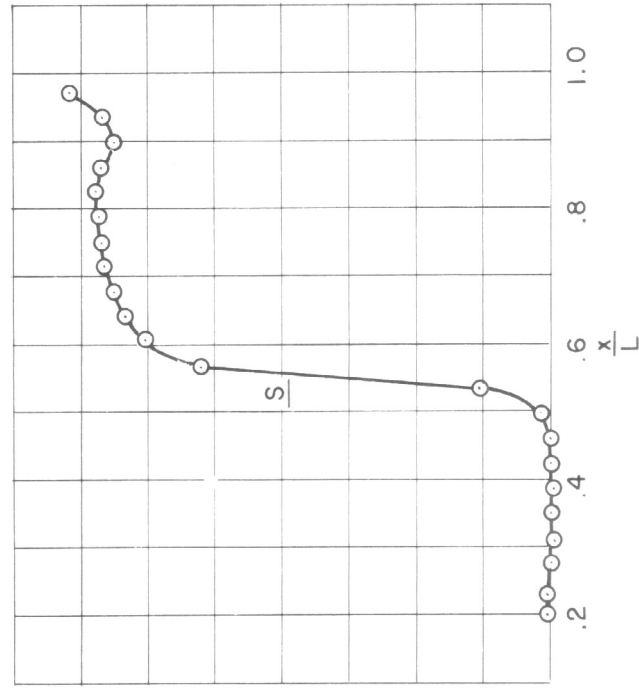
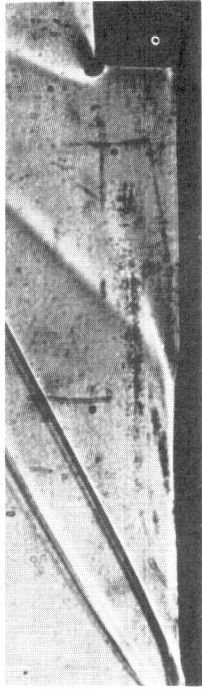


(a)  $16.5^\circ$ -I;  $M_0=2.4$ ;  $R_L=0.054 \times 10^6$

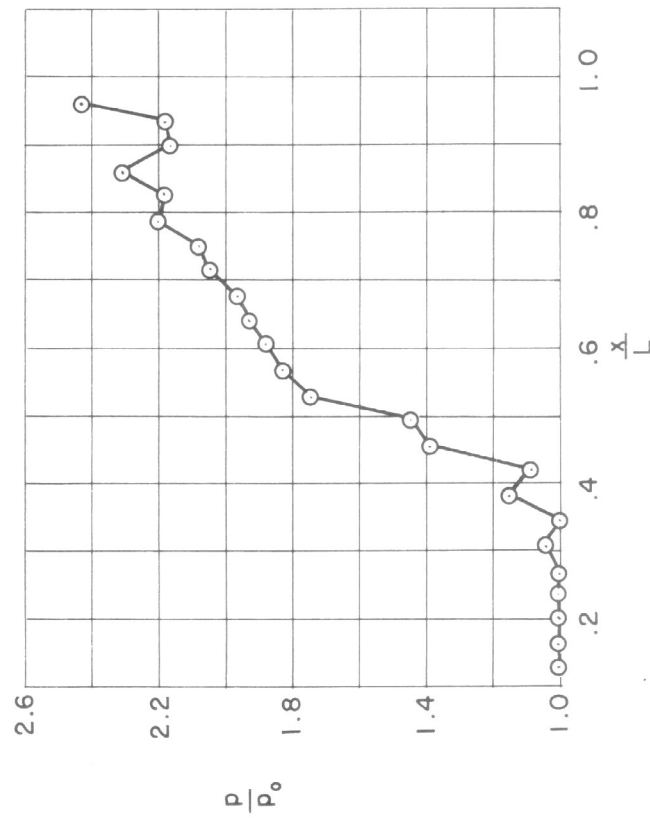
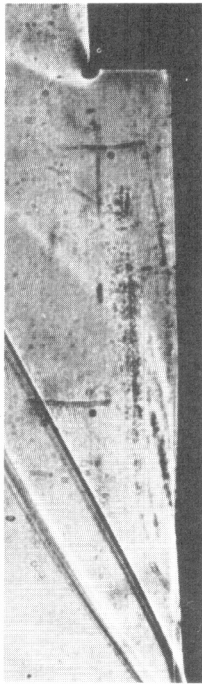


(b)  $16.5^\circ$ -I;  $M_0=2.4$ ;  $R_L=0.176 \times 10^6$

Figure 18.—Pure laminar and transitional separations induced by an incident shock wave;  $M_0=2.4$



(b) Turbulent separation established;  
 $S=6$ (trip 1);  $M_0=2.1$ ;  $R_L=0.51 \times 10^6$



(a) Conversion from transitional to turbulent  
separation;  $S=6$ (trip 1);  $M_0=2.1$ ;  $R_L=0.39 \times 10^6$

Figure 19.— Example of unsteady flow during conversion from transitional to turbulent flow.

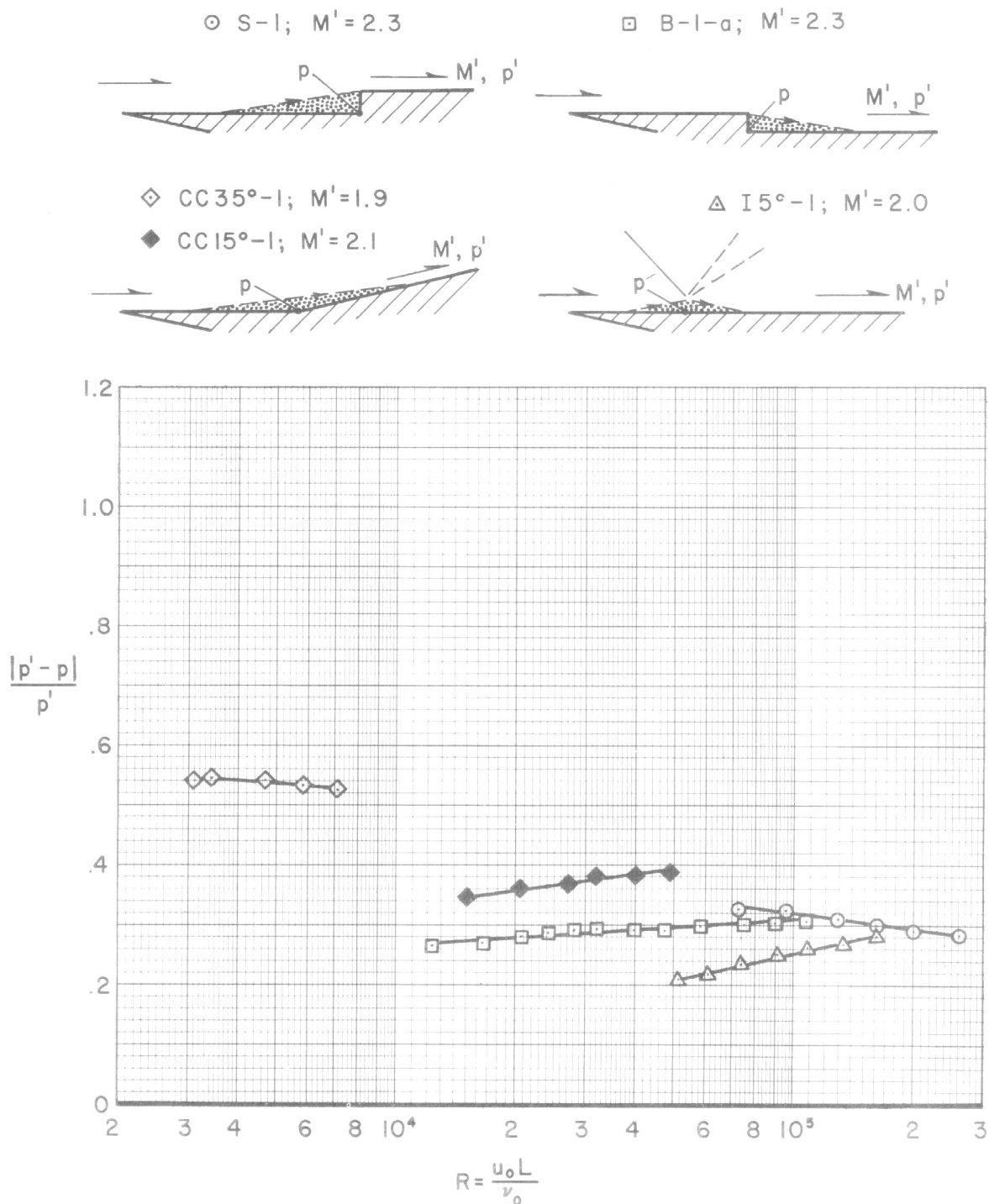
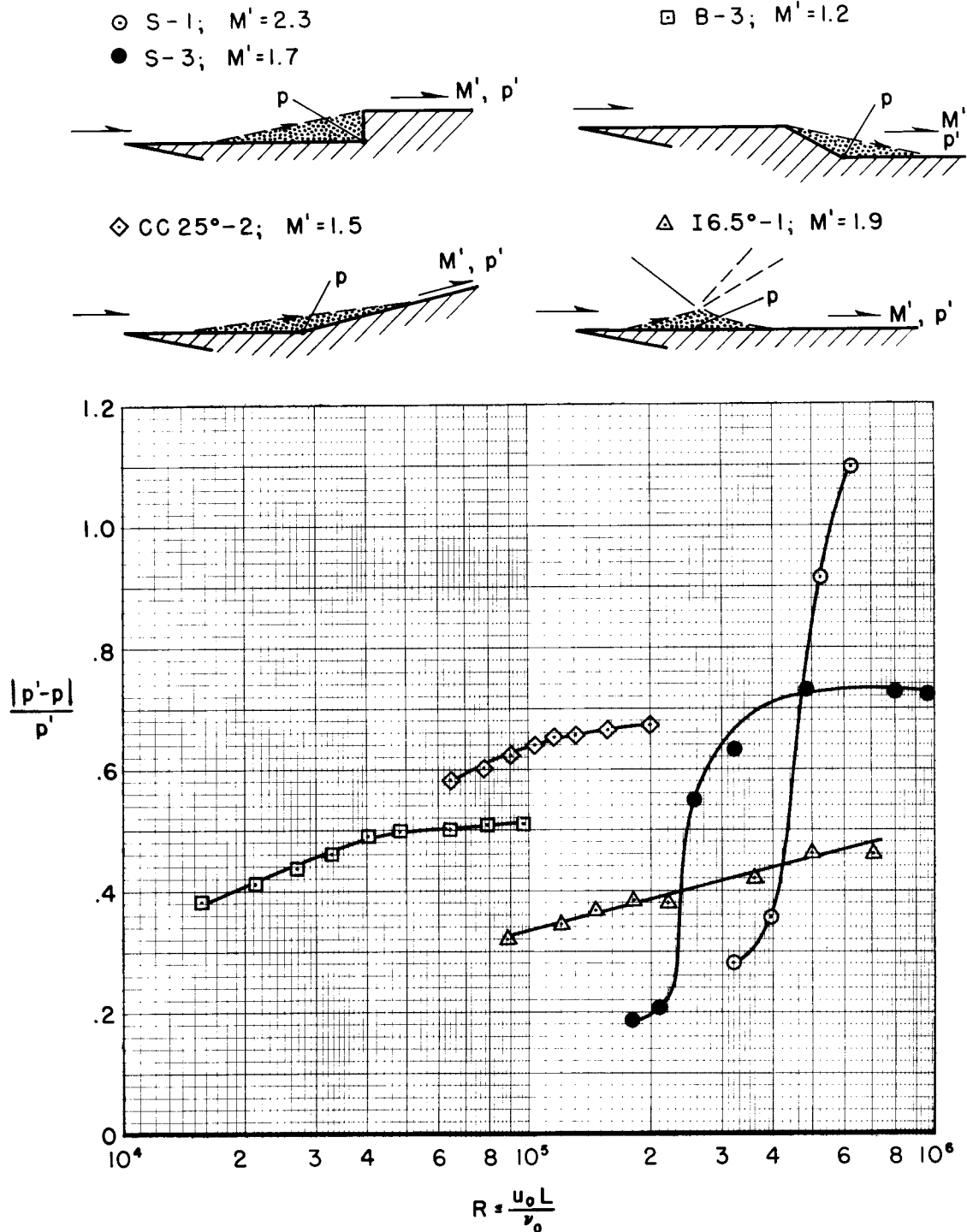
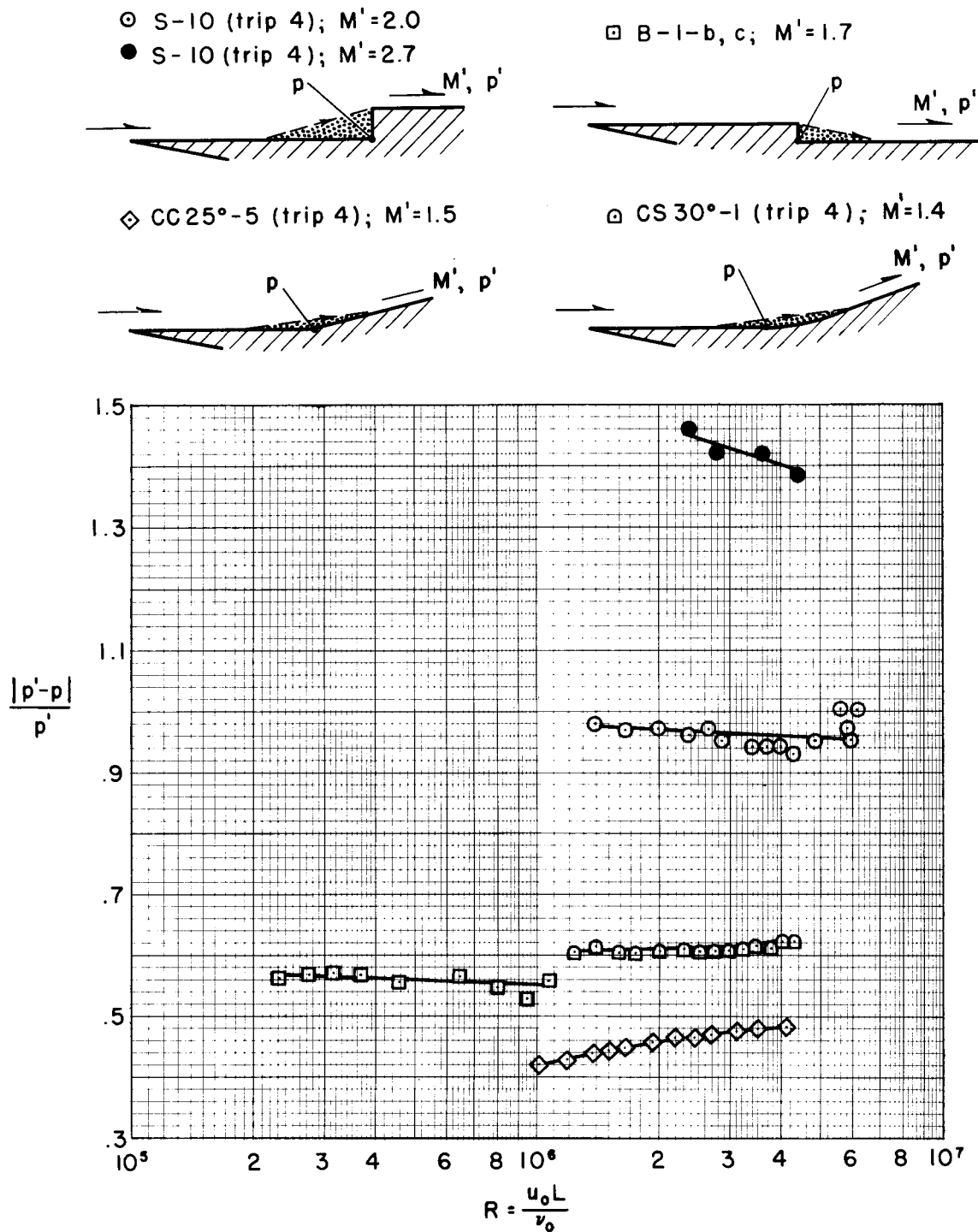


Figure 20.-Characteristic effect of Reynolds number variation on pressure differential for the three regimes.



(b) Transitional separation.

Figure 20.—Continued.



(c) Turbulent separation.

Figure 20.—Concluded.

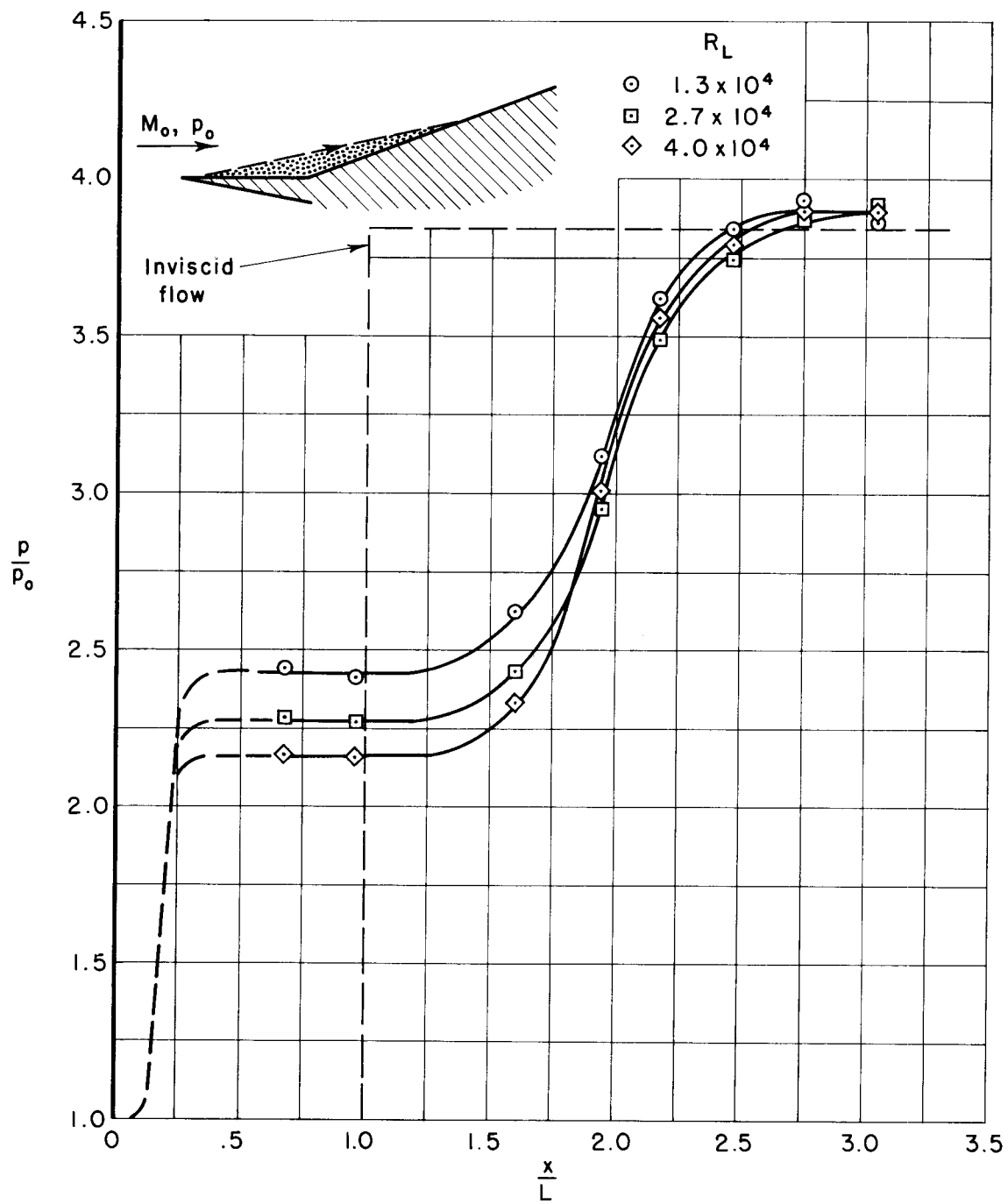
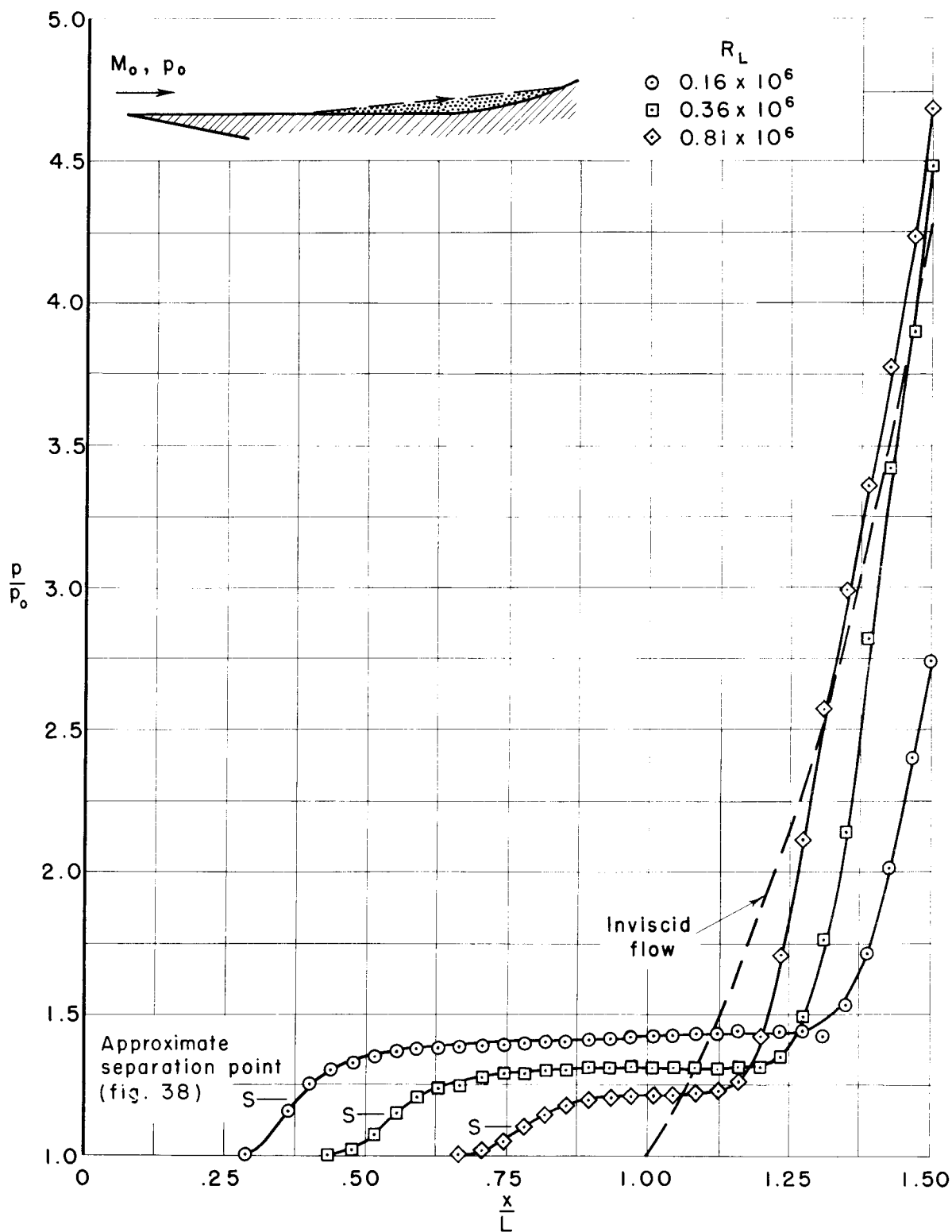
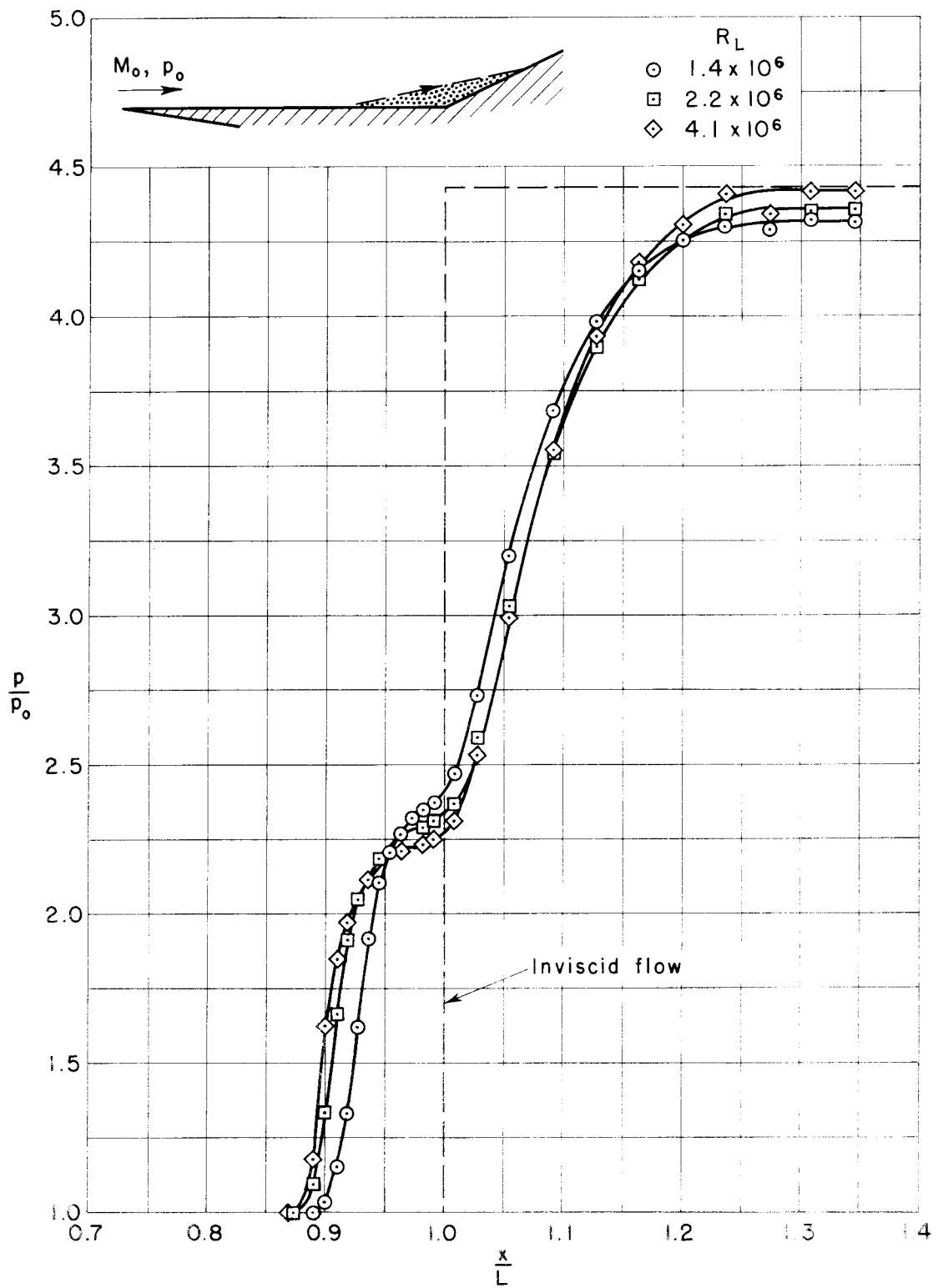
(a) Pure laminar separation; CC20°-1;  $M_0=3.0$ 

Figure 21.—Reynolds number effect on pressure distribution for the three flow regimes.

(b) Transitional separation; CS25°-1;  $M_0 = 2.7$



(c) Turbulent separation; CG25°-5 (trip 4);  $M_0 = 2.7$



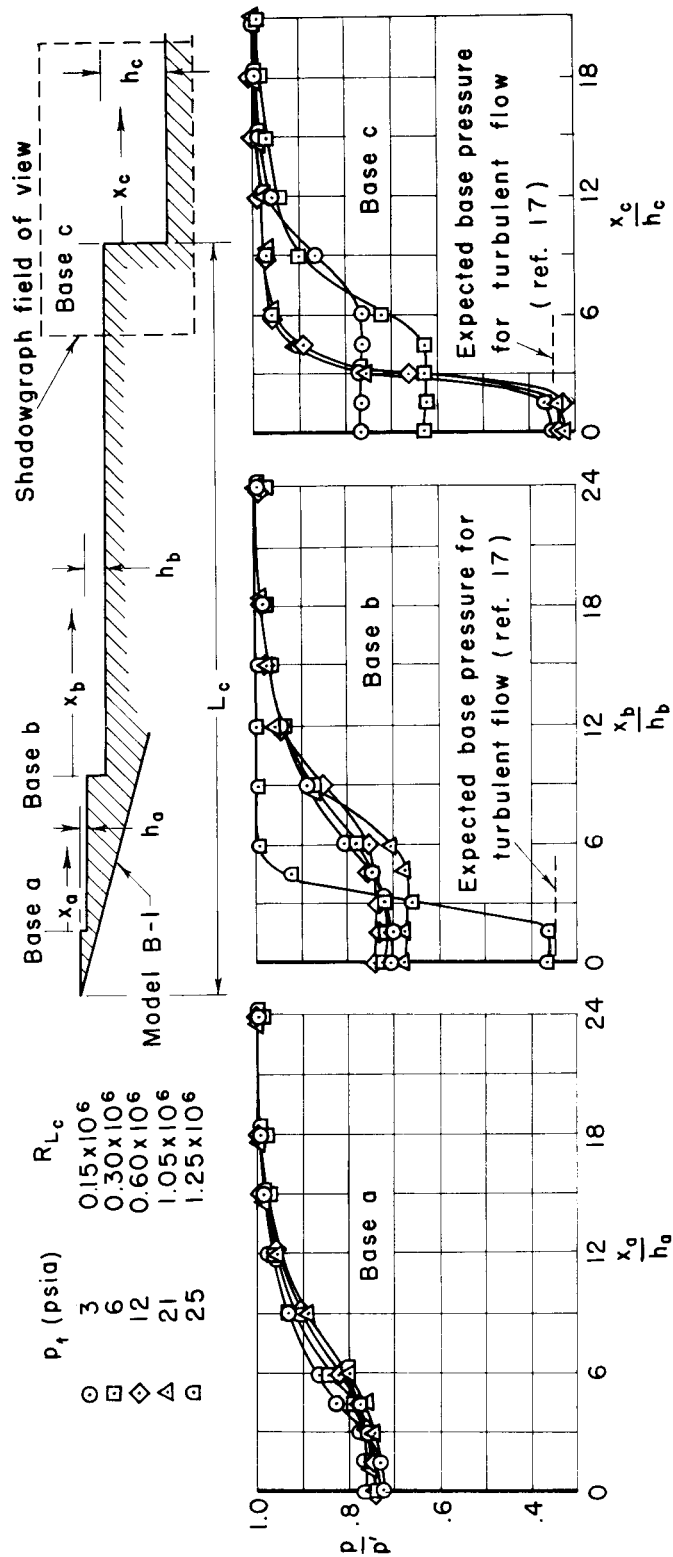
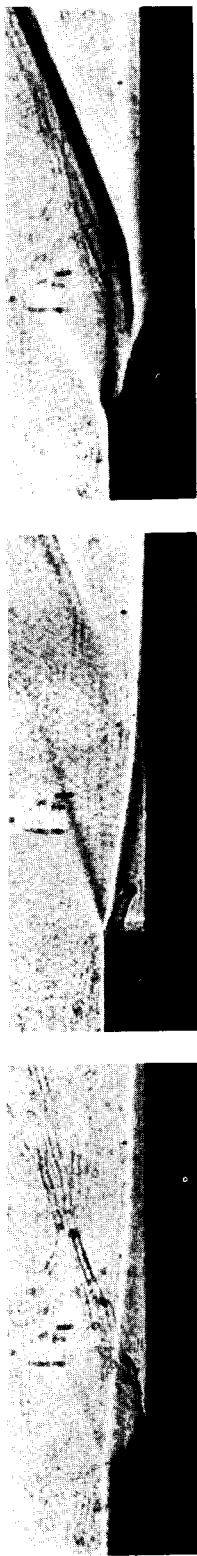
(a) Pressure distribution;  $M_0=2.0$  $\odot$   $p_t=3$  psia $\square$   $p_t=6$  psia $\diamond$   $p_t=12$  psia(b) Representative shadowgraphs of flow over base c;  $M_0=2.0$ 

Figure 22.-Model having three bases in series illustrating characteristic Reynolds number effect for each flow separation regime.

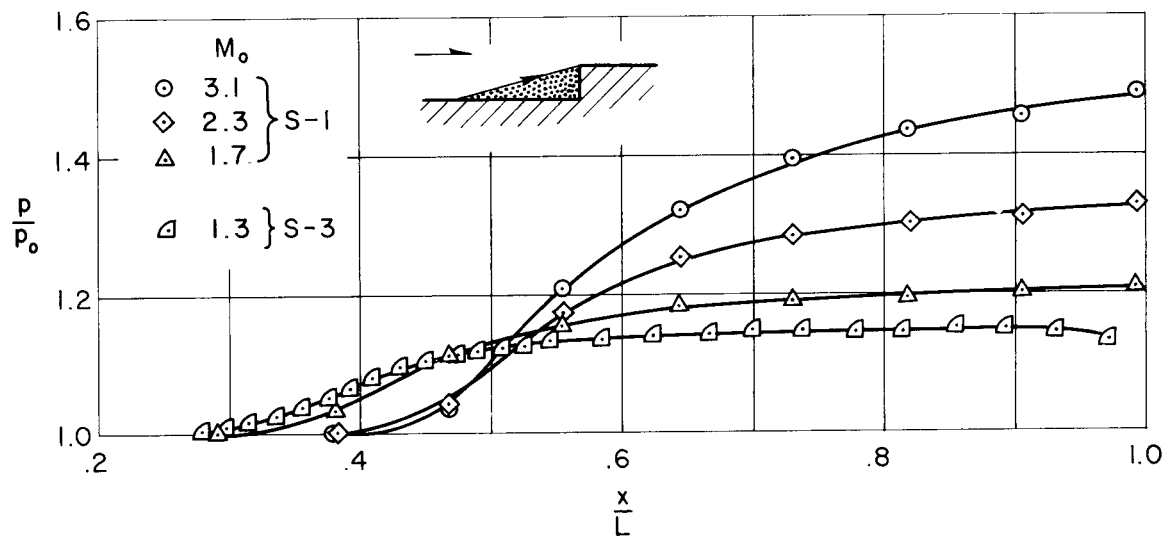
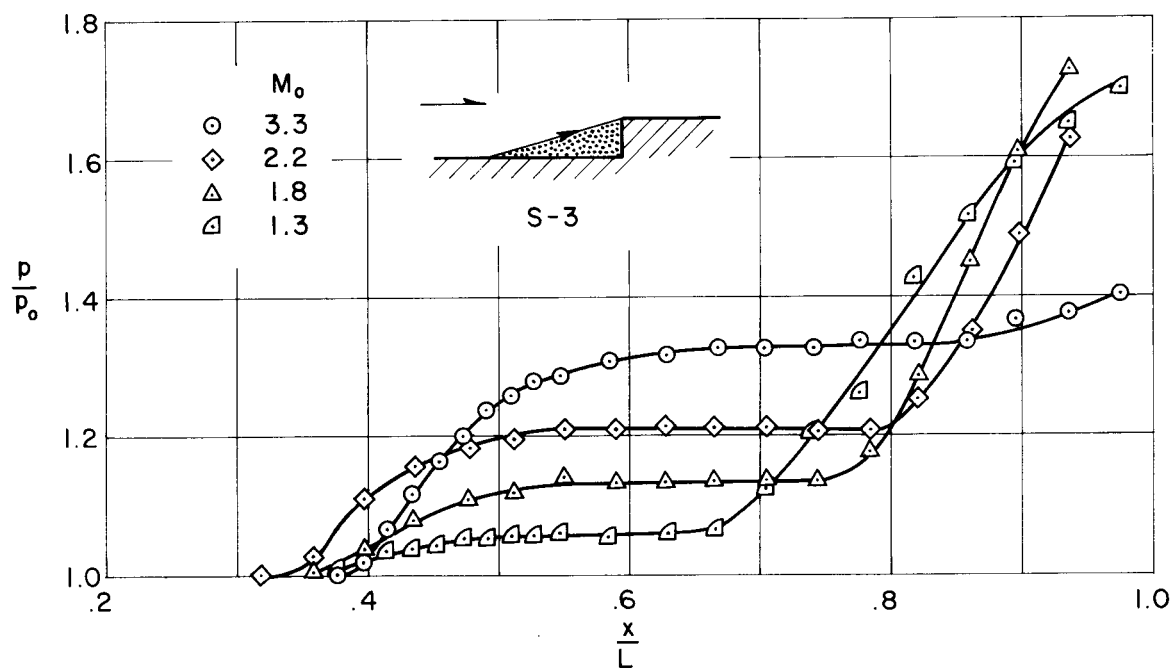
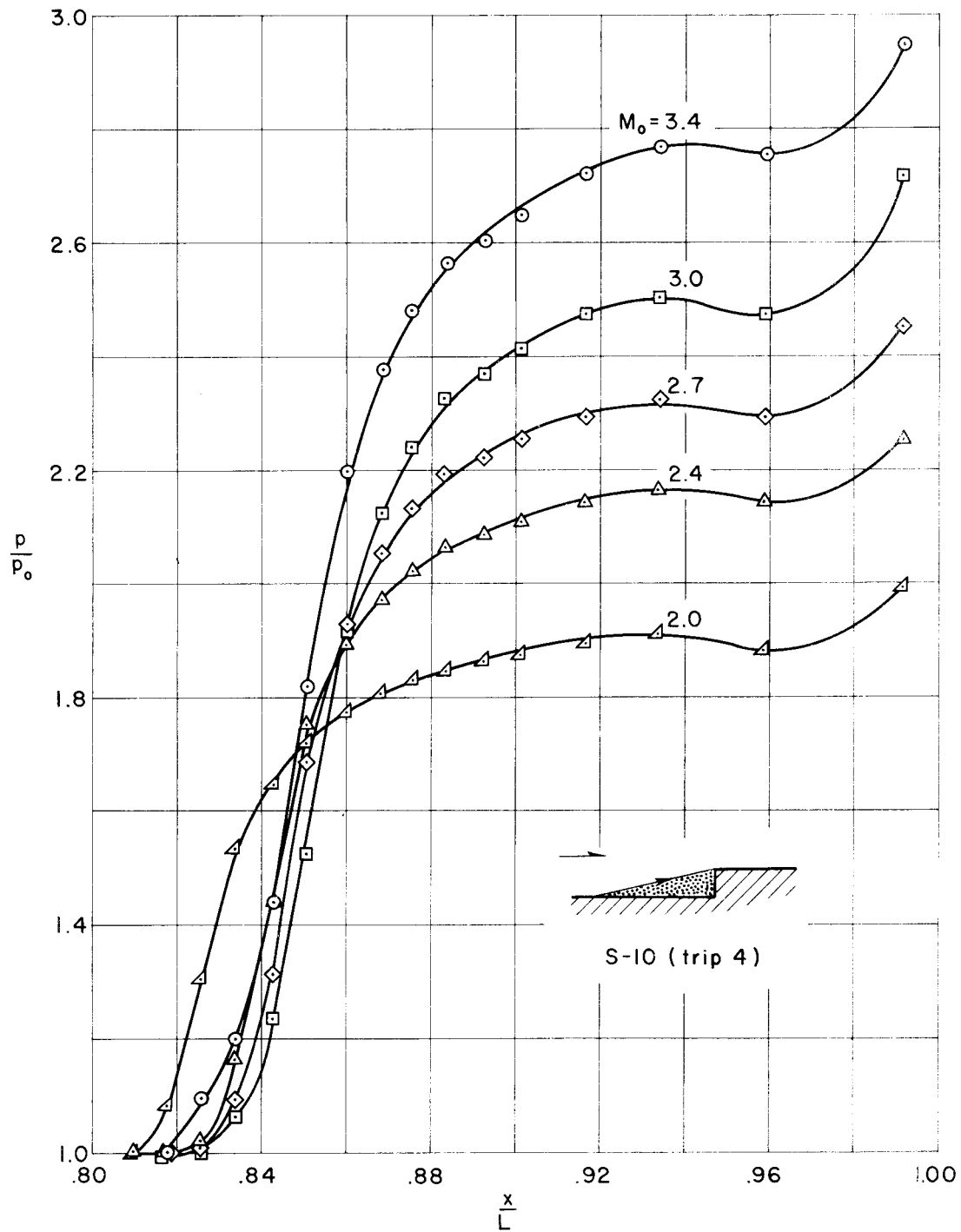
(a) Pure laminar separation;  $R_L \approx 0.13 \times 10^6$ (b) Transitional separation;  $R_L \approx 0.60 \times 10^6$ 

Figure 23.— Effect of Mach number on the pressure distribution on a step for the three flow regimes.

(c) Turbulent separation;  $R_L \approx 2.6 \times 10^6$

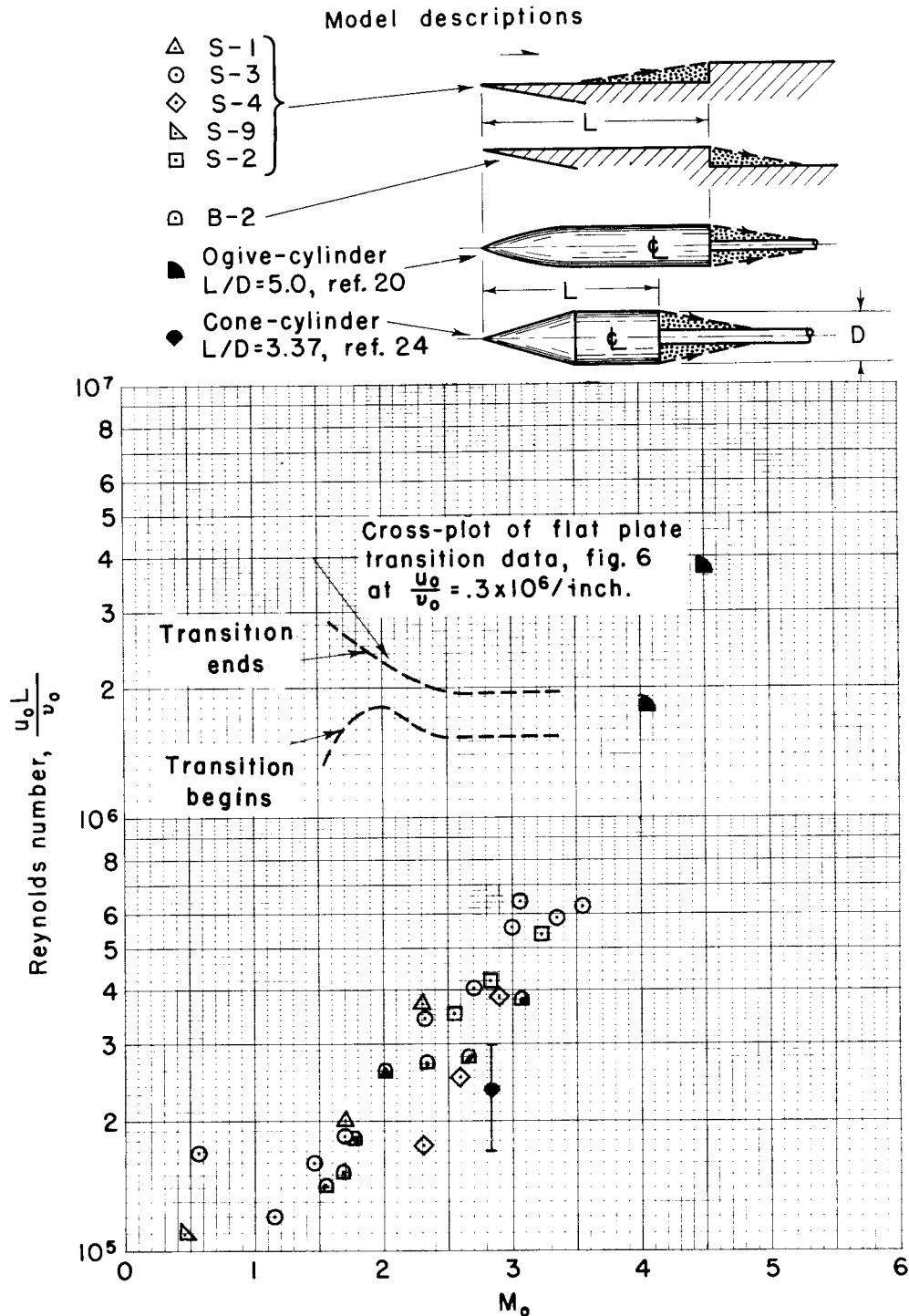
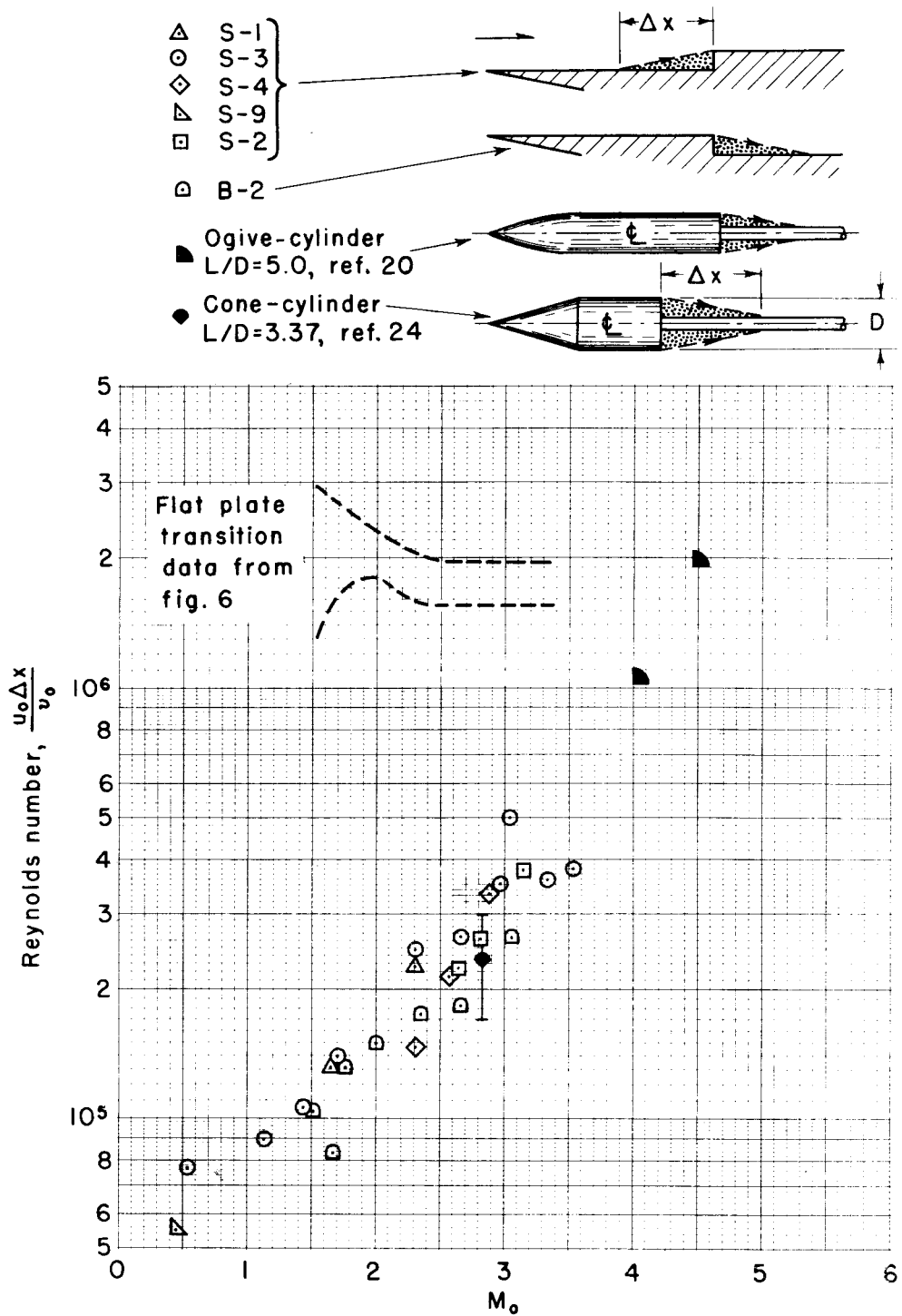


Figure 24.—Maximum Reynolds number for pure laminar type separation.



(b) Reynolds number based on length of separated layer.

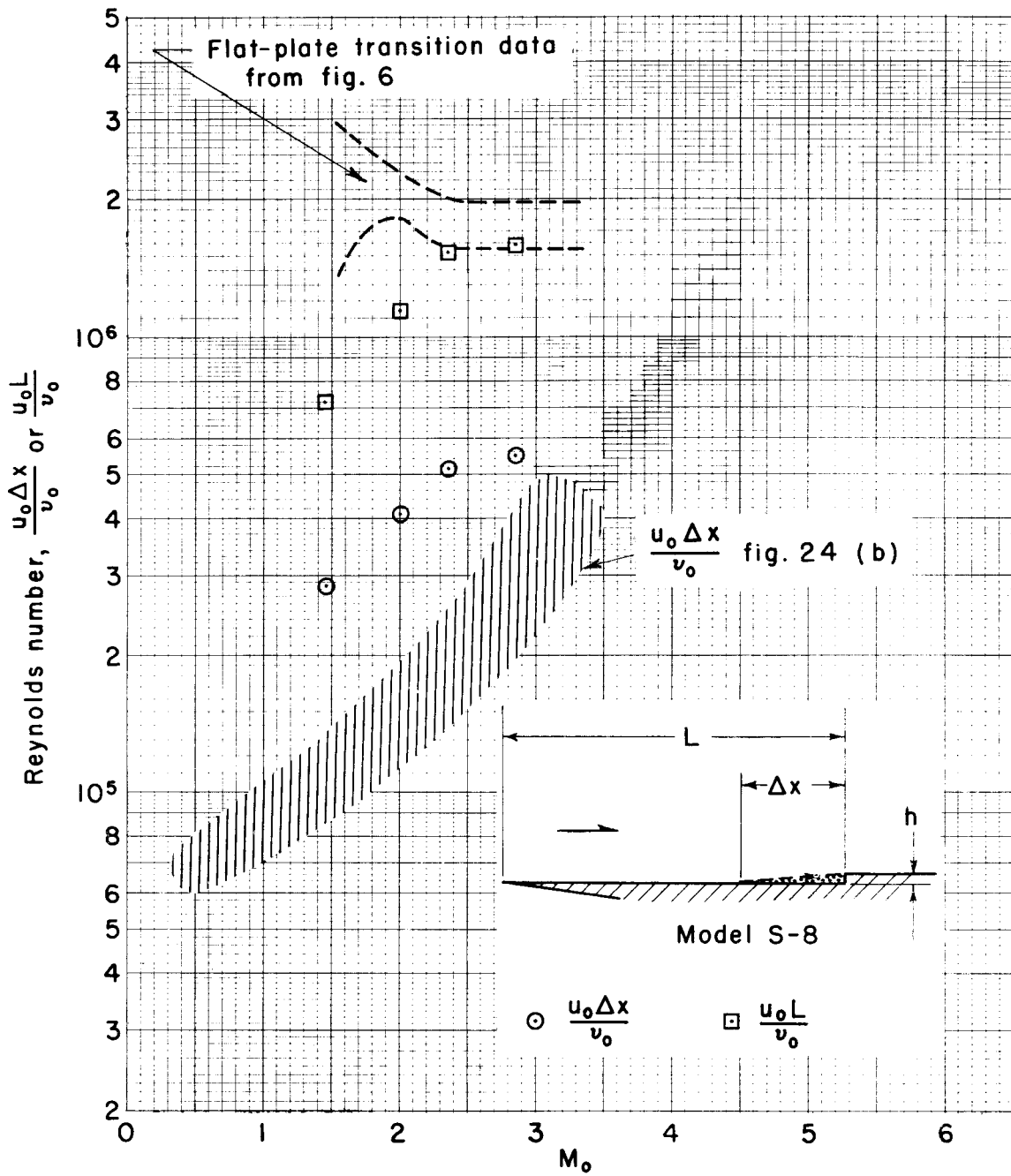


Figure 25.-Maximum Reynolds number for pure laminar separation on step of small height;  $\frac{h}{L} = .009$

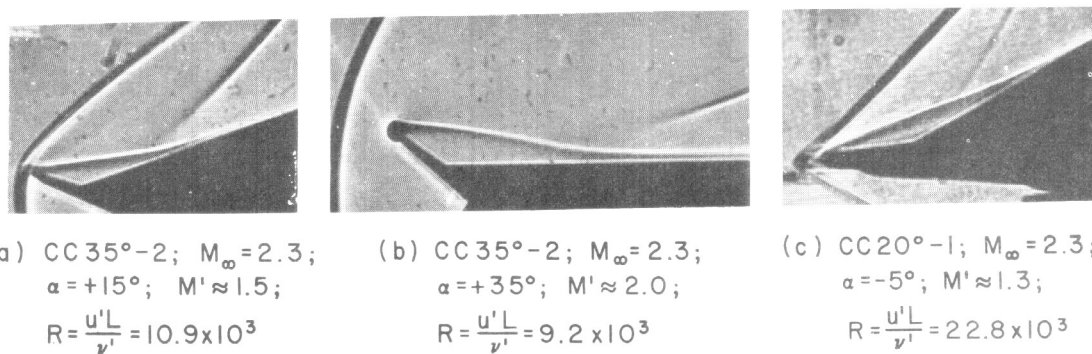


Figure 26.— Pure laminar separations with negligible boundary-layer thickness at separation.

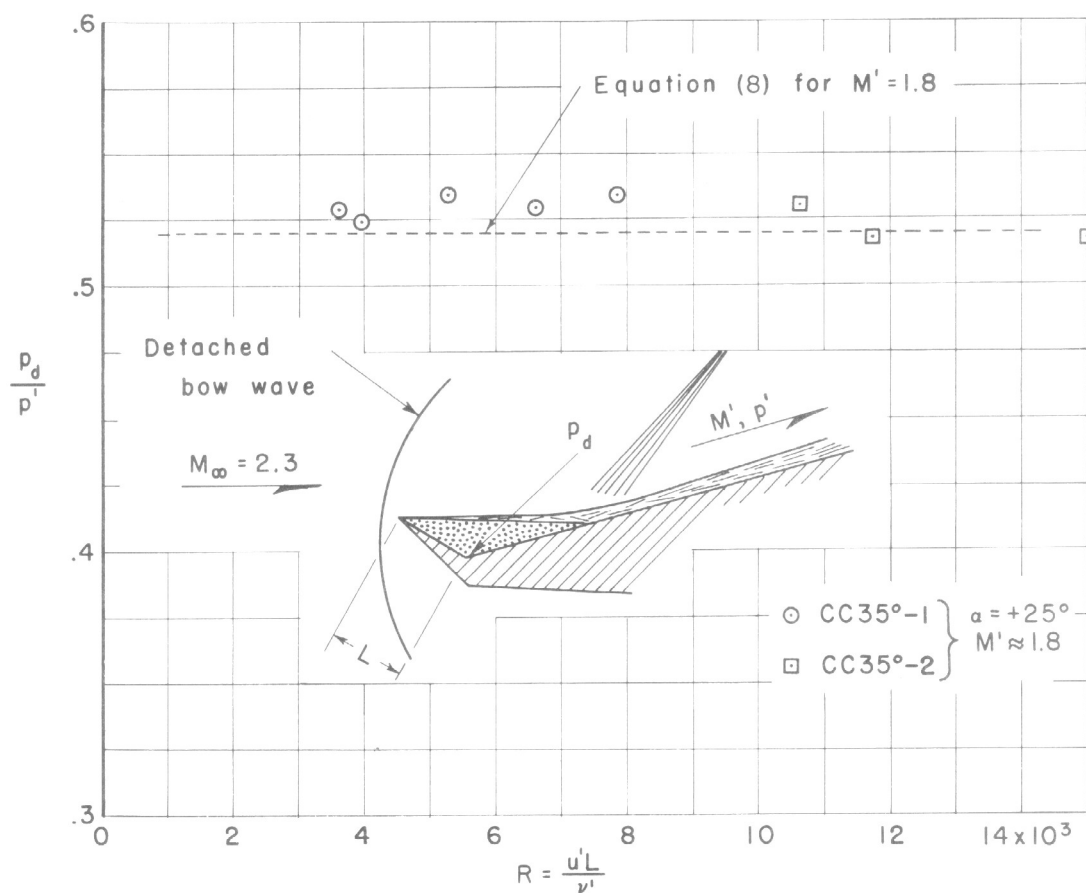


Figure 27.— Absence of significant Reynolds number effect on dead-air pressure for wedge models with leading-edge laminar separation.

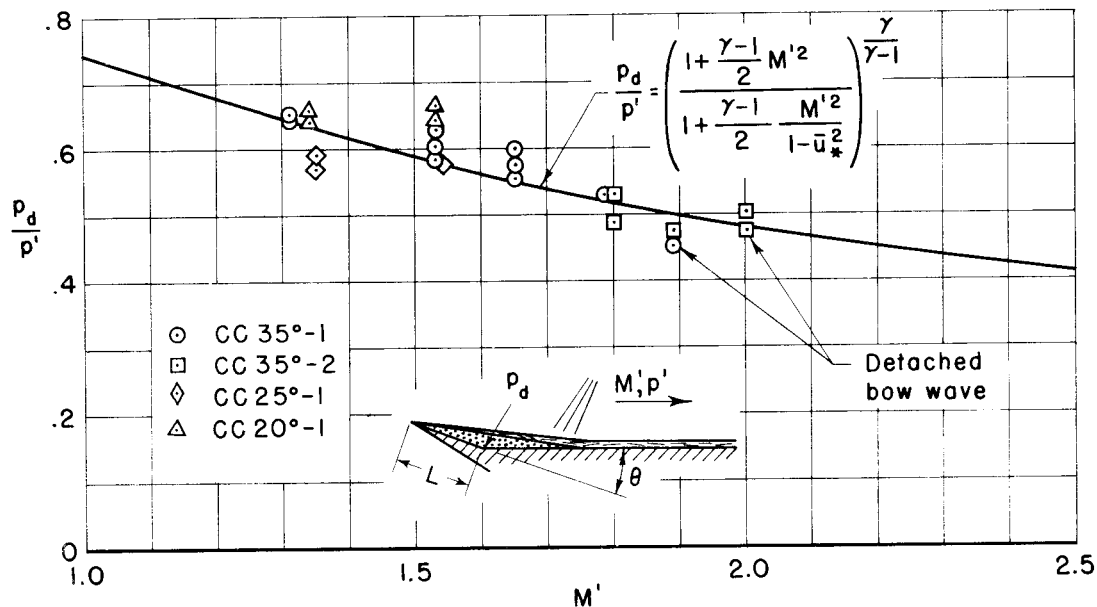


Figure 28.—Comparison of theory and experiment for pure laminar separations with negligible boundary-layer thickness at separation.

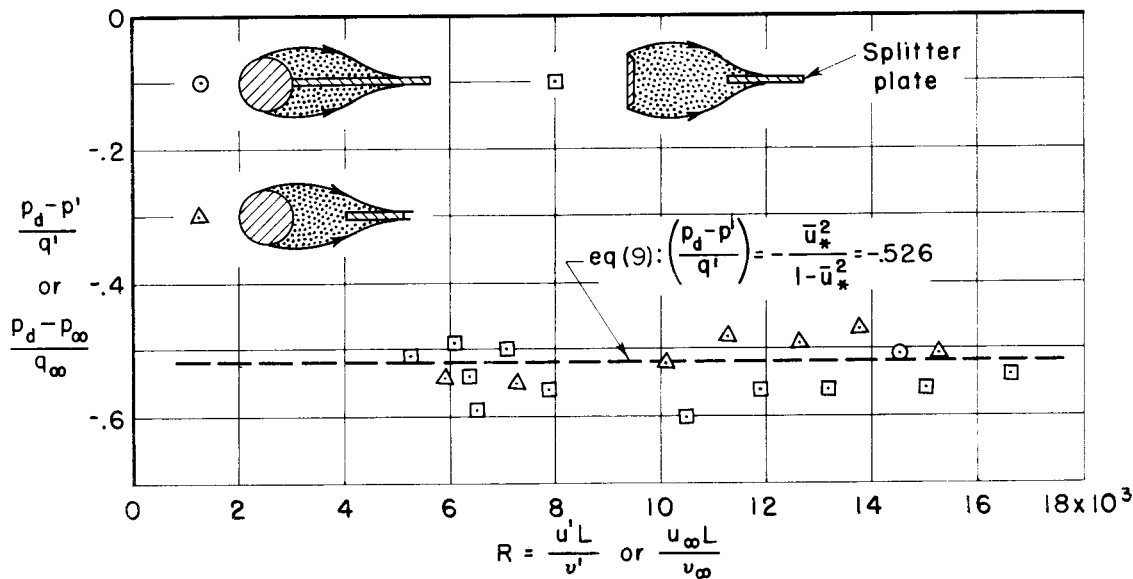


Figure 29.—Comparison of theory with experiments of Roshko conducted at low speed;  $M' \approx 0$



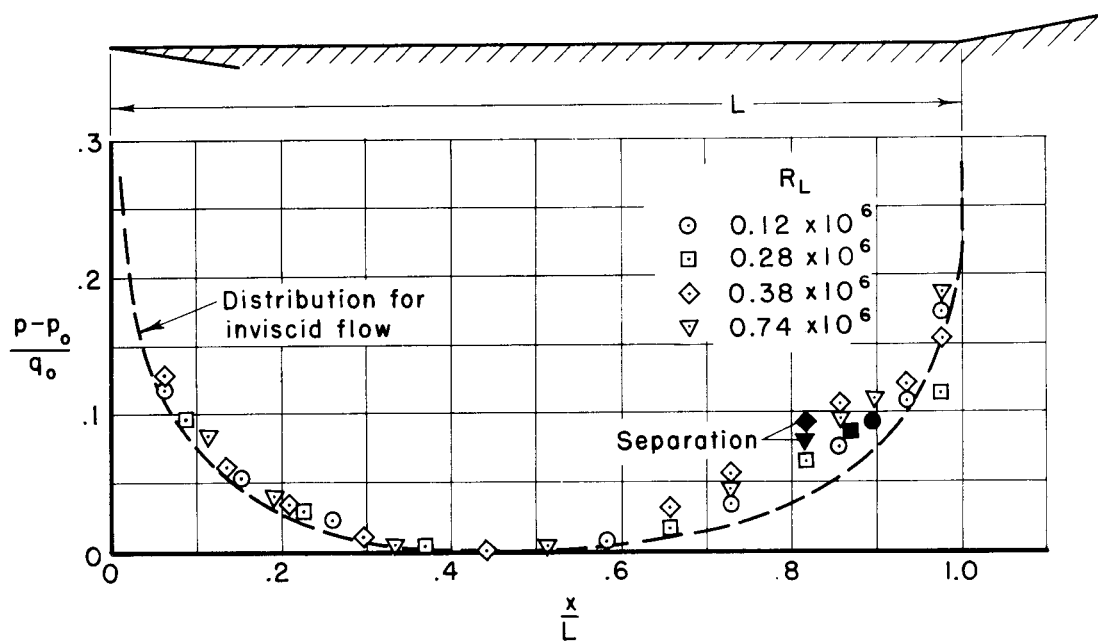
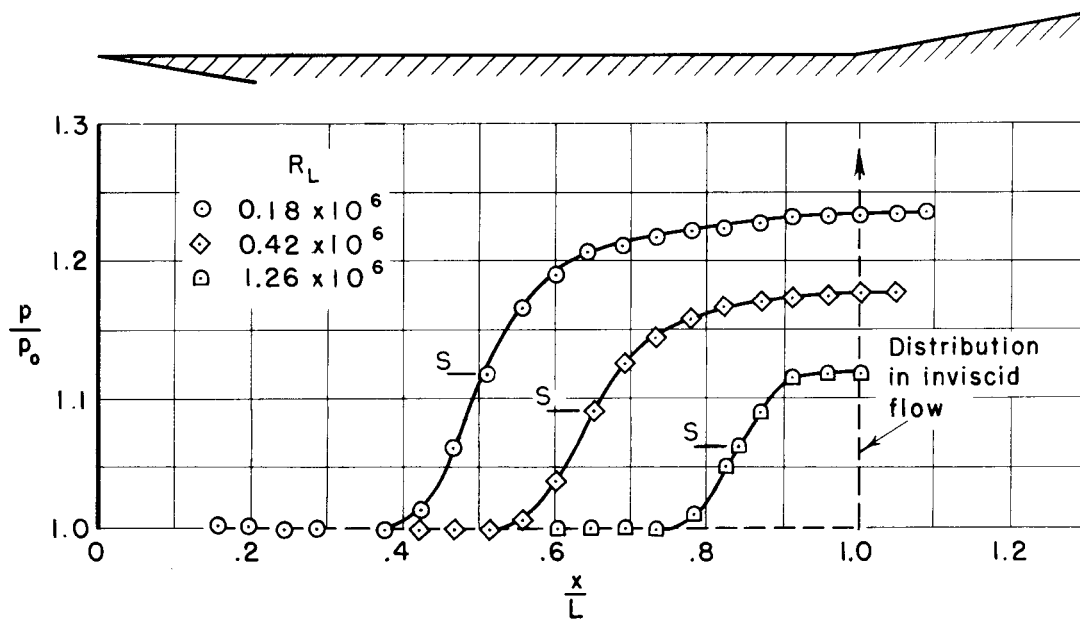
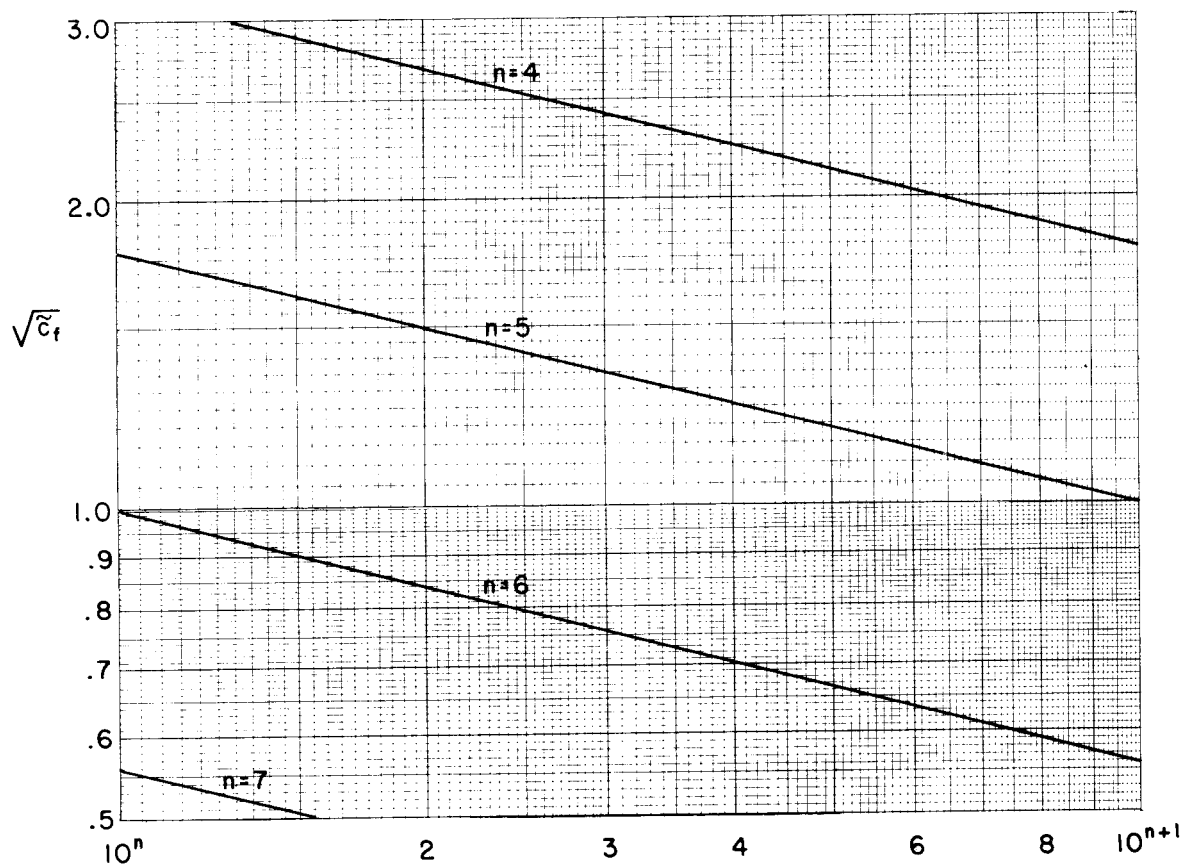
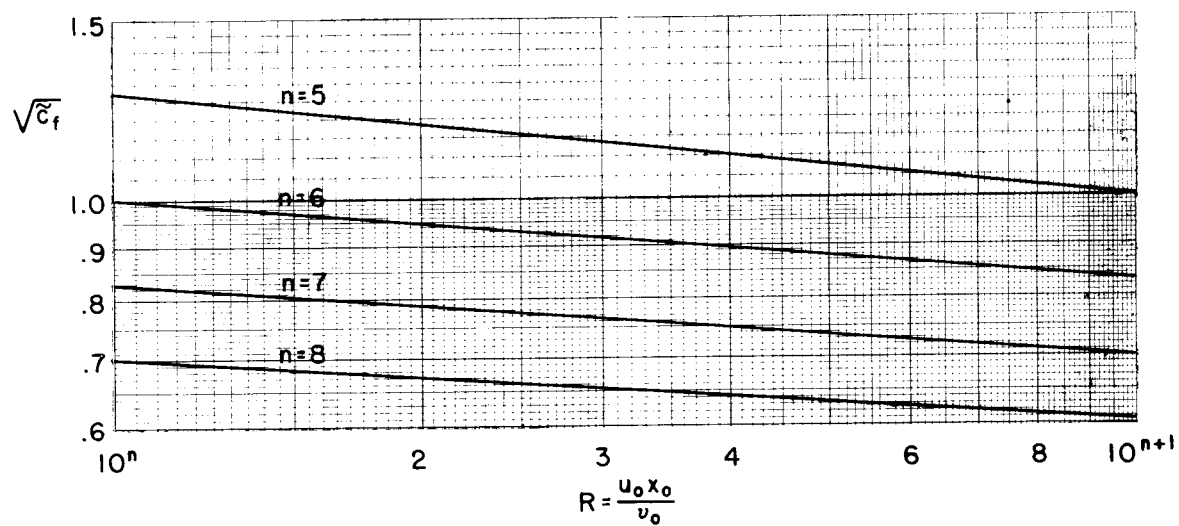
(a) Subsonic;  $CC10^\circ-3$ ;  $0.4 < M_\infty < 0.8$ ;  $\alpha = -4^\circ$ (b) Supersonic;  $CC10^\circ-2$ ;  $M_0 = 2.0$ 

Figure 30.—Comparison of subsonic and supersonic flows at various Reynolds numbers.



(a) Laminar flow.



(b) Turbulent flow.

Figure 31.—Square root of local skin friction as function of Reynolds number.

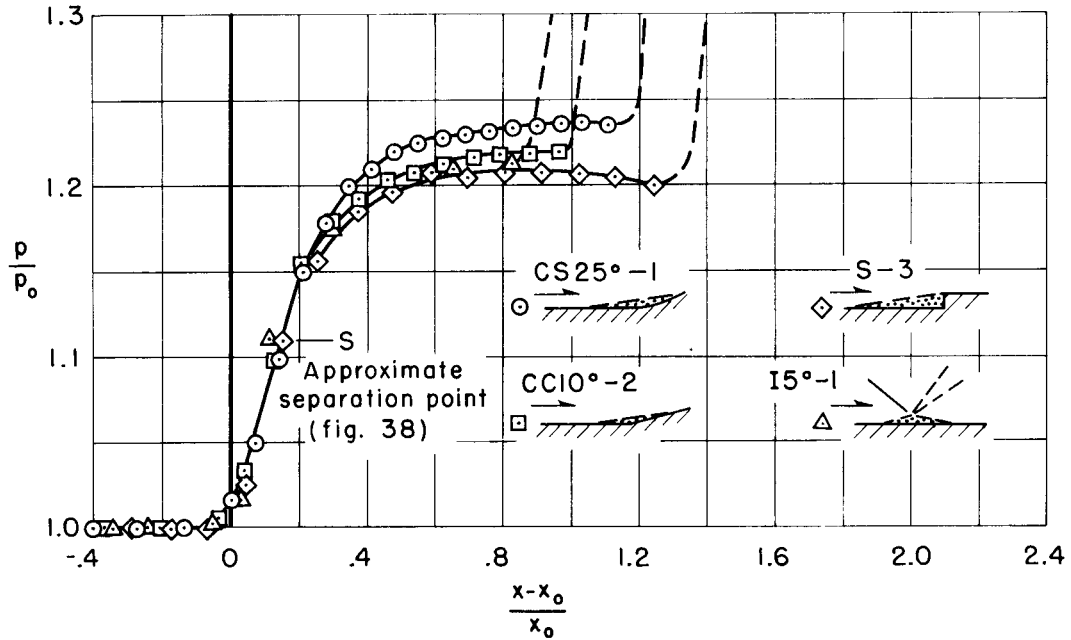


Figure 32.—Independence of pressure distribution and method of inducing laminar separation;  $M_0=2.3$ ;  $R_{x_0}=0.20 \pm .01 \times 10^6$ .

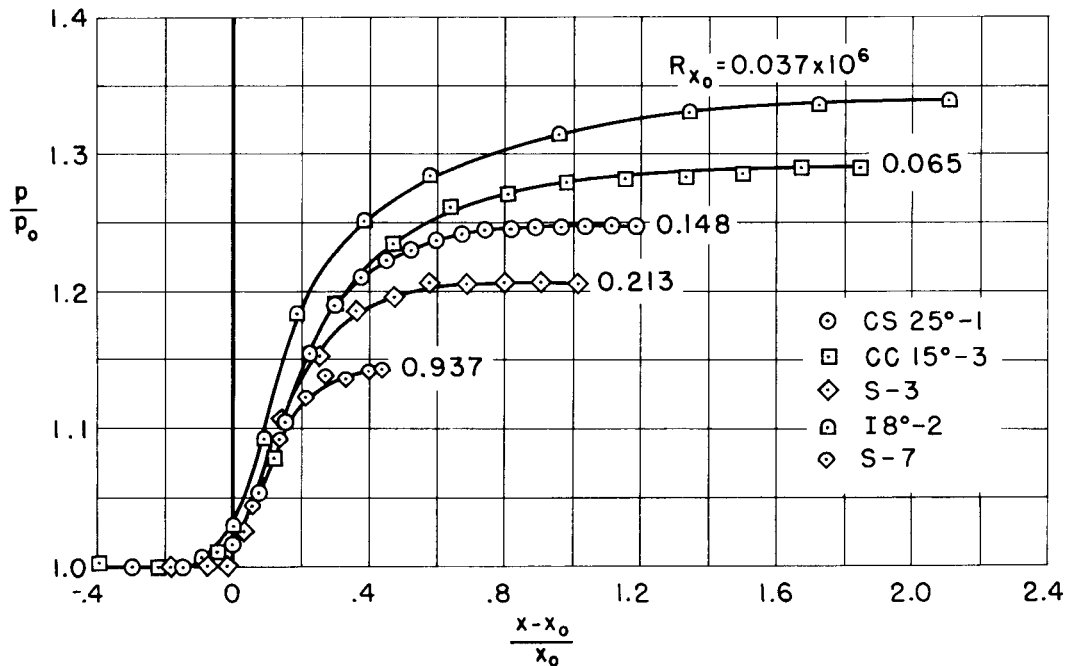


Figure 33.—Effect of Reynolds number on pressure distribution in laminar separation;  $M_0=2.3$ .

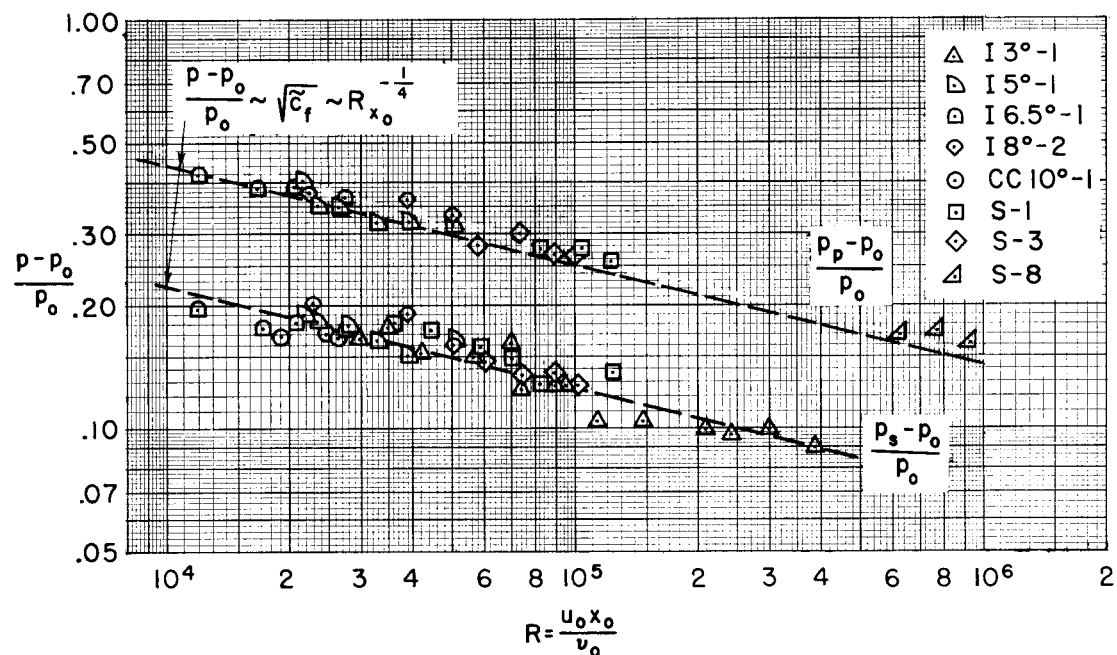
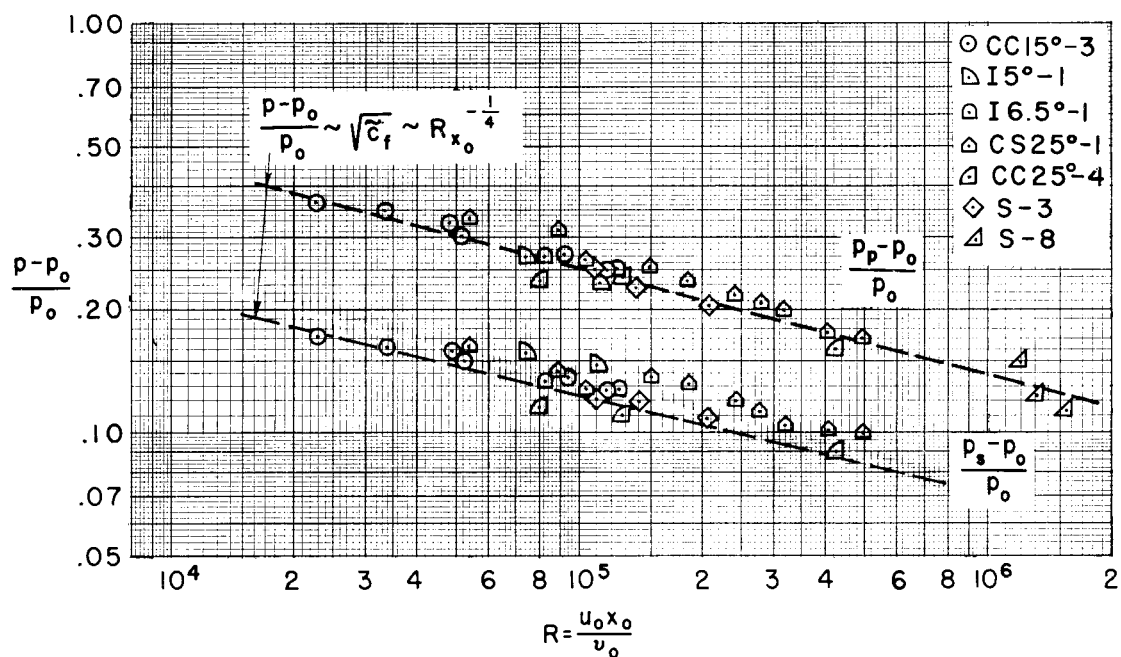
(a) Pure laminar separation;  $M_0 = 2.3$ (b) Transitional separation.  $M_0 = 2.3$ 

Figure 34.—Effect of Reynolds number on pressure rise to separation and plateau pressure.

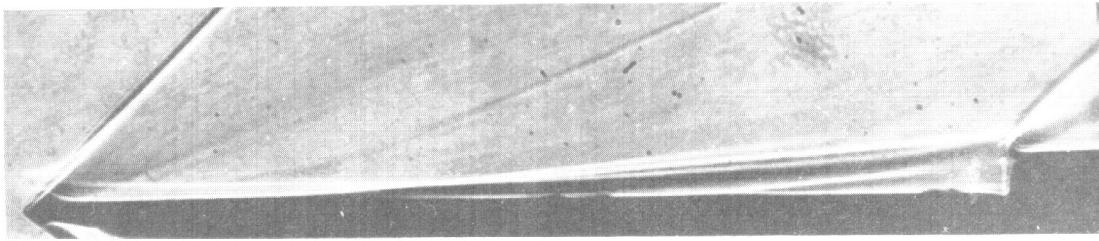


Figure 35.-Shadowgraph indicating lack of two-dimensional flow;  
S-3;  $M_0=3.0$ ;  $R_L=0.57 \times 10^6$ .

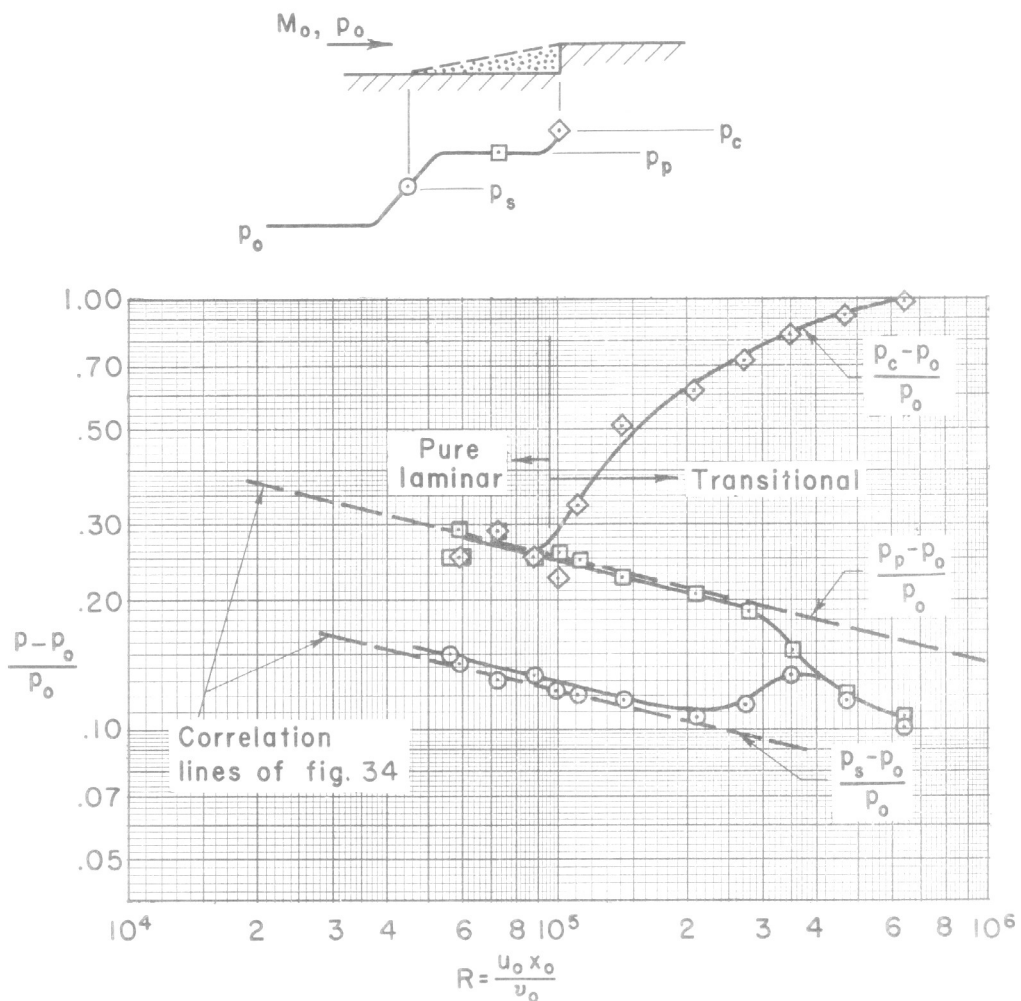


Figure 36.-Data illustrating restriction for correlation of transitional data; S-3;  $M_0=2.3$ .

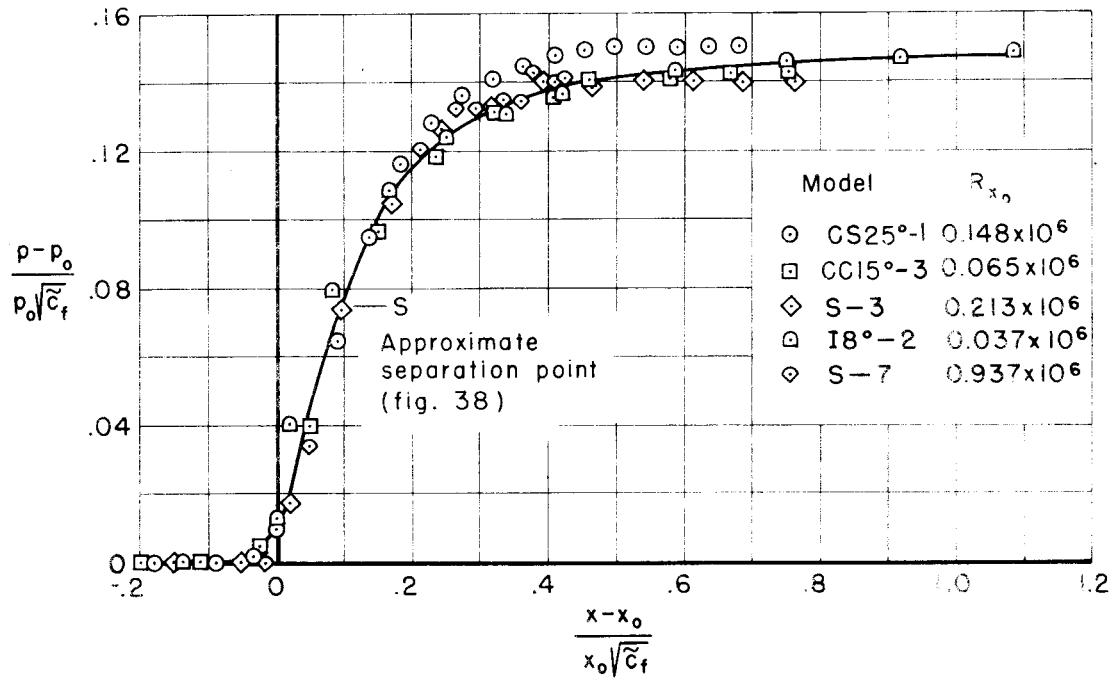


Figure 37.—Correlation of pressure distribution for laminar separation for various model configurations and Reynolds numbers;  $M_0=2.3$

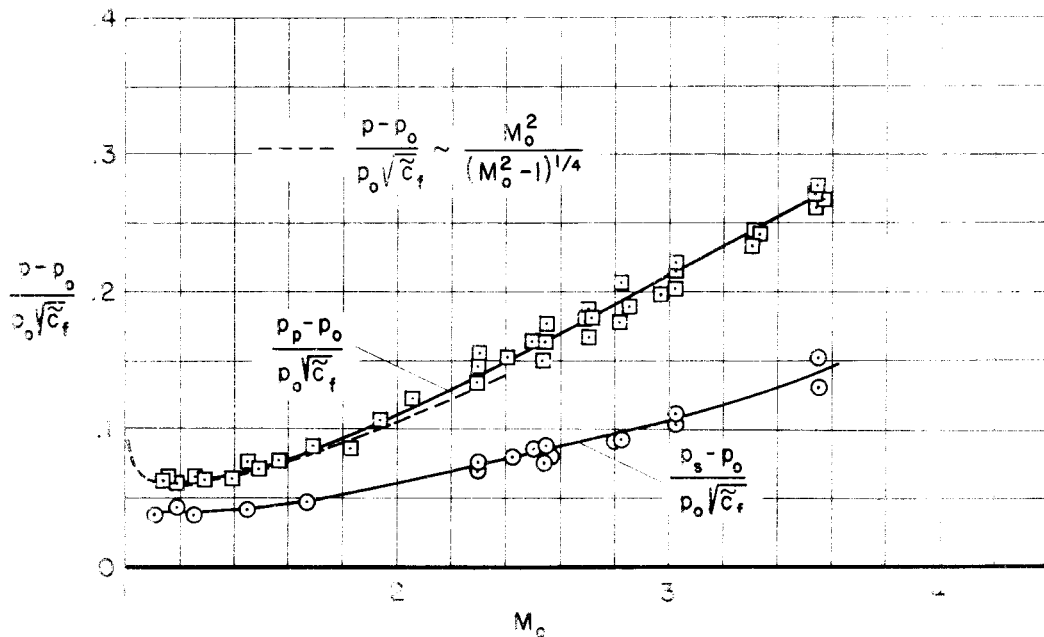


Figure 38.—Effect of Mach number on characteristics of laminar separation for a series of model configurations and Reynolds numbers.

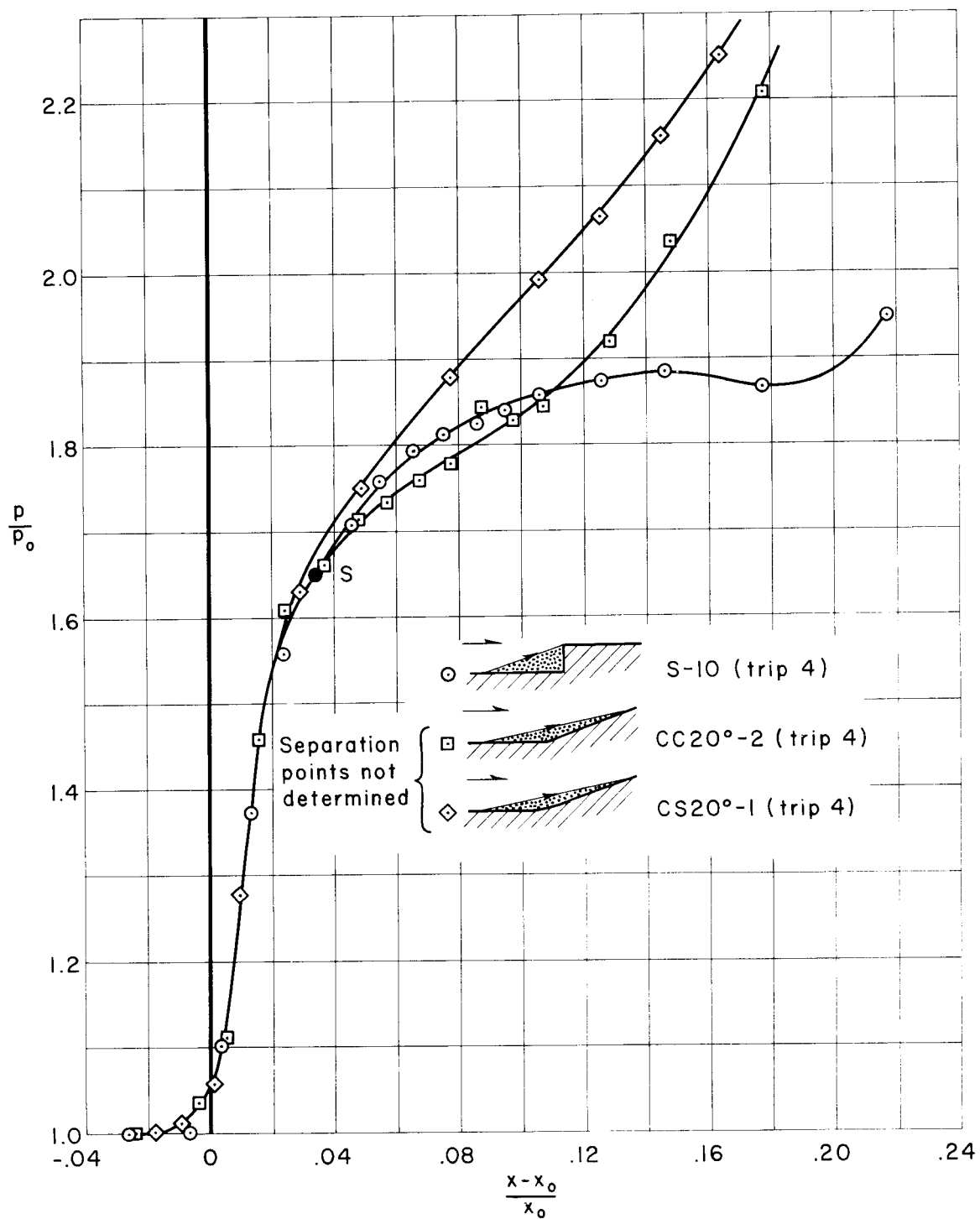
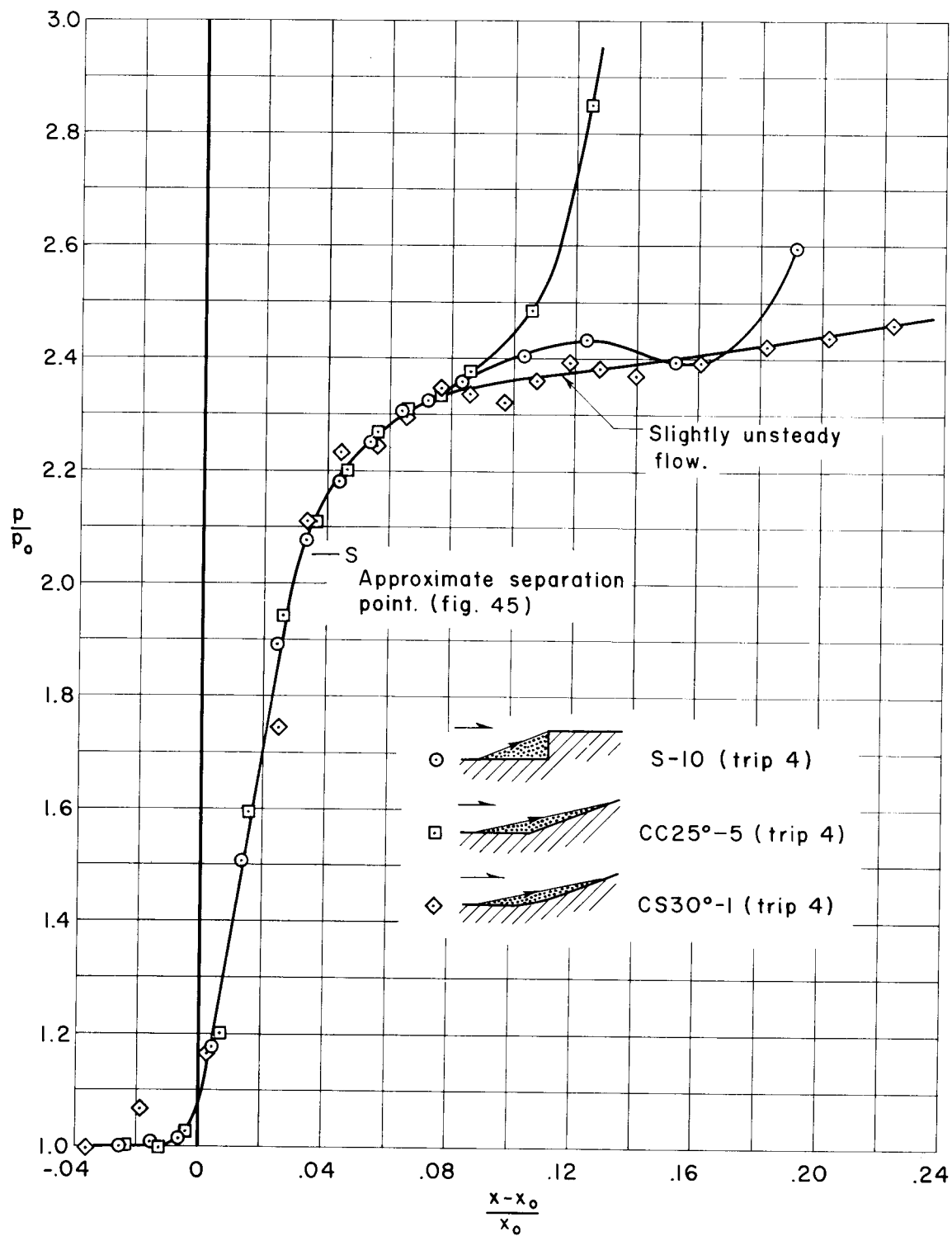
(a)  $M_0=2.0$ ;  $R_{x_0}=3.1 \times 10^6$ 

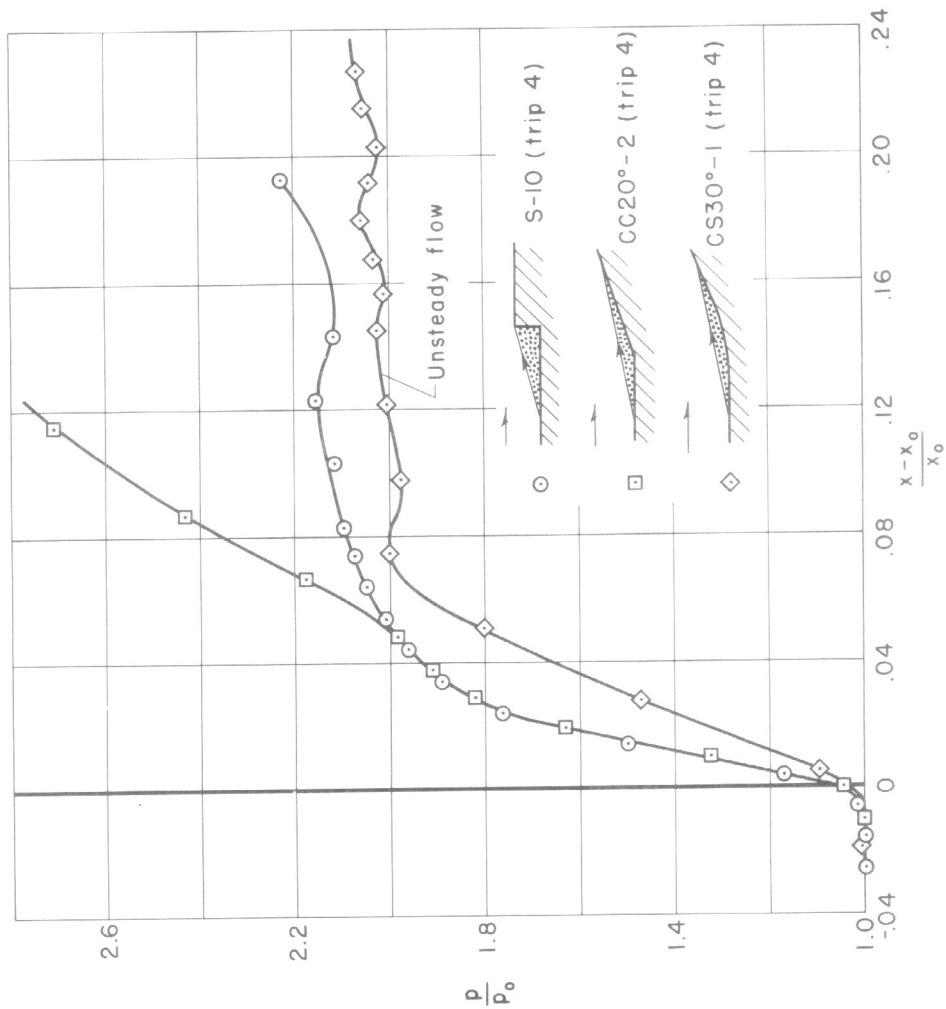
Figure 39.—Effect of body shape on the pressure distribution for turbulent separation at a fixed Mach number and Reynolds number.



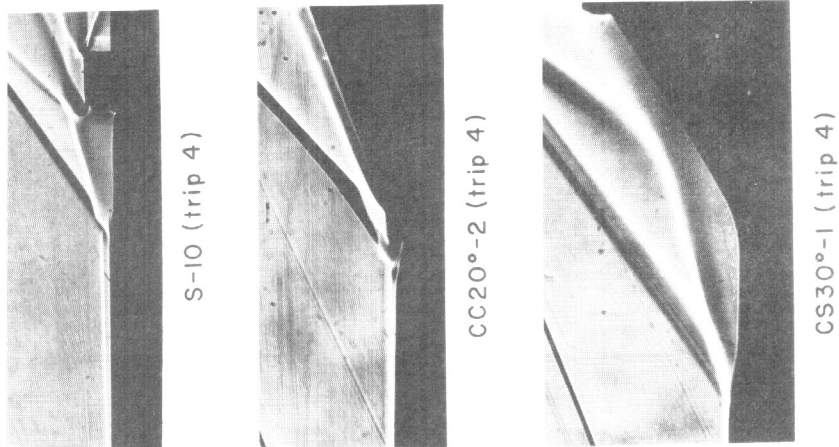
(b)  $M_0=3.0$ ;  $R_{x_0}=3.1 \times 10^6$

Figure 39.—Concluded.





(a) Pressure distribution.



(b) Shadowgraphs.

Figure 40.— Effects of flow unsteadiness on the pressure distribution and the corresponding shadowgraphs for turbulent separation;  $M_0 = 2.4$ ;  $R_{x_0} = 2.7 \times 10^6$ .

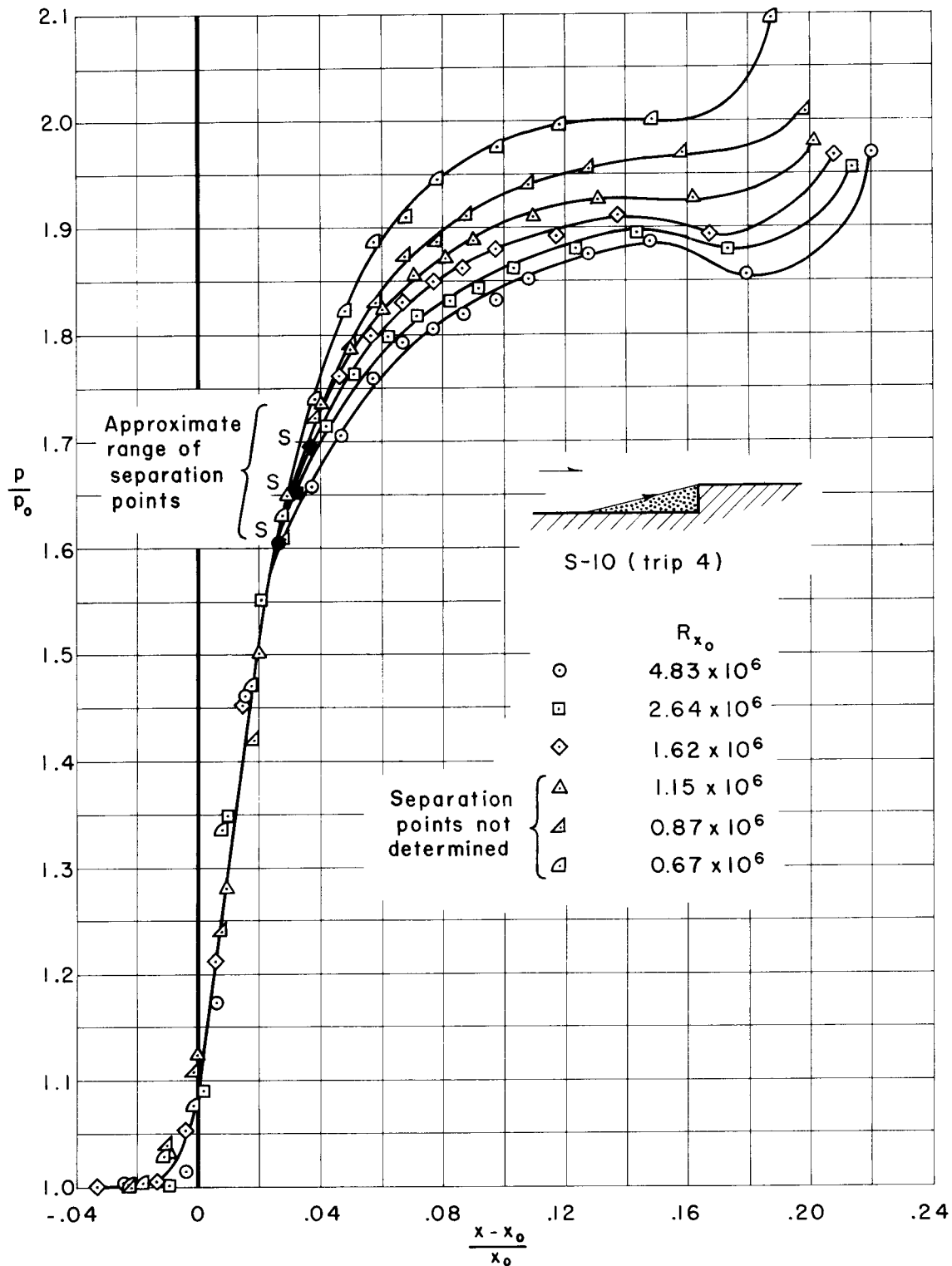
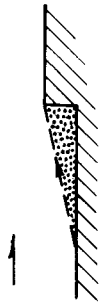


Figure 41.—Effect of Reynolds number on the pressure distribution for a step with turbulent separation;  $M_0=2.0$ .

Open symbol—Transition near the base of the boundary-layer trip.

Filled symbol— Transition location between the base of the boundary-layer trip and the beginning of pressure rise; therefore the correct Reynolds number is less than the value shown.



S-10 (trip 4)

$$\frac{P_p - P_o}{P_o} \sim \sqrt{C_f} \quad (\text{See fig. 31})$$

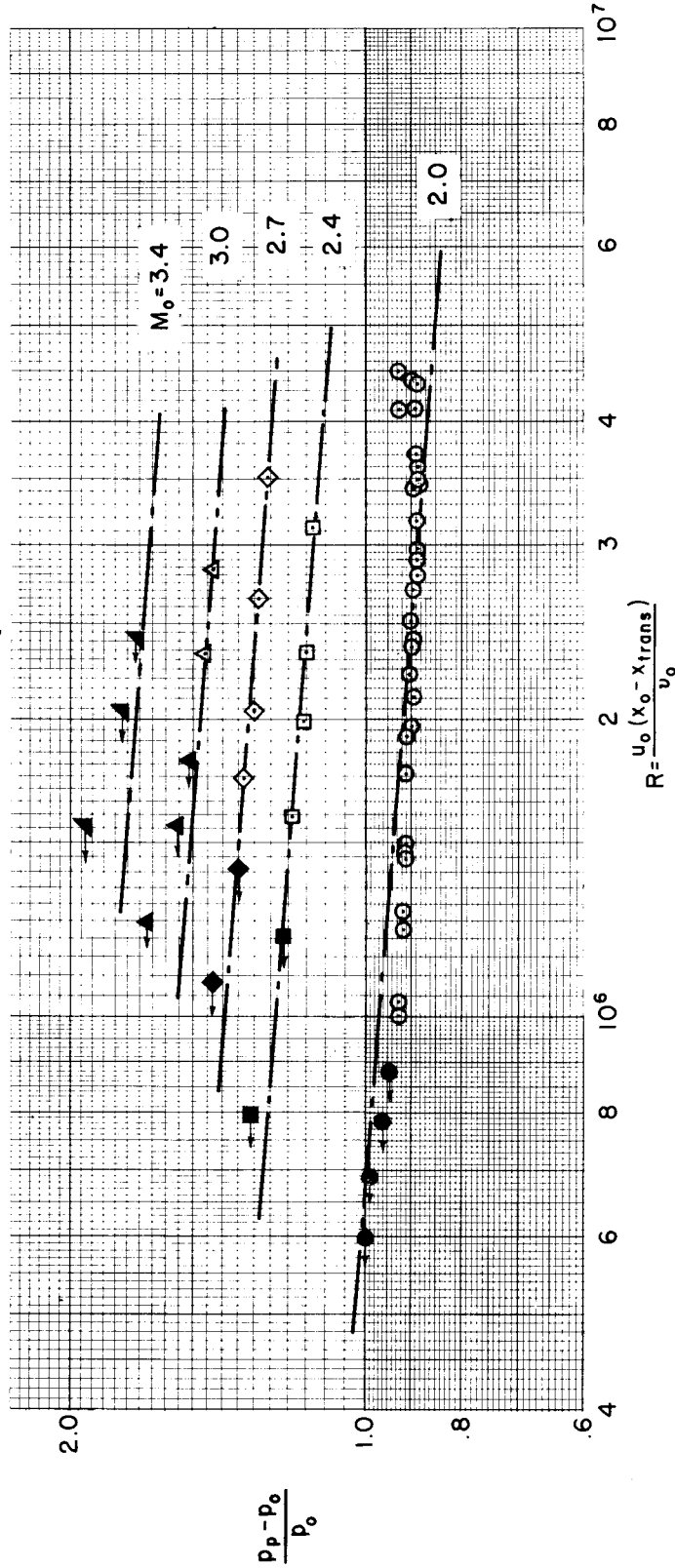


Figure 42.—Reynolds number effect on the peak pressure ratio for a step with turbulent separation at various Mach numbers.

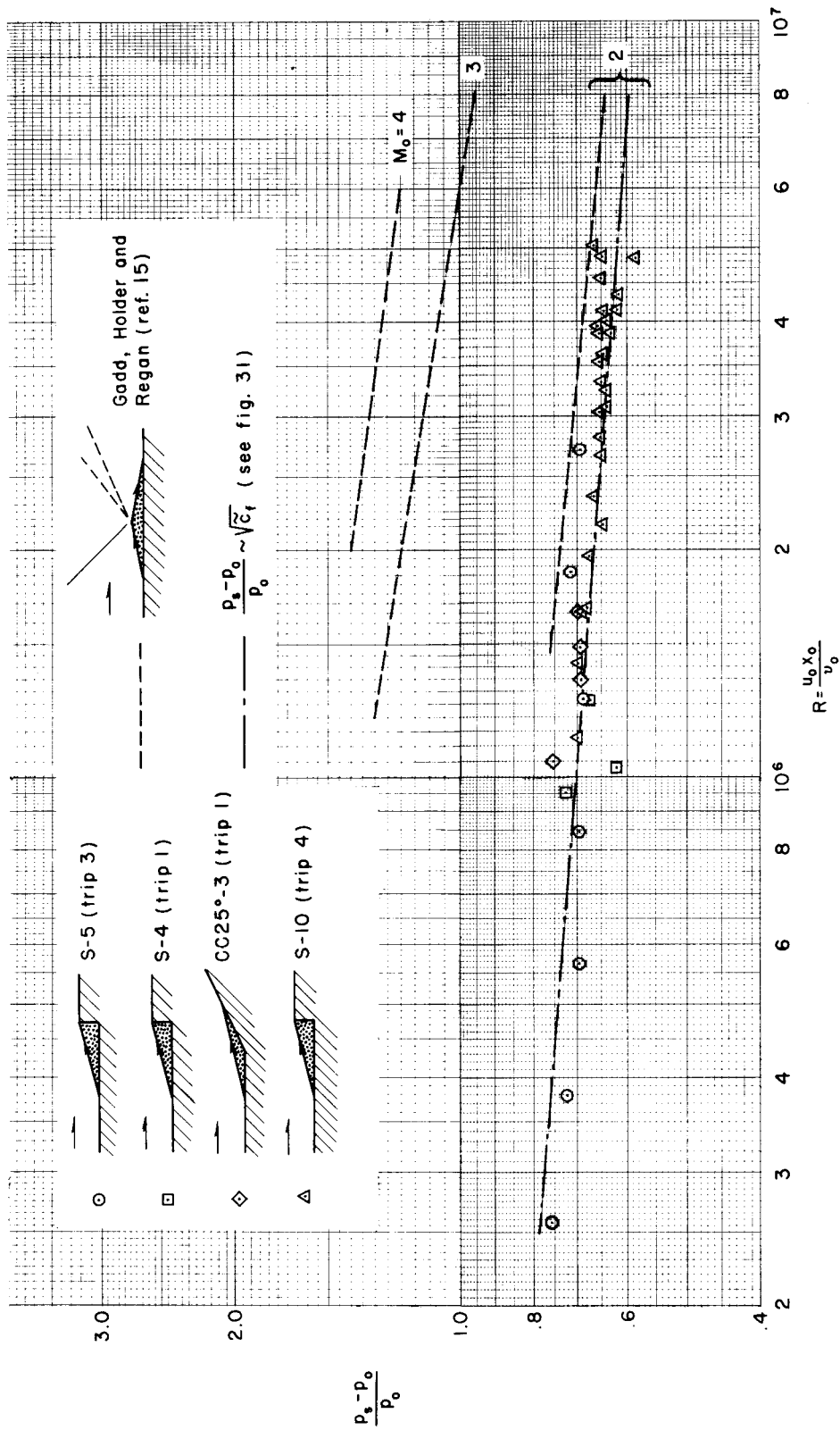


Figure 43.—Reynolds number effect on pressure rise to turbulent separation for various Mach numbers.

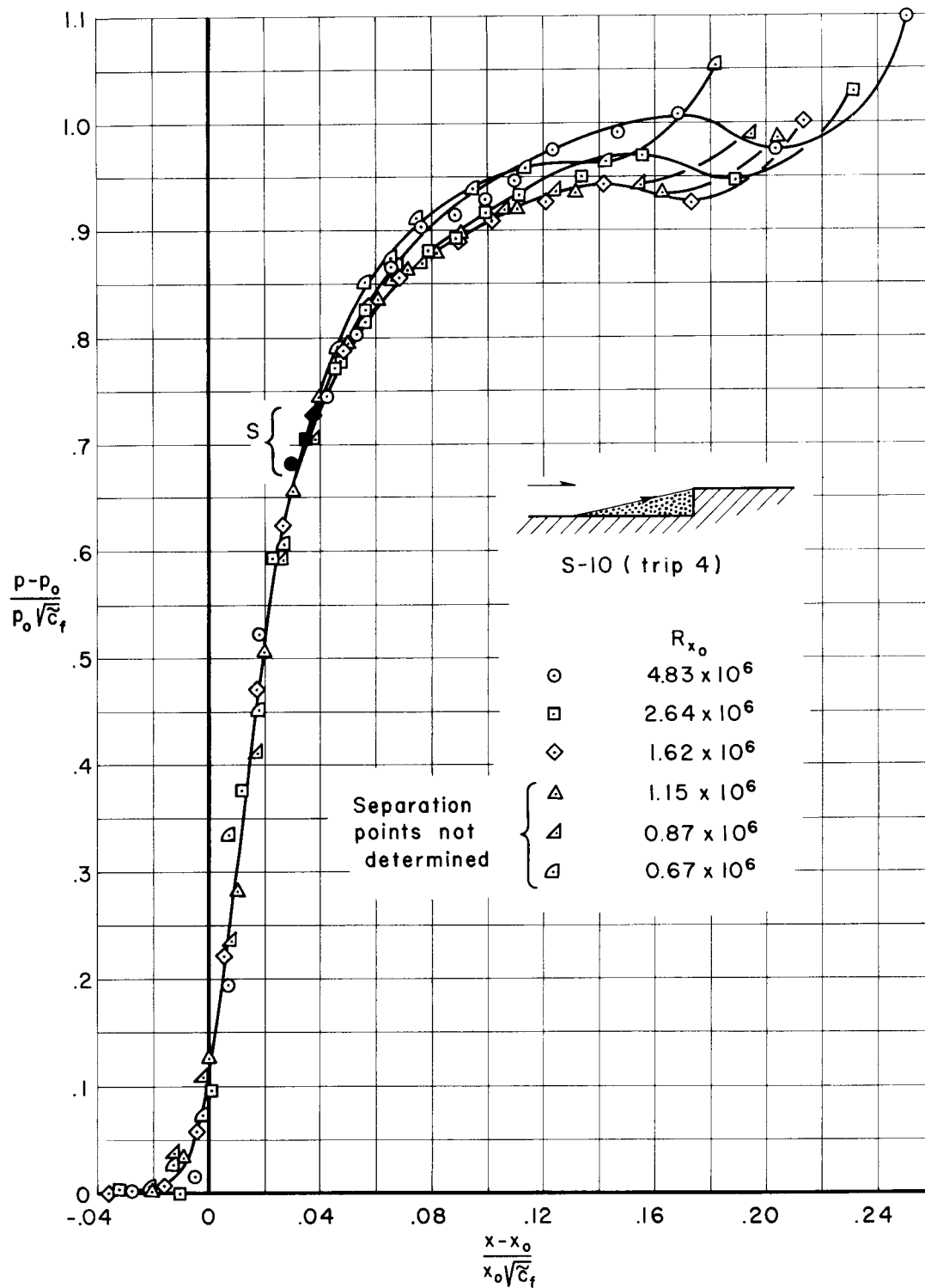


Figure 44.-Correlation of pressure distribution at various Reynolds numbers for turbulent separation over a step;  $M_0 = 2.0$ .

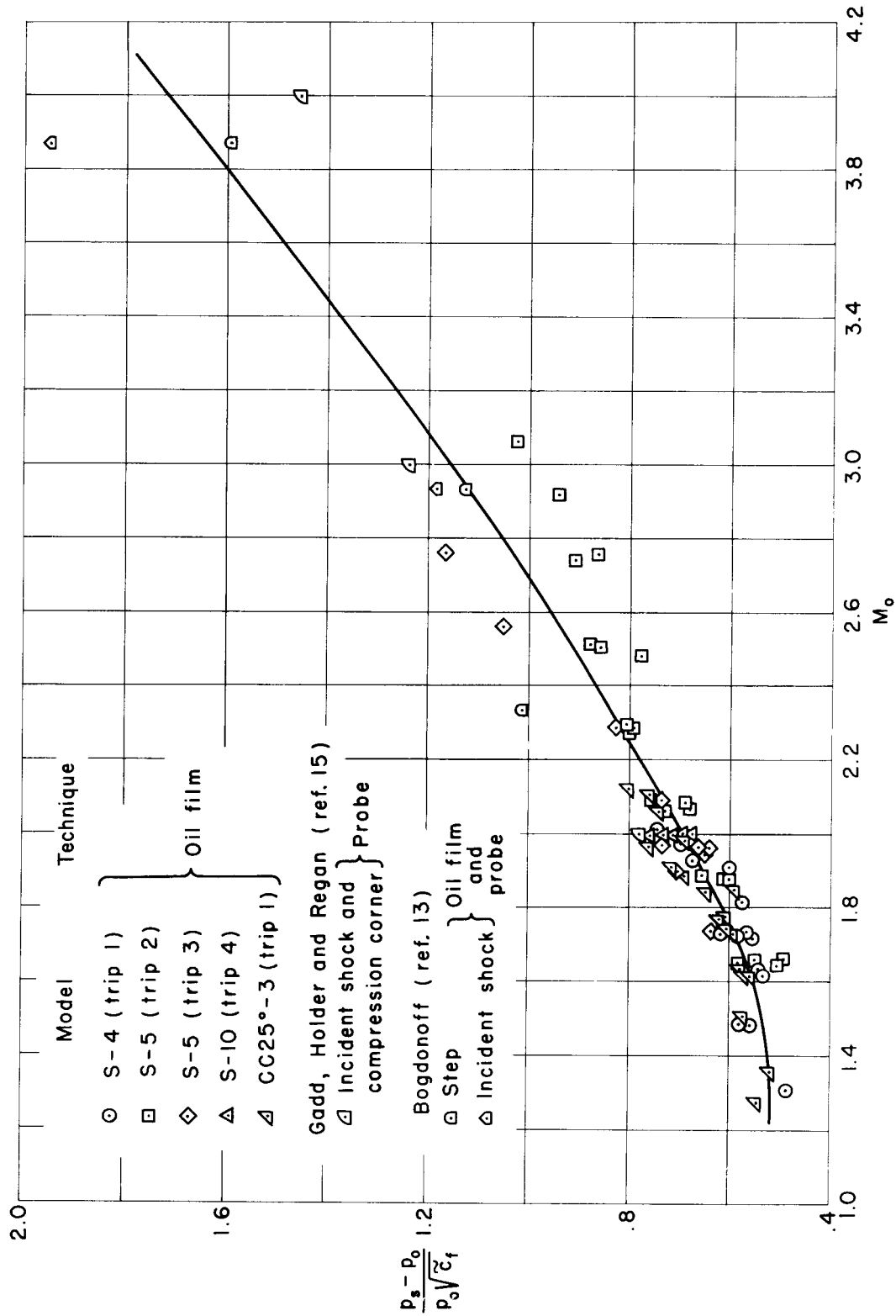


Figure 45.—Effect of Mach number on pressure rise to separation point for turbulent flow for steps, compression corners, and incident shocks.

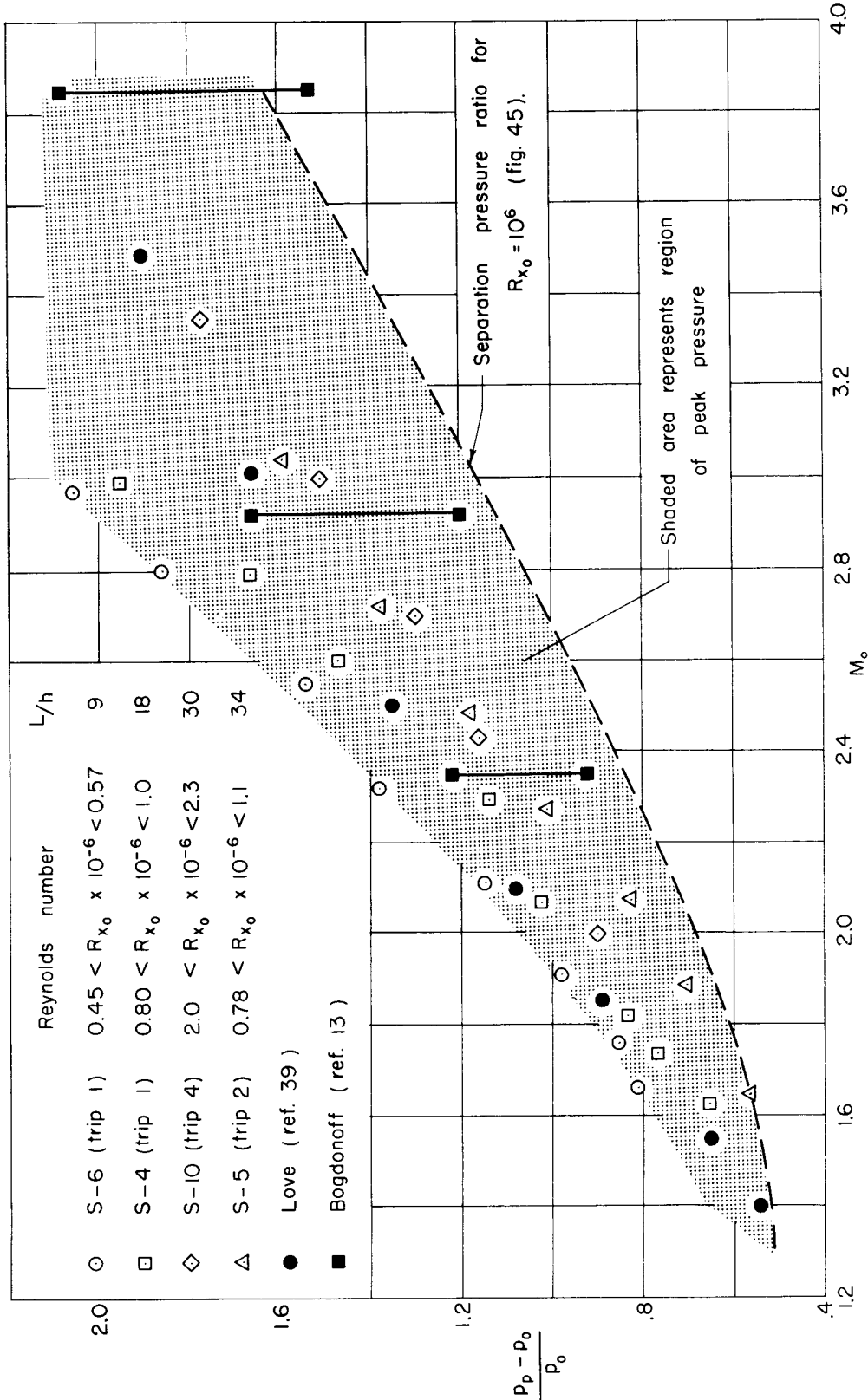
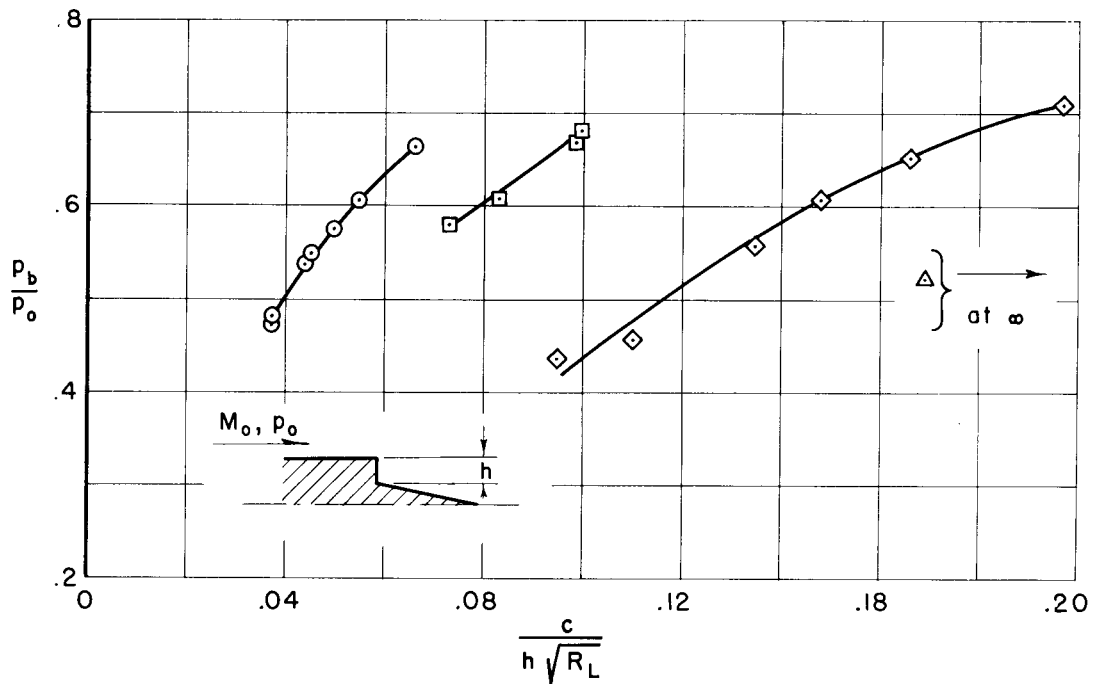
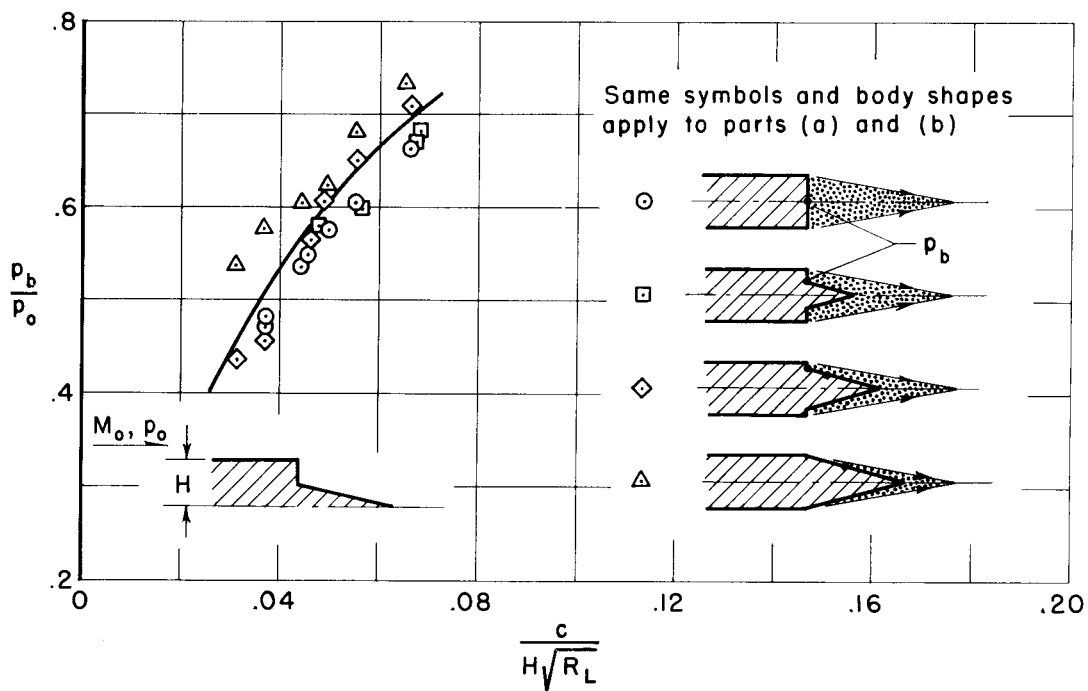


Figure 46.- Effect of Mach number on peak pressure ratio for steps with turbulent separation.



(a)  $h'$  as characteristic length.



(b)  $H$  as characteristic length.

Figure 47.— Base pressure measurements for transitional type separation with various wedge inserts in the dead air region;  $M_0=2.0$ .